UNIWERSYTET IM. ADAMA MICKIEWICZA W POZNANIU

Antonio Santana i Ros

Physical models of single and binary asteroids from photometric surveys: preparation of Gaia data scientific exploitation

Rozprawa doktorska

Praca wykonana pod kierunkiem
Prof. dr hab. Tadeusza Michałowskiego
i dr Przemysława Bartczaka
w Obserwatorium Astronomicznym
Wydziału Fizyki UAM

POZNAŃ 2015

Oświadczenie autora pracy

Ja, niżej podpisany mgr Antonio Santana i Ros oświadczam, że przedkładaną rozprawę doktorską pt:

Physical models of single and binary asteroids from photometric surveys: preparation of Gaia data scientific exploitation

napisałem samodzielnie. Oznacza to, że przy pisaniu pracy, poza niezbędnymi konsultacjami, nie korzystałem z pomocy innych osób, a w szczególności nie zlecałem opracowania rozprawy lub jej istotnych części innym osobom, ani nie odpisywałem tej rozprawy lub jej istotnych części od innym osób.

Oświadczam ponadto, że wydrukowana oraz elektroniczna wersja pracy są identyczne.

Acknowledgements

I would like to show my special appreciation to my advisor Professor Tadeusz Michałowski, not only for supporting me from the very beginning of my career as a minor planet astronomer, but also for leading me through the hard path of learning Polish. A special thanks to my favorite "kabaret" performer Dr Przemysław Bartczak, who was also my second advisor and has taught me the secrets of non-convex modelling of asteroids. I also want to thank Dr Ania Marciniak for her enormous patience and enthusiasm when teaching me how to gather good lightcurves and for her precious comments on this work. I warmly thank Dr Paolo Tanga for welcoming me to the Observatoire de la Côte d'Azur, for kindly replying to all my long emails full of questions and for making me feel part of the DPAC from the very beginning. This work would not have been possible without the collaboration of Dr Alberto Cellino who put at my disposal the use of the genetic algorithm for the inversion of *Gaia* disk-integrated photometry of asteroids. I am also very grateful to Dr François Mignard for putting at my disposal the use of the *Gaia* simulator of Solar System observations. At the end, I would like to thank all my colleagues from the Gaia Research for European Astronomy Training (GREAT-ITN) network, with special reference to Dr Nicolas Walton, who has enthusiastically led the project and to Dr Francesca Figueras who encouraged me to join this fantastic group of people.

Vull dedicar un especial agraïment a les meves famílies. A l'originària a Catalunya per ajudar-me a fer de mi qui sóc i seguir incondicionalment cadascun dels meus passos. I a la d'acollida a Polònia, per fer-me sentir com a casa durant aquests anys. I a l'Ania, la meva dona, amb la que he compartit el camí que m'ha dut fins aquí, i amb la que seguirem recorrent el sender de la vida.

This work has been funded by the European Union Seventh Framework Programme (FP7/2007-2013) under grant agreement no. 264895.

Al Nil, i als que encara han de venir.

Modele fizyczne planetoid pojedynczych i podwójnych otrzymane na podstawie przeglądów fotometrycznych: przygotowanie do naukowego wykorzystania danych z kosmicznej misji Gaia

Antonio Santana i Ros

Streszczenie

Celem naukowym niniejszej pracy było sprawdzenie realności algorytmu genetycznego, który będzie wykorzystany do analizy danych fotometrycznych planetoid, zebranych przez misję Gaia, wystrzeloną przez Europejską Agencję Kosmiczną.

W czasie swojej pięcioletniej misji, Gaia zgromadzi dane fotometryczne dla ponad 300000 planetoid. Wykorzystując te pomiary spodziewamy się określić kształty dla ponad 10000 planetoid, co oznacza wzrost o czynnik 100 w stosunku do obecnie znanych modeli. Wykorzystanie tak dużego zbioru danych obserwacyjnych będzie wymagało opracowania całkowicie automatycznych algorytmów, zdolnych do otrzymywania rozwiązań podczas nieprzerwanych procesów obliczeniowych trwających kilka tygodni.

W przeciwieństwie do klasycznej fotometrii planetoid, Gaia nie będzie dostarczała pełnych krzywych zmian jasności a tylko pojedyncze, niezbyt częste pomiary. Liczba detekcji zależy od orbity konkretnego obiektu, co średno powinno dać 60-70 rejestracji dla planetoid z Głównego Pasa. Te dane będą pokrywały szeroki zakres warunków obserwacyjnych, w szczególności szeroki zakres długości ekliptycznych, dając w rezultacie właściwy zakres zmian kąta aspektu. Takie dane będą podobne do rzadkich pomiarów zgromadzonych w Asteroids Dynamic Site. Co więcej, Gaia dostarczy danych fotometrycznych 10 razy dokładniejszych i co jest bardzo istotne, będą one jednorodne w tym sensie, że zostaną otrzymane pojedynczym instrumentem.

Głownym wyzwaniem przy analizie rzadkich danych jest prawidłowe określenie okresu rotacji planetoidy. Rozwiązanie tego problemu w tradycyjny sposób dla więcej niż 300000 planetoid, wymagałoby ekstremalnie dużych mocy obliczeniowych. Z tego powodu techniki obliczeniowe, przygotowane do analizy specyficznych danych z misji Gaia, bazują na algorytmie genetycznym, gdzie rozwiązanie problemu jest zcharakteryzowane przez najlepsze dopasowanie układu parametrów, które są otrzymywane na drodze kilku przypadkowych zmian w procesie mutacji genetycznych.

W celu testowania algorytmu przeprowadzono kilka symulacji dla 10000 planetoid mających różne orientacje osi rotacji, okresy obrotów oraz kształty. Procesy analizy zostały przeprowadzone przy wykorzystaniu klastra obliczeniowego (znajdującego się w Obserwatorium UAM w Poznaniu), który składa się 27 stacji roboczych wyposażonych w sześcio-rdzeniowe procesory AMD (3 GHz). Epoki obserwacyjne, użyte w każdej symulacji, zostały uzyskane z symulatora misji Gaia, opracowanego w Obserwatorium Lazurowego Wybrzeża (Francja), a jasności zostały wygenerowane Z-buforem, standardowej metody graficznej. Zbadano także wpływ szumu gaussowskiego, przy różnych wartościach sigma, na otrzymywane wyniki. Badania wykazały korelację pomiędzy wiarygodnością metody a szerokością ekliptyczną bieguna oraz kształtem planetoidy. W szczególności, rezultaty są niepewne dla planetoid o kształtach zbliżonych do sfery oraz

z biegunami o niskich wartościach szerokości ekliptycznych. Ten efekt jest spowodowany przez małą amplitudę zmian jasności obserwowaną przy takich warunkach co wynika z faktu, że periodyczny sygnał może być zagubiony w przypadkowym szumie fotometrycznym, wtedy gdy obie te wartości są porównywalne. Taki zbieg okoliczności powoduje, że wykorzystywana metoda nie daje prawidłowych wyników. Te sytuacje powinny być brane pod uwagę podczas analizy wyników i nie powinny być mylone z realnymi efektami np. z działaniami sił niegrawitacyjnych.

Ponieważ pomiary fotometryczne planetoid będą mogły być wykorzystywane dopiero po czwartej publikacji danych misji Gaia (rok 2019) wykorzystaliśmy rzadkie pomiary fotometryczne planetoid zgromadzone w Asteroids Dynamic Site, aby również przetestować algorytm z realnymi danymi obserwacyjnymi. Rezultaty nie miały dużej wartości, czego należało się spodziewać dla bazy danych o niskiej jakości. Chociaż byłoby ryzykowne wyciągać jakieś konkluzje o własnościach fizycznych planetoid, to jednak przeprowadzony eksperyment pozwala sprawdzić do jakiego stopnia rezultaty otrzymane z danych poznańskiego symulatora odpowiadają rzeczywistym danym.

Drugi zespół symulacji został przeprowadzony dla synchronicznych planetoid podwójnych. Analiza rezultatów prowadzi do potwierdzenia, że takie systemy mogą być modelowane jako proste ciała o kształcie trójosiowej elipsoidy. Na bazie tych symulacji stało sie możliwe opracowanie strategii odkrywania planetoid podwójnych. Ostatecznie, najlepszym użytecznym parametrem są półosie wielkie. Ilościowe rezultaty zawierają wartości półosi wielkich modeli trójosiowych elipsoid z wysokim prawdopodobieństwem, że wskazują one na systemy podwójne.

Taki sam eksperyment z rzeczywistymi danymi z Asteroids Dynamic Site został powtórzony dla znanych planetoid podwójnych. Wybrane obiekty są potwierdzonymi planetoidami podwójnymi synchronicznymi bądź niesynchronicznymi. Jednak nie wszystkie znane systemy podwójne mogły zostać wykorzystane z powodu jakości rzadkich danych dla nich istniejących. Niestety tylko dla najjaśniejszych systemów jakość danych była wystarczająca do wykorzystania.

W sumie tylko sześć synchronicznych planetoid podwójnych mogło być wykorzystanych. Niezależnie od niskiej jakości danych, właściwe okresy (tzn, zgodne z tymi otrzymanymi przez innych autorów na podstawie pełnych krzywych zmian jasności) zostały otrzymane dla pięciu z nich. Dla trzech z nich otrzymane bieguny były również w zgodzie z wcześniej opublikowanymi wartościami, dla jednego otrzymano błędny wynik a dla dwóch dalszych nie było wcześniej opublikowanych żadnych rozwiązań.

Z otrzymanych rezultatów można stwierdzić, że algorytm opracowany dla misji Gaia pracuje prawidłowo z systemami synchronicznymi gdyż one pokazują tylko jedną okresowość i można je przybliżyć pojedynczym obiektem. Jednak systemy niesynchroniczne mają więcej okresowości związanych z rotacjami składników i okresowością zaćmień.

Przeprowadzono również badanie znaczenia anlizy danych, które były kombinacjami pełnych krzywych zmian jasności oraz jednoczesnej fotometrii z misji Gaia. Obecnie wszystkie parametry skanowania nieba przez misję Gaia są już ustalone, więc możemy dokładnie przewidywać sekwencję obserwacji ciał z Układu Słonecznego. To oznacza, że można obserwować ten sam obiekt z powierzchni Ziemi w tym samym czasie co Gaia. W ten sposób możemy bardzo łatwo otrzymać pełną krzywą zmian jasności planetoidy w pobliżu (lub bardzo blisko) czasu izolowanej obserwacji przez misję Gaia. Połączenie tych dwóch zbiorów danych będzie bardzo silne, ponieważ pojedynczy pomiar z misji dostarcza bardzo dokładnej jasności absolutnej, która moze być wykorzystana do

kalibracji obserwacji naziemnych.

Pokazano, że połaczenie obserwacji z misji oraz danych naziemnych redukuje liczbę błędnych rezultatów dla planetoid posiadających mniej niż 50 punktów pomiarowych. To nabiera specjalnego znaczenia przy planowaniu obserwacji naziemnych planetoid, które mogą zwiększyć naukowe znaczenie danych z misji Gaia na naszą wiedzę o Układzie Słonecznym.

W celu wsparcia obserwacyjnej kampanii należałoby publikować sekwencje obserwacji planetoid przez misję Gaia, która pozwoliłaby obserwatorom na otrzymanie krzywych zmian jasności planetoid w czasie gdy będzie je obserwowała Gaia. W tym celu został przygotowany serwis Gaia-Groundbased Observation Service for Asteroids (Gaia-GOSA), który jest dostępny dla potencjalnych obserwatorów na stronie `www.gaiagosa.eu`. Ostatecznym celem tego projektu jest stworzenie sieci obserwatorów woluntariuszy, którzy mogą, pod kierunkiem profesjonalnych astronomów, otrzymać wartościowe dane fotometryczne dla planetoid. Wymagania stawiane w serwisie Gaia-GOSA, prowadzone prace oraz oczekiwane rezultaty są również opisane w niniejszej pracy.

Contents

Abstract

The subject of investigation was the reliability of the genetic algorithm which will be used to invert the photometric measurements of asteroids collected by the European Space Agency *Gaia* mission. To do that, several sets of simulations for 10,000 asteroids having different spin axis orientations, rotational periods and shapes were performed. The observational epochs used for each simulation were extracted from the *Gaia* mission simulator developed at the Observatoire de la Côte d'Azur, while the brightnesses were generated using a Z-buffer standard graphic method. The influence of contaminating the data set with Gaussian noise with different σ values on the inversion results was also explored. The research revealed a correlation between the reliability of the inversion method and the asteroid's pole latitude. In particular, the results are biased against asteroids having quasi-spherical shapes and low pole latitudes. This effect is caused by the low lightcurve amplitude observed under such circumstances, as the periodic signal can be lost in the photometric random noise when both values are comparable, causing the inversion to fail. Such bias should be taken into account when analysing the inversion results, not to mislead it with physical effects such as non-gravitational forces.

A second set of simulations was performed for synchronous binary asteroids. The analysis of the inversion results led to the confirmation that such systems can be successfully modelled with a simple triaxial ellipsoid body. On the basis of these simulations, it was also possible to develop strategies for binary asteroid detection. To that end, the most useful inversion paremeters are the semi-major axis. The presented quantitative results include the semi-major axis values of the triaxial ellipsoid model with a high probability of hosting binary systems.

Finally, it has been studied what impact on the inversion results does it have to combine a full lightcurve and *Gaia* photometry collected simultaneously. It has been shown that using this procedure it is possible to reduce the number of wrong solutions for asteroids having less than 50 data points. The latter result will be of special importance for planning ground-based observations of asteroids aiming to enhance the scientific impact of *Gaia* on Solar System science. On this basis, the Gaia-Groundbased Observation Service for Asteroids (*Gaia-GOSA*) has been developed and is already available for the observing community at `www.gaiagosa.eu`. The requirements for the *Gaia-GOSA* service are described here as well as the development works done and the expected results.

Chapter 1

Overview of the state of the art in asteroid modelling

Asteroids and comets are fundamental objects for studying the Solar System, as they give us clues to its origin and evolution. We can consider them as a big "cosmic laboratory" because their study allows to test and confirm theories, not only concerning astronomy but also with a direct impact on many other fields of physics. As an example, a good understanding of their physical parameters plays a key role in the construction of formation models for exosolar systems. Furthermore, observations of the asteroid orbital perturbations led to the discovery of non-gravitational effects such as Yarkovsky and YORP (Bottke et al. 2001 and Bottke et al. 2006). The Yarkovsky effect is a force acting on an asteroid caused by the anisotropic emission of thermal photons, perturbing its orbit as a long-term result. It depends on the asteroid's spin axis orientation and its period, as well as its size. On the other hand, the YORP effect is affecting the asteroid's rotational period and its spin axis orientation, and it depends on the inclination of the spin axis and the body's shape. Therefore, deriving the asteroid's spin, shape and rotational state is a necessary effort that has to be done in order to proceed further with these investigations. To that end, photometry is by far the most fruitful observational technique. The classical photometric observations of asteroids (henceforth "dense lightcurves") that have been collected during the last decades, are the main source of our knowledge about asteroids and their physical parameters. The usual format of this data for one apparition (the period during which the asteroid is observable from the Earth) is basically dozens of photometric measurements collected during few observing nights (e.g. Fig. 1.1). As a result, the rotational period of the asteroid is well covered but the quantity of information of the body shape is limited, as the geometry orientation of the asteroid is almost constant during this period. Consequently, to obtain a unique spin and shape solution, we need a set of a few tens of dense lightcurves observed during at least four different apparitions. This observational constraint is significantly limiting the number of objects for which we have enough dense observations to derive a complex shape of the body. Around 100 asteroid models have been obtained basing on this classic photometric data. Enlarging the number of derived models using this method requires the organization of observational campaigns, potentially resulting in few tens of new models per year.

The majority of these models were generated using a convex representation of the

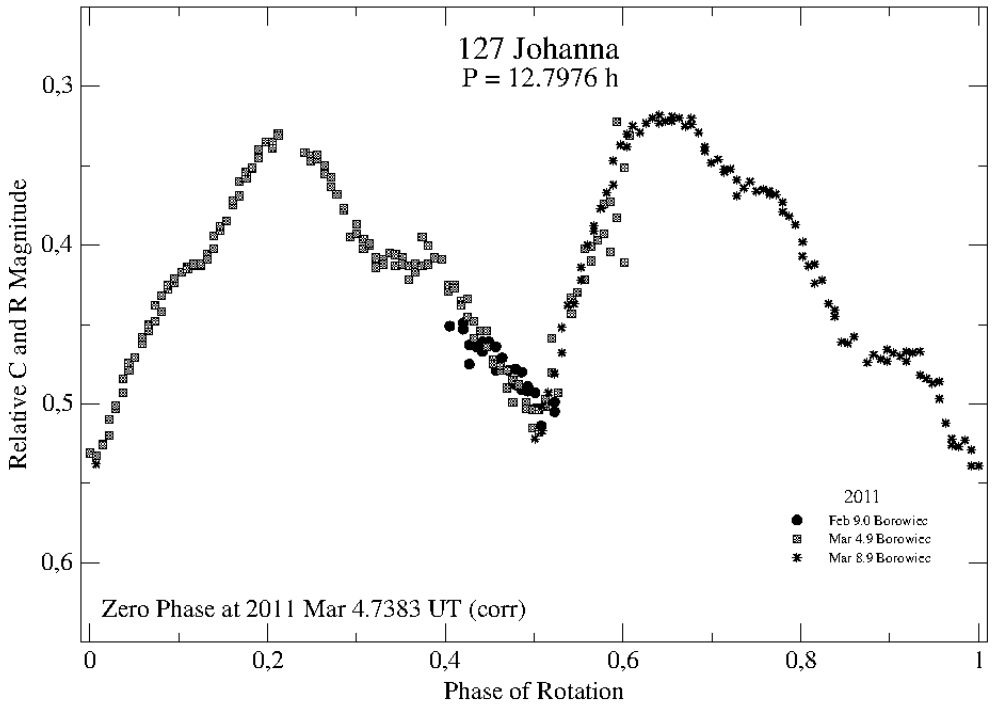

Figure 1.1: Composite lightcurve of asteroid (127) Johanna (Marciniak, Bartczak, Santana-Ros et al. 2012).

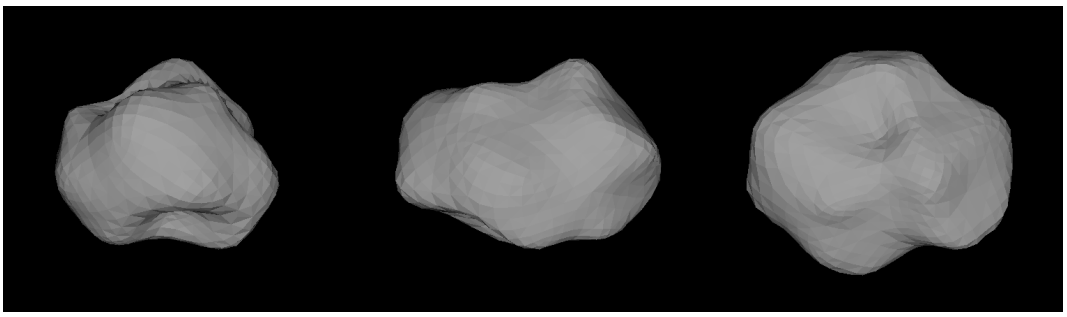

Figure 1.2: Three different spatial views of the non-convex model for 9 Metis shown at equatorial viewing and illumination geometry, with rotational phases 90 apart (two pictures on the left), and the pole-on view at the right (Bartczak, Santana-Ros & Michałowski, 2014).

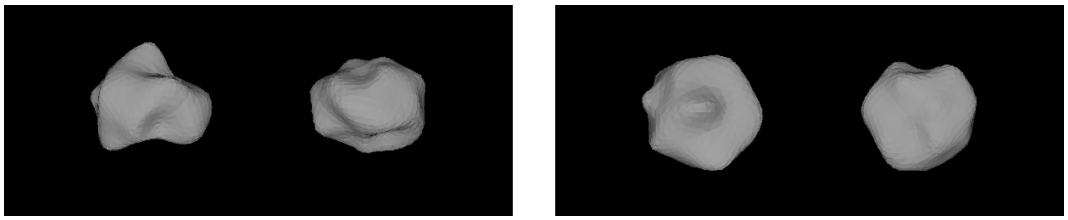

Figure 1.3: Two different spatial views of the nonconvex model for 90 Antiope binary system shown at equatorial viewing and illumination geometry (on the left), and the pole-on view on the right (Bartczak et al. 2014).

asteroid shape (Kaasalainen & Torppa, 2001), which despite being a first-order approximation of the real shape of the body, have been proven to be good enough to fit the lightcurves and to derive asteroid's main physical parameters. However, from direct images obtained during space missions like NEAR Shoemaker or Hayabusa, we know that the real shapes of asteroids are not convex, but generally are full of concavities. In order to obtain a more accurate (realistic) shape model, alternative methods have been presented. For instance, Bartczak, Michałowski, Santana-Ros et al. (2014) recently developed a new inversion method called SAGE (Shaping Asteroids with Genetic Evolution) capable to derive nonconvex shape models for single and binary asteroids relying on their disk-integrated photometric measurements. In this case, the optimization problem is tackled by a genetic algorithm, which randomly mutates the model parameters and selects the best trial solutions until the evolution stabilizes. These models confirm the pole directions and rotation periods derived with previous methods, and additionally the highly detailed description of the asteroids' shape allows a more accurate determination of their physical properties, like the volume and as a consequence, their density. An example of the models obtained using the SAGE technique can be seen in Fig. 1.2 for the single asteroid case and in Fig. 1.3 for the 90 Antiope binary system.

The most popular photometric technique for asteroids is, by far, differential photometry. It might seem that performing absolute photometric measurements should be always preferred. However, it is preferable to use relative photometric measurements, for the following reasons:

- Conditions might not be always photometric. If we rely on absolute photometry, many observational nights might be lost, or the data might be burdened with serious errors.
- Uncertainties of absolute magnitude measurements are normally at the level of few hundreths of magnitude. For asteroids with small amplitude (i.e. lightcurves with amplitude below 0.1 mag) such measurement uncertainty would make the data unsuitable for modelling purposes.

The inversion techniques are thus relying on relative photometry, so the resulting models are also relative in terms of dimensions. In order to scale them, we need an absolute measurement of the asteroid size. This can be obtained from other observation techniques like the time chords recorded during a stellar occultation by an asteroid, or direct imaging techniques, like adaptive optics. For instance, we could use the excellent results obtained during the 2011 Antiope's stellar occultation and project the 3D shape

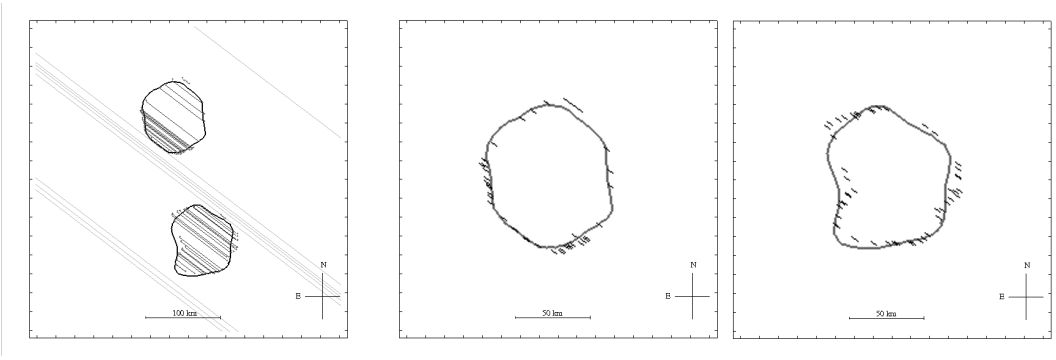

Figure 1.4: Left: best fit of the stellar occultation chords obtained during the 2011 occultation (Colas et al. 2012)) to the solution found for the non-convex shape model of 90 Antiope (Bartczak et al. 2014). Middle and right: timing uncertainties on both projected components due to the unknown diameter of the occulted star (LQ Aqr).

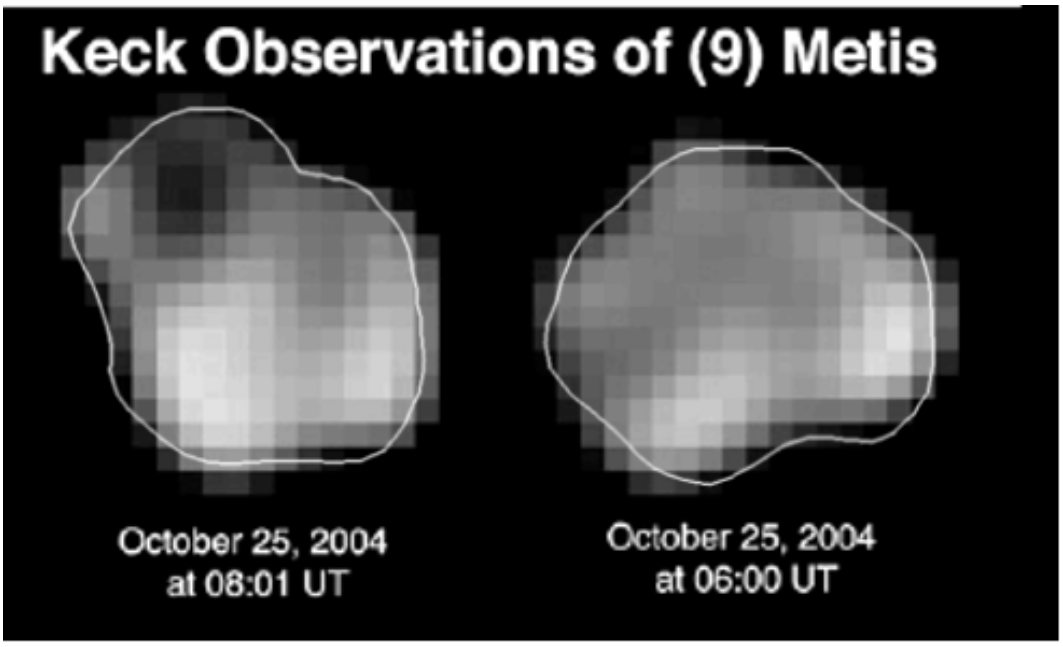

Figure 1.5: Profile comparison of the non-convex solution found for (9) Metis (Bartczak, Santana-Ros & Michałowski, 2014) to the Adaptive Optics observations presented in Marchis et al. (2006) obtained with the Keck NGS AO system.

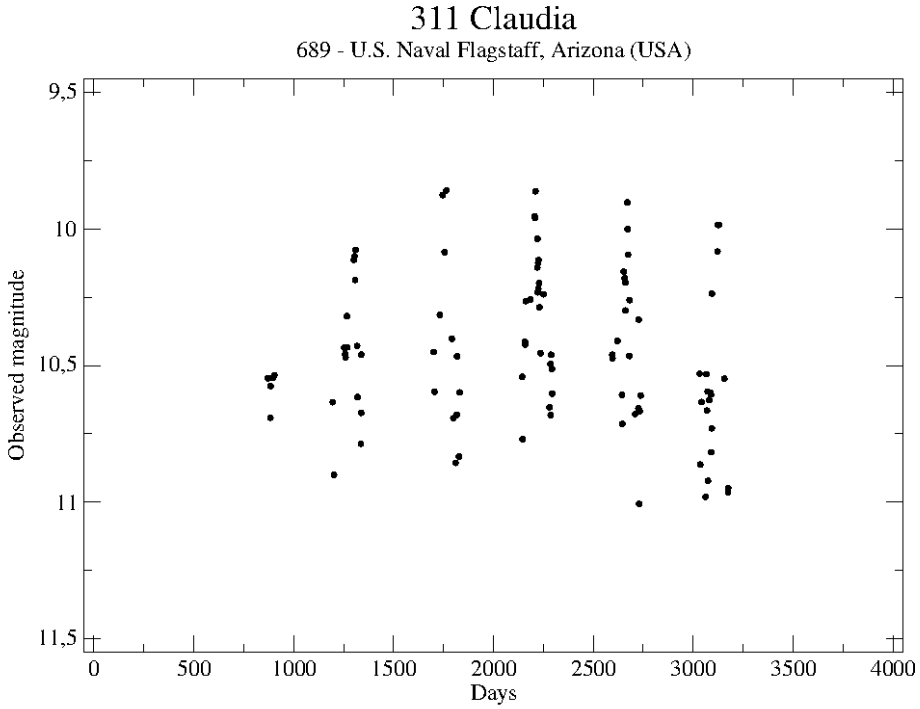

Figure 1.6: Example of sparse-in-time photometric measurements of (311) Claudia obtained by the 689 U.S. Naval Flagstaff observatory during 6 different apparitions.

model onto the asteroid's silhouette derived from the occultation timings (Fig. 1.4). On the other hand, the adaptive optics images of 9 Metis, not only allowed us to scale the relative model, but confirmed the concativies found by our modelling technique (Fig. 1.5).

Other approaches to the multi-data inversion problem have been developed during the last years. For instance, the KOALA (Knitted Occultation, Adaptive optics and Lightcurve Analysis, Carry et al. 2012) algorithm solutions are based on lightcurves and silhouette contours, while ADAM (All-Data Asteroid Modeling, Viikinkoski, Kaasalainen & Durech, 2015) is a collection of functions from which one can tailor an inversion procedure for multiple data sources including direct imaging, radar and interferometry.

During the last years, some observatories around the world have started sky surveys mainly focused to detect new NEAs or to improve their orbit determination (e.g. U.S. Naval Flagstaff, Catalina Sky Survey, La Palma). As a by-product of these astrometric survey programs a huge amount of sparse-in-time photometric measurements for tens of thousands of asteroids have been retrieved. For each object some tens of discrete observations were collected for different asteroid's geometries and illuminations (e.g. Fig. 1.6). Combining these datasets with dense lightcurves allowed increasing the modelled population of asteroids from 100 (classical photometry) to 400 (combination of classical and sparse photometric data).

Generally, the photometric accuracy of such surveys is rather low, at the order of $\sim$0.1 mag in the majority of cases. But still, this accuracy has been proved to be enough to retrieve valuable information of the asteroids' physics and its properties (e.g. Hanus et al. 2013). *Gaia* observations will generate a similar sparse set of photometric measurements during its 5 years operation. But the data increase will be considerable, both in terms of quantity (observations are expected for $\sim$300.000 asteroids, Mignard et al. 2007) and quality (the photometric accuracy is estimated to be $\sim$0.01 mag for asteroids up to 18 magnitude, and $\sim$0.03 mag up to 20 magnitude, Cellino et al. 2006). As a result of this enormous amount of new data, we expect to derive asteroid models for at least 10.000 objects. This means an improvement of two order of magnitudes from our actual knowledge. This will have a direct impact on the Solar System formation theories, as a statistically large sample of objects with known properties may reveal physical effects which play an important role for the whole population.

The present work is devoted to the preparation of the scientific exploitation of *Gaia* photometric measurements of asteroids. In chapter 2, an overall view of the mission contribution to asteroid science is compiled. Due to the fact that these data will be released at the end of the mission (expected for 2019), the results presented have been obtained on the basis of simulations. The tools used for generating these simulations are described in chapter 3, while the data inversion process and the analysis of the results for the case of single and binary asteroids are presented in chapters 4 and 5. In chapter 6 the potential of combining ground-based observations with *Gaia* data in order to enhance the asteroids' scientific output is discussed, while chapter 7 is presenting the *Gaia*-GOSA service, a tool specifically developed to coordinate such observational campaign.

Chapter 2

Gaia contribution to asteroid science

2.1. *Gaia* mission overview

On 19 December 2013, the ESA's *Gaia* space telescope was succesfully launched from Kourou in French Guiana. It took almost one month for *Gaia* to arrive to the L2 point, and after technical calibrations, the spacecraft started its scanning of the sky that should last for at least 5 years. The astrometric focal plane has an area of almost 0.5 m^2 and contains 170 CCDs, which make it the largest digital camera ever flown in space. The mission aims to obtain very precise astrometric measurements for more than a billion objects, from stars to distant galaxies, but also for Solar System objects like asteroids. The focal plane is complemented with a radial velocity spectrometer and a blue and red band photometric instrument (Fig. 2.1).

Gaia perfoms its observations from a controlled Lissajous-type orbit around the L2 Lagrange point of the Sun and Earth-Moon system. The observational strategy for *Gaia* consists of a constant survey of the sky with two telescopes separated by a basic angle of 106.5°. The spacecraft spins around its axis with a constant speed of 60 arcsec $s^{-}1$. The two astrometric fields of view scan across all objects located along the great circle 'perpendicular' to the spin axis, completing a full revolution each 6 hours (Fig. 2.2). Data is being acquired continuously (except for dead time preventing nominal observations), thus the CCDs are operating in time-delayed integration (TDI) mode, which is synchronized with the satellite's rotation rate. The full catalogue of *Gaia* observations will consist of several (from 40 to 150, depending on the object's sky position) astrometric, spectometric and photometric sparsed-in-time precise measurements for all objects with $V \leq 20.7$.

In the case of Solar System science, astrometric, spectrometric and photometric measurements for more than 300.000 asteroids are going to be obtained. Using this data we expect to derive shape models for about 10.000 asteroids, which means increase by a factor of 100 the actual number of known models. Dealing with such big sets of data requires developing totally automatized algorithms, capable to derive the solutions under unattended runs of computation lasting several weeks.

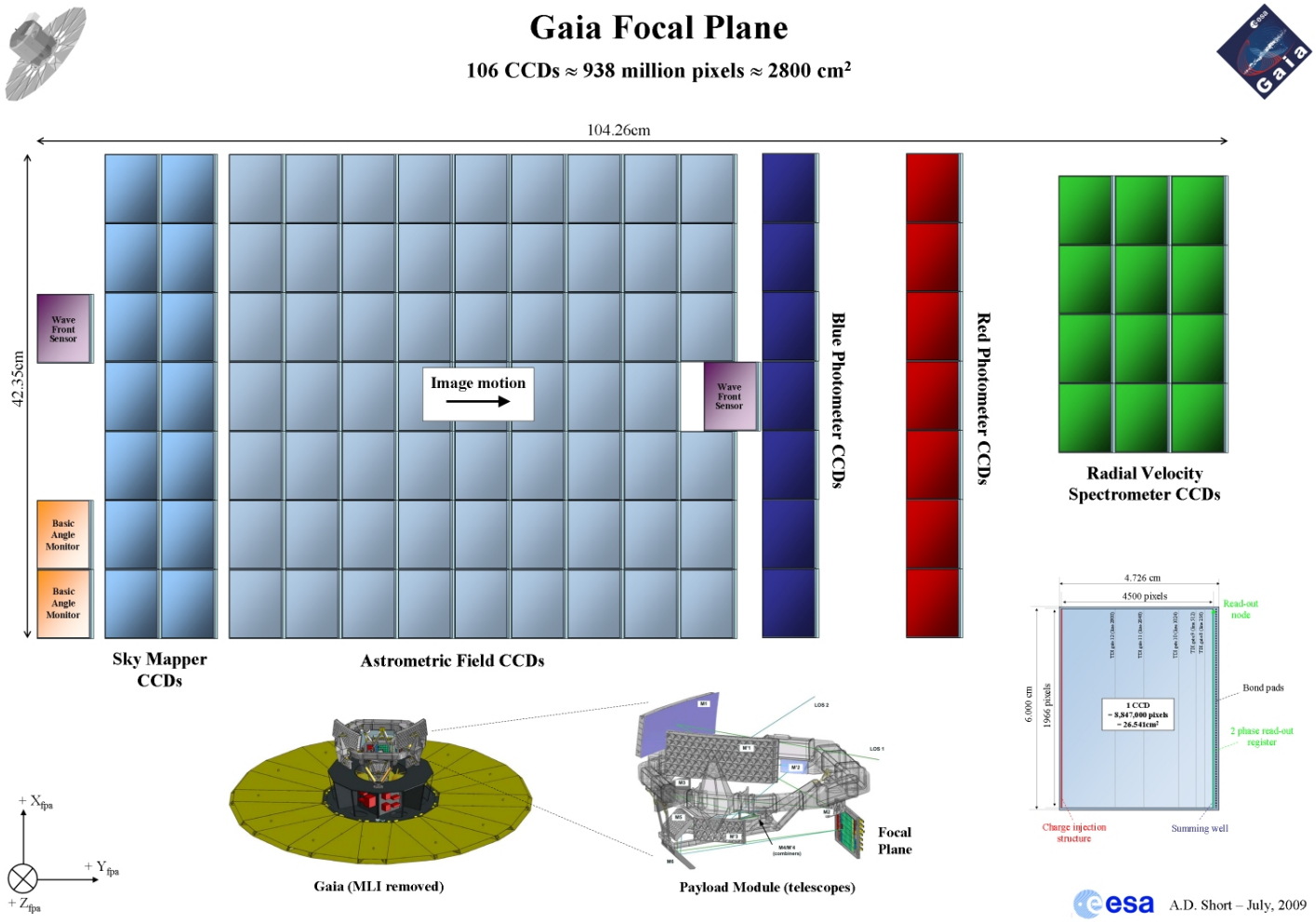

Figure 2.1: Schematic of the *Gaia* focal plane (Credits: ESA).

2.2. Photometry

The big advantage of *Gaia*, with respect to ground-based telescopes, is the fact of being diffraction-limited only. The image of an object on the *Gaia* focal plane is the result of the convolution of the incoming wave front with the optical system of *Gaia*, described by the point spread function (PSF) of the instrument. The PSF contains all information about the optical response of the *Gaia* telescope, depending on the position on the focal plane and the spectral properties of the source. Since the satellite rotates around its spinning axis, any detected celestial source transits across the *Gaia* focal plane, and its optical signal is recorded by a series of CCDs and converted into an electronic signal consisting of a distribution of photoelectrons generated in the CCD pixels.

2.2.1. Physical models from disk-integrated photometry

Knowledge of rotational states of asteroids is fundamental for understanding the history of the Solar System, specifically the accretion of planets or the collisional processes. For instance, it was presumed that due to collisional evolution, the spin-vector distribution of main belt asteroids (MBAs) should be nearly isotropic, possibly with a small excess of prograde spins (Davis et al. 1989).

For this task, the *Gaia* Solar System team has developed a genetic algorithm able to invert sparse data sets of photometric measurements like the ones we expect from *Gaia* (Cellino et al. 2006). The potential of this technique has been shown in subsequent studies (Cellino et al. 2009) where the authors successfully derived the shape models for more than 20 asteroids using the photometry from the Hipparcos mission.

This genetic algorithm is able to invert a set of sparse disk-integrated photometric data using a model that contains the following unknown and adjustable parameters, to be determined during the inversion process:

- the sidereal rotation period of the object: P
- the ecliptic coordinates of the asteroid north pole (λ, β)
- the axial ratios b/a and c/a of the triaxial ellipsoid shape
- an initial rotational phase ϕ_0 of the object corresponding to the epoch of the first observation in the dataset
- the coefficient k of a linear relation of absolute magnitude as a function of phase angle

Based on this model, the photometric behaviour of a given object can be generated for a set of epochs and observing circumstances. For this purpose, analytic functions are used to compute the apparent illuminated area of a triaxial ellipsoid object. Despite not being the most accurate method, this choice is a good approximation and makes the algorithm less demanding in terms of CPU time.

Assuming for simplicity that the object is not in a tumbling rotational state, and it has relaxed state of rotation (it is a rigid body rotating around its principal axis of the maximum moment of inertia), the formulae described by Pospieszalska-Surdej & Surdej (1985) can be used to compute the fraction of the illuminated surface visible to *Gaia*. At a given epoch, the apparent illuminated cross-section of a triaxial ellipsoid can be characterized by four angles: the phase angle α (the angle between the directions to

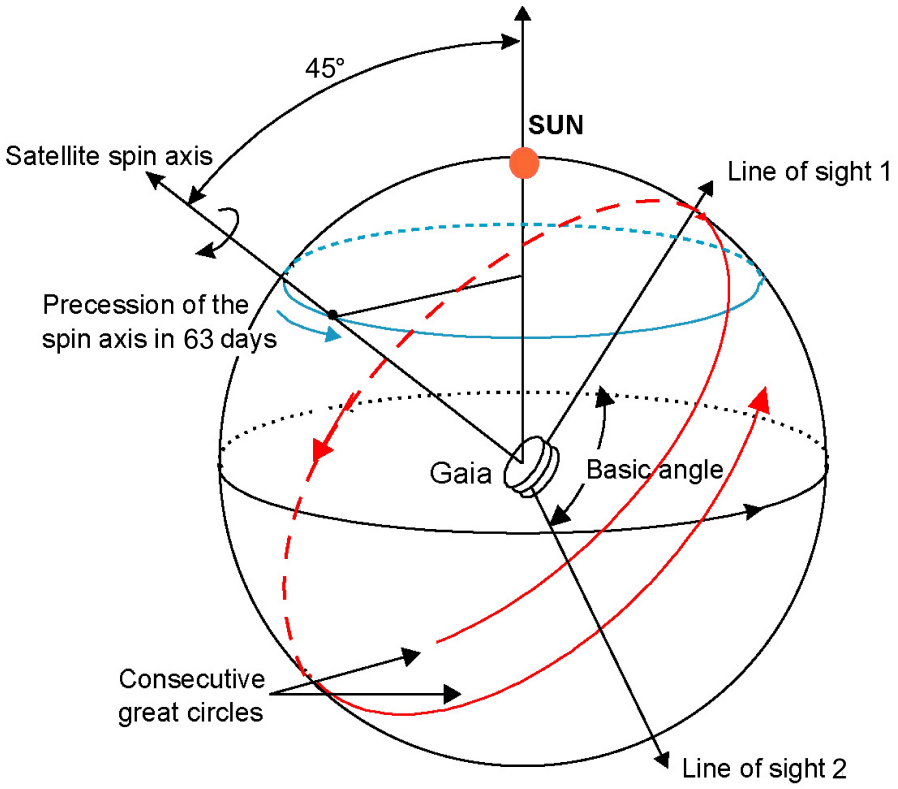

Figure 2.2: *Gaia*'s spin axis does not point to a fixed direction in space (or on the sky) but is carefully controlled so as to precess slowly on the sky (Credits: ESA).

the Sun and to *Gaia* as seen from the asteroid), the rotation angle ϕ (the rotational phase of the object at the given epoch), the aspect angle γ (the angle between the direction of the object's spin axis and the direction to *Gaia*), and the obliquity angle χ (the angle between the plane containing *Gaia*, the asteroid and its spin axis, and the plane perpendicular to the asteroid-*Gaia*-Sun plane). Knowing the above angles and the triaxial semi-axes ($a = 1 > b > c$), the visible illuminated surface S is given by the Pospieszalska-Surdej & Surdej (1985) formulae:

$$S = \frac{S_1 + S_2}{2} \tag{2.1}$$

where S_1 and S_2 are given by the following expressions

$$S_1 = \pi abc\sqrt{\Big(\frac{1}{a^2}\sin^2\phi + \frac{1}{b^2}\cos^2\phi\Big)\sin^2\gamma + \frac{1}{c^2}\cos^2\gamma} \tag{2.2}$$

and

$$S_2 = \pi abc\frac{(V_{11}\cos\alpha + V_{12}\sin\alpha)}{\sqrt{V_{11}\cos^2\alpha + V_{22}\sin^2\alpha + 2V_{12}\sin\alpha\cos\alpha}} \tag{2.3}$$

where V_{11}, V_{12}, V_{22} are

$$V_{11} = \sin^2\gamma\Big(\frac{1}{a^2}\sin^2\phi + \frac{1}{b^2}\cos^2\phi\Big) + \frac{1}{c^2}\cos^2\gamma \tag{2.4}$$

$$\begin{aligned} V_{12} = \frac{1}{a^2}(-\sin\phi\sin\gamma)(\cos\phi\cos\chi + \sin\phi\cos\gamma\sin\chi) \\ +\frac{1}{b^2}\cos\phi\sin\gamma(\sin\phi\cos\chi - \cos\phi\cos\gamma\sin\chi) \\ +\frac{1}{c^2}\cos\gamma\sin\gamma\sin\chi \end{aligned} \tag{2.5}$$

$$\begin{aligned} V_{22} = \frac{1}{a^2}(\cos\phi\cos\chi + \sin\phi\cos\gamma\sin\chi)^2 \\ +\frac{1}{b^2}(-\sin\phi\cos\chi + \cos\phi\cos\gamma\sin\chi)^2 \\ +\frac{1}{c^2}\sin^2\gamma\sin^2\chi \end{aligned} \tag{2.6}$$

The method includes one more simplification pertaining to the magnitude–phase function: absolute magnitude of the object varies linearly with phase angle. This assumption can be introduced for *Gaia* observations due to the spacecraft particular scanning law, which avoids observations close to the asteroid's opposition or for large phase angles (Fig. 2.3. In particular, *Gaia* observations of main-belt asteroids will be obtained for phase angles between 10 and 30 degrees.

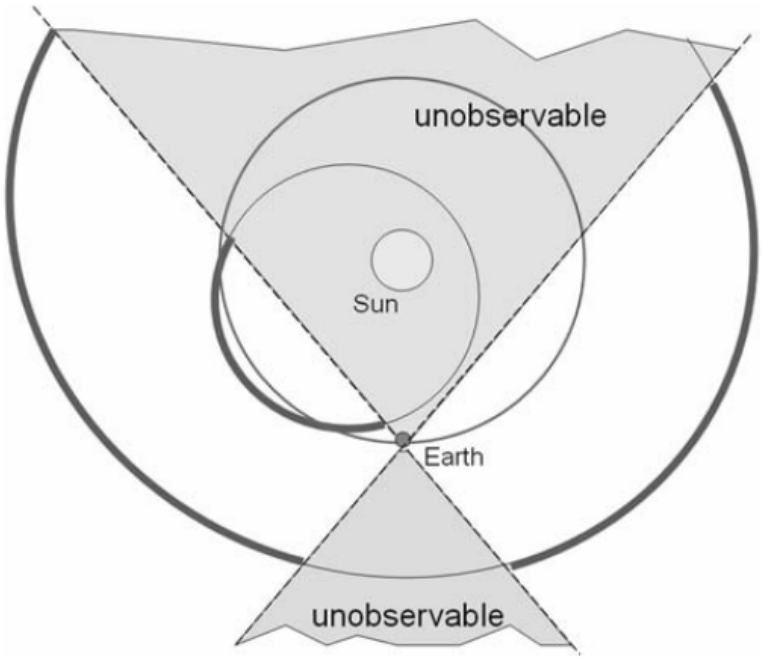

Figure 2.3: The region not reached by *Gaia*, projected on the ecliptic plane (Mignard et al. 2007).

The genetic routines control the evolution of the model parameters following the mechanism of natural selection. In other words, the strongest individuals in this framework are those that produce the closest fit to the set of photometric data. Starting from random parameter values, the genetic mutations are repeated many times (between 300.000 and 1.000.000, depending on the configuration file) and at the end a list with the N best solutions is saved in the output file. This method was chosen in order to save computational time, due to the obvious constrain to the inversion problem that represents the huge amount of data produced by *Gaia*. However, it is worth mentioning that the presence of a small number of wrong inversion solutions is, in any case, unavoidable, due to the way the genetic approach works. There is always the possibility that several genetic inversion attempts for the same object will not be sufficient to find the right solution. Increasing the number of attempts per object would certainly improve further the performances, but this is not recommended in the *Gaia* scenario due to CPU time constraints, as the inversion algorithm will have to process a number of the order of half a million of asteroids (meaning two months of computations in our observatory computer cluster).

The solution of the inversion problem consists of a set of model parameters which provides the best fit to *Gaia* photometric data. This fit can be quantitatively evaluated with a minimization of the observed and computed magnitudes

$$\epsilon = \sqrt{\frac{\sum_{i=1}^{N} w_i (O_i - C_i)^2}{\sum_{i=1}^{N} w_i}} \tag{2.7}$$

where O_i and C_i are, respectively, the observed and computed magnitudes of the ith observation, w_i is the assigned statistical weight of the ith observation and N is the number of photometric observations for a given asteroid.

An example of the output of the *Gaia* inversion algorithm is shown in Fig. 2.1

Despite the good results obtained during the algorithm tests, its reliability is limited by some constraints coming from the distribution of *Gaia* observations. In the case of Solar System objects, the average number of measurements per object will be between 60 and 70, spread over 5 years. For comparison, the classical inversion relies on some tens of lightcurves, each containing dozens of (usually) relative disk-integrated measurements. Thus, there are few questions that need to be answered: under which circumstances such sparse in time observations are enough to derive an acceptable model solution? Is the method's performance correlated with any physical parameter of modelled asteroids? Is it possible to improve the results by adding ground-based observations of selected targets?

During the last three years I have been studying this particular problem in order to answer these questions. As a result of collaboration with P. Tanga (manager of the *Gaia* Data Processing and Analysis Consortium - Coordination Unit 4 and leader of the *Gaia* Solar System team in the Observatoire de la Côte d'Azur) and the work within the Poznań's photometric team, we have developed a *Gaia* mission simulator that is able to simulate the asteroid's *Gaia* photometry of asteroids using random body shapes and different scattering laws. We have started using this tool to test the performance of the *Gaia* inversion algorithm and some of the conclusions obtained have been published in Santana-Ros, Bartczak, Michałowski et al. (2015). These investigations allowed us

Table 2.1: Example of the best solutions found by the *Gaia* inversion algorithm for a given asteroid. The model parameters (λ, β, P, b/a, c/a, ϕ_0 and k coefficient) are ordered by the χ^2 of the fit (last column on the right), which reflects the goodness of the solution.

λ	β	P	b/a	c/a	ϕ	k	χ^2
291.65	70.27	6.081763	0.65	0.65	0.09	0.004	0.054009
292.19	70.49	6.081761	0.65	0.65	0.09	0.006	0.054029
294.81	70.38	6.081761	0.65	0.65	0.08	0.003	0.054073
161.61	62.29	6.081774	0.66	0.66	0.45	0.004	0.054551
157.47	61.64	6.081773	0.65	0.65	0.46	0.001	0.054567
200.58	45.89	6.083700	0.62	0.62	0.45	0.004	0.081964
199.79	46.56	6.083699	0.63	0.63	0.45	0.003	0.081965
201.40	45.56	6.083702	0.62	0.62	0.44	0.003	0.081966
200.95	45.68	6.083701	0.62	0.62	0.45	0.003	0.081970
289.16	56.28	5.888275	0.66	0.66	0.11	0.001	0.089874
211.96	32.68	5.887591	0.50	0.50	0.39	0.001	0.097259
304.06	20.26	6.082687	0.61	0.61	0.10	0.001	0.097423
283.95	60.85	12.332628	0.68	0.68	0.13	0.002	0.113324
18.72	77.75	10.761168	0.63	0.63	0.42	0.005	0.116432

to identify a relation between the asteroid's pole latitude and the correctness of period determination. Such effects could result in a biased *Gaia* catalogue, that might have a direct impact in the theories developed by astronomers a posteriori. Thus our work has been focused on a correct interpretation of the *Gaia* inversion results for asteroids, to remove the bias caused by the method limitations which would lead to wrong theories on the formation of the Solar System. The aforementioned tests and the results obtained are presented in section 4.

2.2.2. Measurement of asteroid sizes

Asteroids are not point-like sources, therefore it is certain that, above some given limit of apparent angular size, and depending also on the apparent magnitude at the epoch of observation, an asteroid signal produced on the *Gaia* focal plane will be different with respect to the ideal case of an unresolved star.

The results of the simulations produced by Mignard et al. 2007 indicate that above a size of 30 km in diameter, more than 50% of the known main-belt asteroids will have their size measured at least once during the Gaia operational lifetime with an accuracy better than 10% (see Fig. 2.4). The number of useful measurements rapidly increases for increasing size. In the size range between 20 and 30 km, more than 20% of the objects will also be measured at least once, or even a few times.

2.3. Spectro-photometry

Gaia gathers spectro-photometric data using two different detectors. The astrometric field measures white-light G magnitudes from unfiltered fluxes, while low resolution prism spectra is measured in the blue (330–680 nm) and red (640–1050 nm) CCDs

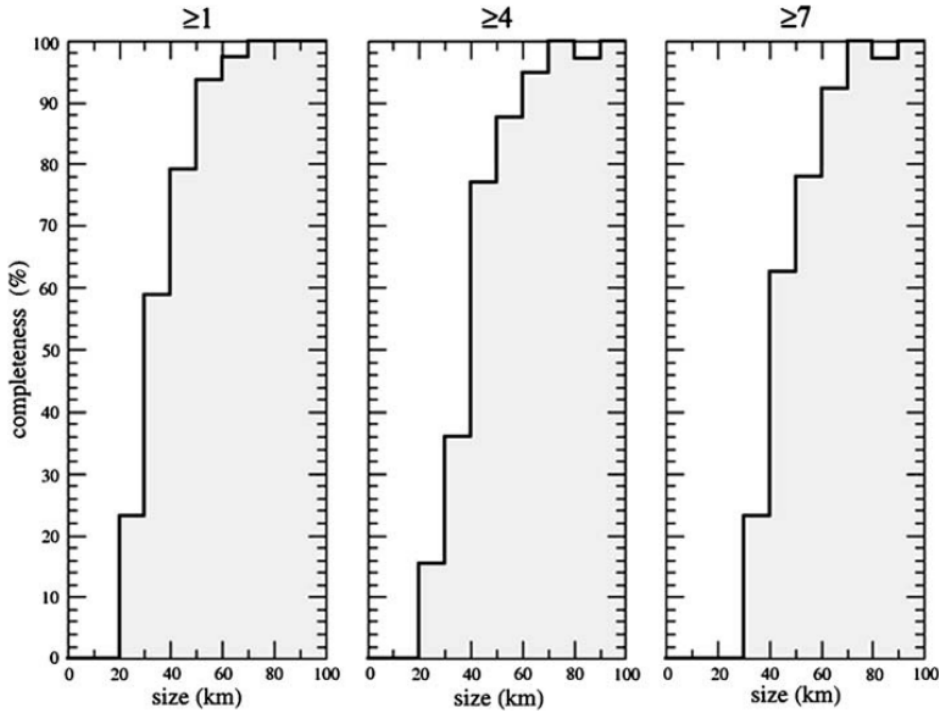

Figure 2.4: Predicted percentage of the existing main-belt asteroids that will have their apparent angular sizes measured by *Gaia* with an accuracy better than 10% at least once, four and seven times (from left to right) during the *Gaia* operational lifetime, as a function of their actual sizes (Mignard et al. 2007).

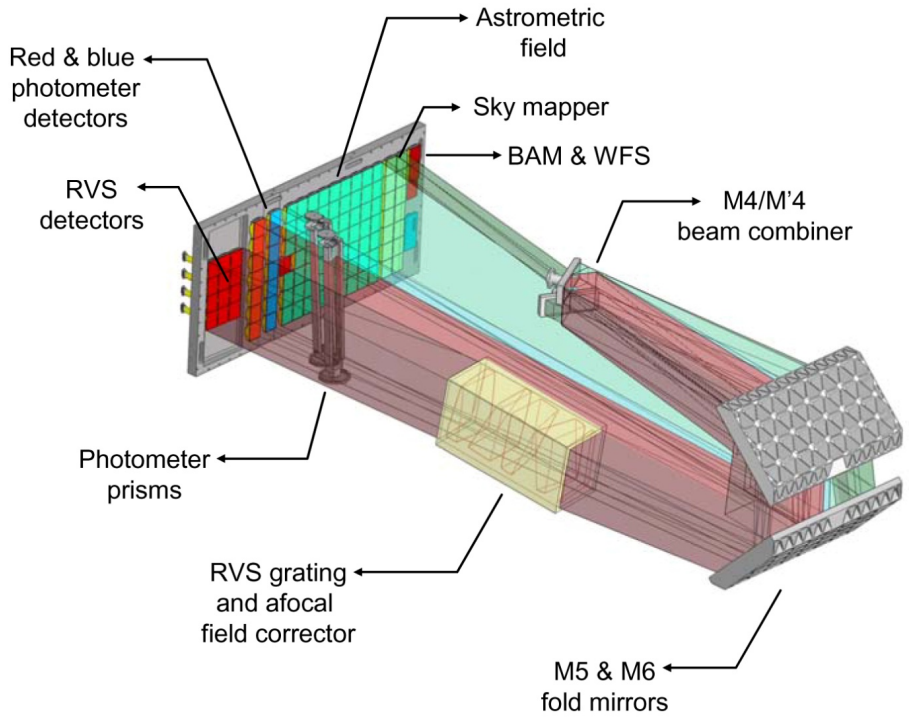

Figure 2.5: The *Gaia* spectro-photometric instrument consists of two low-resolution fused-silica prisms dispersing the light entering the field of view (Credits: ESA).

(Fig. 2.5). The integrated flux of these blue photometer and red photometer spectra yields G_{BP} and G_{RP} magnitudes as two broad passbands. We expect to use the data obtained by these detectors to derive reflectance spectra for more than 100,000 asteroids (Delbo et al. 2012). Such data is meant to be a great source for the taxonomy classification of asteroids. It is noteworthy that the blue part of the reflectance spectrum will allow the study of sub-classes of the C-complex, which is not achievable from ground-based observations.

In the beginnings of the asteroid taxonomy studies the method of principal component analysis (PCA) was used by Tholen (1984) to define the first asteroid taxonomic classes based on 7-color spectra (Eight Color Asteroid Survey, Zellner et al. 1985). This first classification scheme was extended with infrared data from IRAS (Barucci et al. 1987), and more recently by Bus & Binzel using data from the SMASSII (Small Main Belt Asteroid Spectral Survey II, Bus & Binzel, 2002a). The actual feature-based taxonomy includes 26 classes following the increased discriminative ability of CCD spectra (Fig. 2.6).

Gaia low resolution spectro-photometry will allow sampling of asteroid reflectance spectra for a representative fraction of the known population. In order to obtain the best possible signal-to-noise ratio, each asteroid spectra will be obtained from the average of all transits (being the expected number of transits ∼60-70 for a main belt object). These data will yield the study of the asteroids' composition and their classification as a function of their origin.

It was shown in Warell & Lagerkvist, 2007 that both photometric systems of *Gaia*

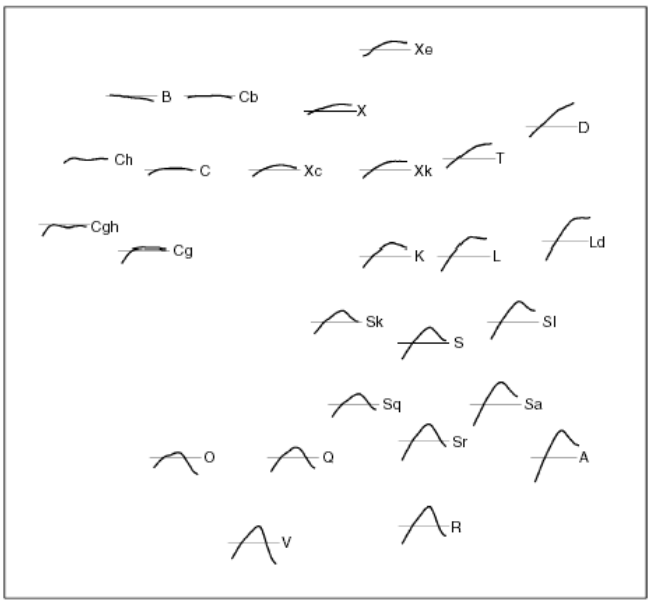

Figure 2.6: Reflectance spectra for the 26 classes from the SMASSII taxonomy (Bus & Binzel, 2002b).

are able to discriminate between all of the Tholen asteroid classes while the medium band system is able to discriminate between the majority of the 26 SMASSII asteroid classes. These classes can lead to a mineralogical interpretation in terms of the reflectance spectra as shown in Fig. 2.7, which is a unique source to study the asteroid surface mineralogy and their origin and history.

Due to the huge amount of data produced during five years of continuous scanning, *Gaia* taxonomic classification algorithm was built as an automated code developed to generate scientific results from unattended runs. The *Gaia* taxonomy algorithm for each collected reflectance spectra checks which class best fits the data. An example of a simulation of the reflectance and the clone generated is shown in Fig. 2.8. The enormous quantity of data expected will be enough to raise significant conclusions about the taxonomy within asteroid families. On the other hand, basing the analysis on *Gaia* data alone will have two major advantatges:

1. It will be a homogeneous dataset, in the sense that is being collected by a single instrument
2. For most objects, it will include the blue region of the spectrum, not available for taxonomic classifications based on spectroscopic surveys from the ground

The latter data are of special interest, as it can be used to distinguish among different sub-classes of primitive, low-albedo objects.

2.4. Astrometry

Gaia is the most ambitious astrometric mission ever built. Its main goal is to construct a 3D model of our galaxy based on the astrometric measurements of 1 billion

Asteroid taxonomic classes and their general interpretation.

Type	Probable Surface Mineralogy	Albedo	Abundance	Bell's Superclass
A	Olivine or olivine-metal	High	Rare	Igneous
B, *F*, *G*	Hydrated silicates, carbon, organics	Low	Fairly rare	Metamorphic
C	"	Low	Common	Primitive
D, *P*	Carbon/organic-rich silicates	Very low	Common	Primitive
E	Enstatite, iron-free silicates	Very high	Rare	Igneous
M	Metal, metal + enstatite	Moderate	Moderately rare	Igneous
Q	Olivine + pyroxene + metal	Moderate	Rare	Primitive
R	Pyroxene + olivine	Moderate	Rare	Igneous
S	Metal, olivine, pyroxene	Moderate	Common	Igneous
T	Similar to *P* and *D* (?)	Moderate	Rare	Metamorphic
V	Pyroxene, feldspar	Moderate	Rare	Igneous

Figure 2.7: Surface mineralogical interpretation of the asteroid classes (Cellino 2000).

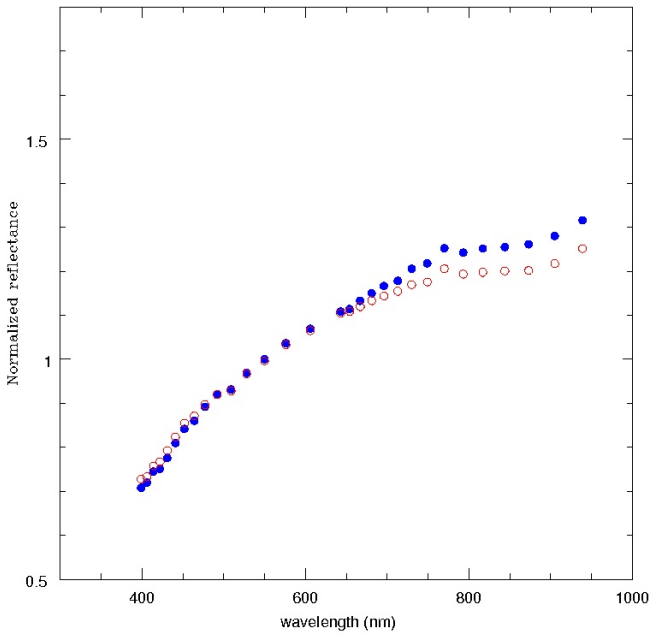

Figure 2.8: Example of a simulation of the reflectance spectra expected from *Gaia* and the clones produced to test the *Gaia* taxonomy algorithm (Cellino 2014).

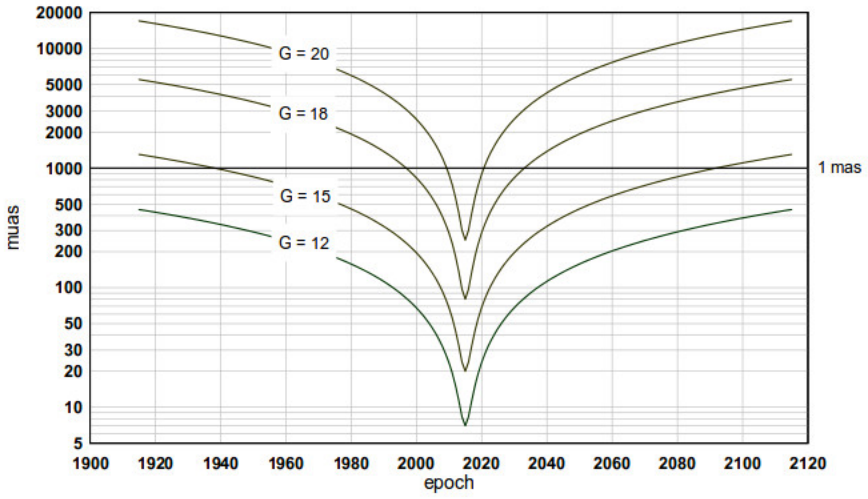

Figure 2.9: Evolution of the accuracy of the *Gaia* positional stellar catalogue with time due to the uncertainty in the annual proper motions of stars (Mignard 2011).

stars. However, *Gaia* will also provide valuable astrometric data of our immediate neighbourhood: the Solar System. These data will permit a precise determination of the asteroid orbits, but it will also allow the direct measurements of gravitational perturbations for a few tens of asteroids, leading to the determination of their masses with a good accuracy. Moreover, the resulting *Gaia* stars catalogue will bring about a revolution on the prediction of stellar occultations by asteroids, which are nowadays limited by the Hipparcos/Tycho catalogues.

2.4.1. Computation of orbits

Orbit determination and improvement are central activities in the analysis and scientific exploitation of the *Gaia* Solar System data. At the end of the mission, the asteroids' positional precision is expected to reach the sub-milliarcsecond level. The exact positional precision will depend in each case on the number of transits for a given object. In a second term, the computation also depends on the body shape, surface properties, observed magnitude or the observation distribution. An initial orbit computation will be already available for the first observations (Muinonen et al. 2005). Actually, for more than two observations, the statistical ranging technique allows a Monte Carlo sampling of the phase space of the orbital elements. However, the global solution for asteroid orbits will not be available until the end of the mission. This is because the full statistical inverse problem should also take into account the sizes, shapes, masses and relativistic effects due to the precision of the *Gaia* astrometry (Mignard et al. 2007).

The accuracy of the resulting positional catalogue will degrade at a rate of 0.2 - 0.3 μas yr^{-1} from the moment of the last observation due to the proper motion uncertainty (see Fig. 2.9). When it comes to System Solar objects, the degradation will include an annual fluctuation due to the variable geometry between the Earth and the asteroid (see Fig. 2.10).

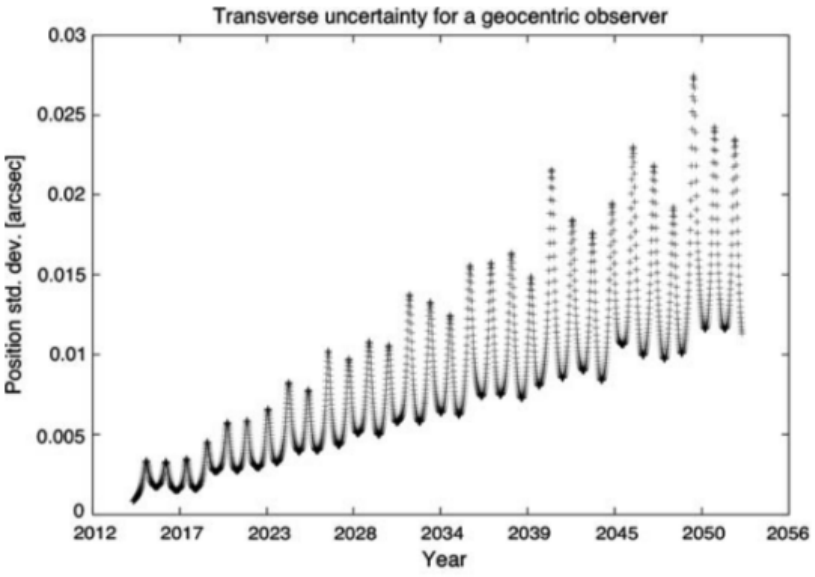

Figure 2.10: The ephemeris uncertainty of (1) Ceres for a geocentric observer as function of time. The fluctuation is due to the variable geometry between the Earth and the object (Mignard et al. 2007).

2.4.2. Mass determination

The astrometric precision provided by *Gaia* will allow the measurement of gravitational perturbations during close approaches of target asteroids. In particular Mouret, Hestroffer & Mignard, (2008) found that at least 42 asteroid masses will be derived with a precision better than 10% and 150 (asteroid masses) with a precision better than 50%. These precise determinations will result in an unprecedent improvement of the dynamical modelling of the Solar System and will have a direct impact on our knowledge of the physics of asteroids.

Mass of the pertubers will be determined according to a two-body ballistic approach where the relative trajectory of the target asteroid with respect to the perturber can be modelled by a hyperbola (see Fig. 2.11).

From the hyperbolic two-body problem the deflection angle θ is given by,

$$\tan\frac{\theta}{2} = \frac{G(m+M)}{v^2 b} \tag{2.8}$$

where G is the constant of gravitation, M is the mass of perturber, m that of the target asteroid, v the relative velocity of the encounter and b the impact parameter which can be reduced to the minimal distance between the two asteroid trajectories in the case where we do not take into account their mutual perturbations.

The mass of an asteroid is a hard physical property to be determined with a good accuracy. Knowing the size of the asteroid, the mass yields its bulk density, which in turn allows the calculation of the porosity (the part of the void which makes up the

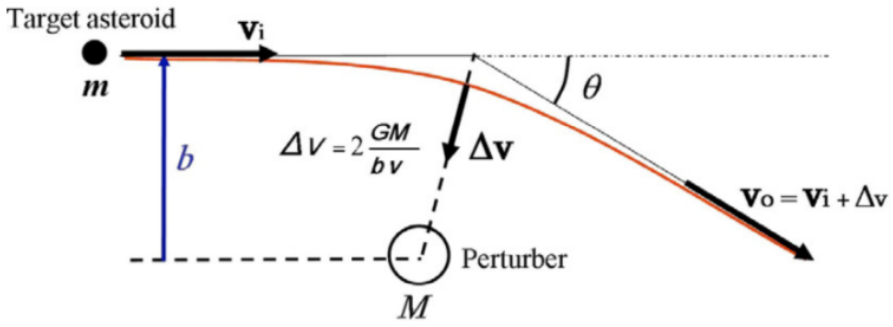

Figure 2.11: Impulse approximation of a small target asteroid perturbed by a larger one. v_i and v_o are respectively the incoming and outgoing velocity vector. The effect of the perturbation is expressed by the vector Δv (Mouret, Hestroffer & Mignard, 2008).

asteroid). The latter measurement is of great interest to evaluate the hypotheses of the Solar System's formation.

However, in order to obtain a full physical characterization of asteroids, further investigation is required (especially of the shape, spin state, rotation axis orientation). Surface characteristics can also be extremely valuable (i.e. surface composition, surface light scattering properties and albedo).

2.4.3. Stellar occultations

One of the main ground-based techniques to obtain information of the asteroid's shape consist in recording the time of a stellar occultation due to the asteroid's transit from the observer point of view. Thanks to organized observational campaigns involving several observers, a 2D snapshot of the asteroid's silhouette can be retreived from the occultation timings. This technique, that may seem unsophisticated, results in an invaluable opportunity to obtain direct observations of the body shape, no matter its size. Moreover, as orbital elements are well known for the great majority of catalogued asteroids, the body size can be directly retrieved from the occultation timings.

Nowadays predictions of stellar occultation events are constrained by the accuracy of asteroid orbits and, even most importantly, the star positions accuracy. In particular, occultation predictions for objects with diameters below 50 km are actually poor, with an uncertainty of the occultation path prediction which, sometimes, might be greater than the Earth's radius (Fig. 2.12. Moveover, the number of stars for which such predictions are feasible is restricted to the Hipparcos/Tycho catalogues. For that reason, on average only $\sim$0.1 events per object per year are predicted.

With *Gaia* astrometric measurements, we expect an oncoming golden epoch for stellar occultations. As soon as the Gaia catalogue is available, the accuracy of star positions and asteroid orbits will increase dramatically, boosting the possibility of obtaining a positive observation of such events. An overall enhancement on the prediction of these events is expected, as the asteroids' orbit determination will improve by a factor of 100. With such ephemeris, the prediction uncertainty will became smaller than the asteroid's size for objects greater than 20 km. A mid-size telescope (i.e. 1 meter

[†] `www.lesia.obspm.fr/perso/bruno-sicardy/07dec08_varuna/`

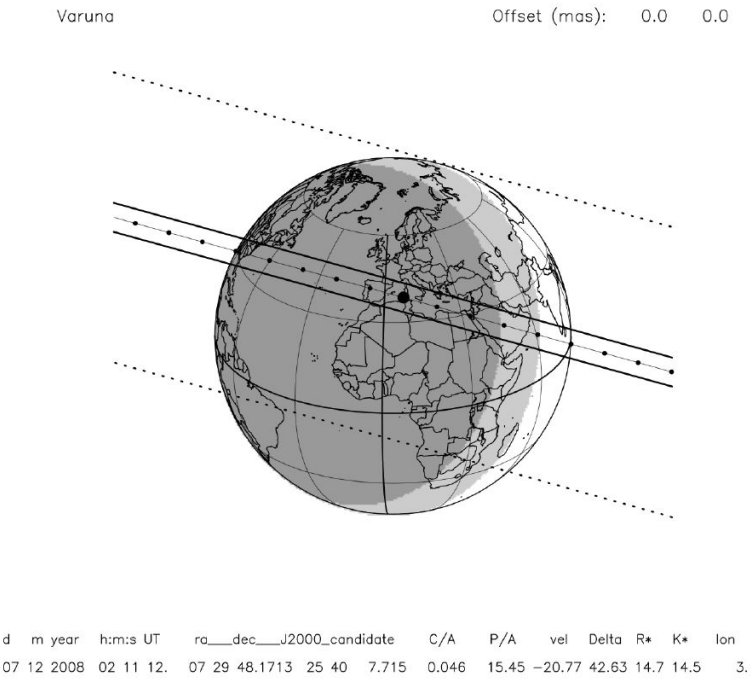

Figure 2.12: Example of a stellar occultation path prediction with an uncertainty comparable to the size of the Earth (B. Sicardy's site[†]).

telescope) will potentially observe from a single site between 20 and 40 events for such objects per year. Observational campaigns in a few years should allow the completeness of the diameter survey of asteroids greater than 20 km. From such data, we will be able to derive shape projections, useful for fine-detailed modelling, but also very precise size measurements will be feasible. Finally, occultations may include a science surprise in the form of a binary asteroid discoveries (when a secondary component is observed in the occultation timings) or even a ring system, as was discovered recently around the Centaur (10199) Chariklo (Braga-Ribas et al. 2014).

2.5. Expected results from combined techniques

The sections above show that *Gaia* data will have a direct impact on almost all the fields of asteroid science. However, even more science will come out from combining these multi-technique measurements.

When physically characterizing an asteroid, the most valuable property without a shadow of a doubt is the body's bulk density. This property can be calculated when knowing the asteroid's mass (deducible from astrometry or from Kepler's third law in case of an asteroid with satellites), its size and shape. *Gaia* is providing all these physical properties, up to some extent, for several asteroids. In particular, the triaxial ellipsoid shape model resulting from the *Gaia*'s disk-integrated photometry inversion is a crude first-order approximation of the body's real shape. Thus, in case of asteroids which masses are determinated with *Gaia* observations, it would be appealing to organize an observational campaign to obtain the required disk-integrated photometry in order to derive a complex shape solution of the body.

Finally, considering the reflectance spectra obtained and the calculated bulk densities, it will be possible to research for an interpretation of the taxonomy in terms of the composition and internal structure of the asteroid. Such accurate characterization of some asteroid's physical properties might bring out their importance as a "Rosetta stone" to understand the origin an evolution of the Solar System.

Chapter 3

Gaia photometry of asteroids

3.1. Sparse-in-time data

The potential of the sparse photometric data to provide physical information about asteroids has been extensively proved by several authors (Cellino et al. 2006; Durech et al. 2007). Generally, the inversion methods used to derive information about the physical properties of asteroids are taking profit of the fact that a simplified version of the asteroids' real shape (triaxial ellipsoid or a convex representation) is, in the majority of cases, good enough to describe the asteroid brightness variation due to its rotation in a given period. If the observations are spread over a variety of aspect angles, it is then possible to derive the orientation of the asteroid spin axis.

The main challenge when inverting sparse data is the correct determination of the rotation period. One possible approach to solve this issue is to fit an asteroid spin and shape on a given period interval (Kaasalainen 2004). If the period is not known, it is necessary to scan along a range of possible solutions for a sample of spin orientation and shape candidates. An example of a periodogram for a given shape and spin axis is shown in Fig. 3.1. Using a convex representation of the asteroid's body shape, some authors have successfully solved the inversion problem for a couple of hundreds of asteroids (Durech et al. 2009; Hanus et al. 2013). If any *dense* lightcurve is available for the object, the interval is reduced to a small range around the observed period, saving a lot of computational time and increasing the solution reliability. But, unfortunately, obtaining full lightcurves of asteroids is a highly time consuming task, thus such observations are actually available only for ∼5,000 asteroids (stored in the Minor Planet Lightcurve Database*). It is estimated that the *Gaia* mission will produce photometric measurements for more than 300,000 asteroids, which means that for the majority of inversion trials the period scanning shall span almost all the possible period values, namely from 2 hours to several days (Eyer & Mignard, 2005).

Unlike classical asteroid photometry, *Gaia* will not obtain full lightcurves, but sparse, single photometric data spread over five years. The number of detections depends on the orbits of the objects, being the average around 60–70 snapshots for main-belt asteroids. These data will cover a wide range of observational circumstances, and in particular wide range of ecliptic longitudes, resulting in a good coverage of aspect angle variation. In terms of observational cadence, these measurements will be

*http://www.minorplanet.info/lightcurvedatabase.html/

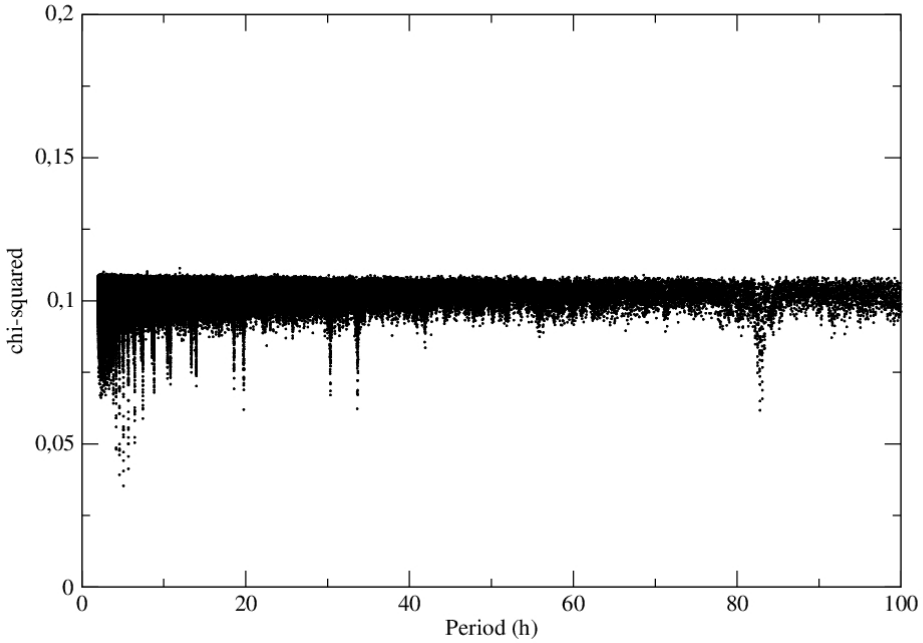

Figure 3.1: Example of a periodogram. The period value with the smallest chi-squared found is considered the problem solution.

similar to the sparse data stored in the Asteroids Dynamic Site (AstDys). However, *Gaia* snapshots will be photometrically ten times more accurate, and what is more important, homogeneous, in the sense that they will be measured by a single instrument. To put it in other words, these sparse data can be considered as the single points of a time-extended lightcurve, describing the photometric variation of the asteroids not over a single rotation period, but over five years, characterized by a continuous change of the observing circumstances. Actually, the inversion problem related with deriving physical parameters of asteroids from such measurements has become a topical issue, since not only *Gaia*, but also new ground-based survey telescopes such as the Large Synoptic Survey Telescope (LSST) will produce this kind of data.

In the case of *Gaia*, solving the inversion problem for more than 300.000 asteroids by brute force with the periodogram method mentioned aboved, would require an extremly high CPU usage. For this reason, the inversion technique specifically developed to invert the *Gaia* sparse data for asteroids (Cellino et al. 2006) is based on a genetic algorithm, where the solution of the inversion problem is characterized by the best fit of a set of parameters that have been obtained by means of several random variations during a genetic mutation process. This solution should mitigate the risk of falling in local minima of the parameter space and its capability to derive the *correct* inversion solution has been shown in some experiments with *Gaia* simulated observations and also with real data collected during the ESA Hipparcos mission (see for instance Cellino et al. 2009 or Carbognani et al. 2012). On the other hand, adding existing ground-based observations for a given asteroid is not speeding up the performance of this method (in fact the inversion becomes slower with greater number of measurements) and whether such observations can improve the method performance or not is a topic that needs to be studied.

This work is devoted to make a more general and detailed reassessment of the expected performances of the *Gaia* inversion algorithm. To do that, the inversion algorithm was fed with simulations for tens of thousands of asteroids with different spin axis orientations, different rotational periods and random shapes. Such work is necessary to correctly analyse the results generated with the *Gaia* inversion algorithm at the end of the mission, when asteroids' photometric observations will be released.

3.2. Simulations of the observational epochs of asteroids

The *Gaia* transit predictor for Solar System objects has been developed by F. Mignard at the Observatoire de la Côte d'Azur (Mignard 2015). For a set of minor planets, the program computes the crossing times in the fields of view of *Gaia*. In particular, the following equation is solved for the ith asteroid and for each field of view f over an interval of time $[T_b, T_e]$,

$$\boldsymbol{G}_F(t) = \boldsymbol{U}_i(t) \tag{3.1}$$

where $\boldsymbol{U}_i(t)$ is the unit vector of the planet proper direction at time t and $\boldsymbol{G}_F(t)$ stands for the pointing direction of *Gaia* field of view F. The left-hand-side is the *Gaia* nominal scanning law, while the right-hand-side resulted from the integration of the planetary motion.

Over a certain interval of time the program finds all the roots $t_1, t_2, \ldots, t_r k$ of Eq. 3.1. The solutions are found with an iterative process to locate a first approximation within a spin period of *Gaia* and then accurately compute the solution with a Newton-Rapshon method.

The transit predictor is based on the following general inputs:

- The osculating elements of the minor planets from the Astorb file mantained at Lowell Observatory
- The *Gaia* scanning law
- The orbit of *Gaia*
- The nominal description of the *Gaia* focal plane assembly, giving the relative position of the CCDs and the nominal optical projection
- Time coverage between T_b and T_e
- Range of magnitude in which detection are achievable

The positions and velocity of the planets are computed by a numerical integration from the osculating epoch, using gravitational perturbations from the 8 planets (Mercury to Neptune) with the main component of the relativistic contribution.

The Solar term with relativistic effect is computed as,

$$\frac{d\boldsymbol{v}}{dt} = -\frac{GM_\odot \boldsymbol{r}}{r^3} + \frac{GM_\odot}{c^2 r^3}\left(4GM_\odot \frac{\boldsymbol{r}}{r} - v^2\boldsymbol{r} + 4(\boldsymbol{r}\cdot\boldsymbol{v})\boldsymbol{v}\right) \tag{3.2}$$

with $\boldsymbol{r} = \boldsymbol{r}_p - \boldsymbol{r}_\odot$ for the heliocentric position vector of the planet.

The planetary perturbations are given by,

$$\sum_k GM_k\left[\frac{\boldsymbol{r}_k - \boldsymbol{r}}{|\boldsymbol{r}_k - \boldsymbol{r}|^3} - \frac{\boldsymbol{r}_k}{r_k^3}\right] \tag{3.3}$$

where $\boldsymbol{r}_k$ is the heliocentric position vector of the kth planet. Solar System ephemeris are taken from INPOP10e expressed in the barycentric frame with international celestial reference frame orientation and using barycentric coordinate time as an independent variable.

3.3. Simulations of the *Gaia* photometry for single asteroids

During 2012 I had the opportunity to visit P. Tanga in the Observatoire de la Côte d'Azur (Nice). He is the manager of the DPAC CU4, and he is leading the research of the *Gaia* Solar system group. As a result of my stage, I could understand better the potential of the *Gaia* mission to derive physical information of asteroids, but also after some enriching conversation with P. Tanga, I could be aware of the major challenges and drawbacks not solved yet for the exploitation of the *Gaia* data for asteroids. Thanks to this collaboration I could also test the *Gaia* Solar system predictor (described in section 3.2) and obtain a copy of the algorithm. Relying on the epochs calculated with the *Gaia* predictor and taking profit of the experience in asteroids modelling of the Poznań's Observatory photometric team, we could develope a tool that is able to simulate the asteroid's *Gaia* photometry using different body shape models (elipsoid or nonconvex shape, single and binary) and scattering laws (geometric, Lambert, Lommel-Seeliger or Bowell). The performance of the Poznań's *Gaia* simulator is described in the following sections.

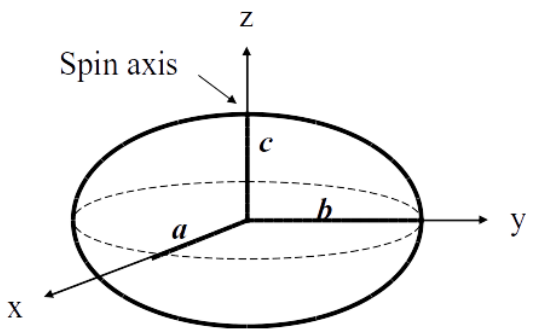

Figure 3.2: An ellipsoid defined in a given reference frame rotating about its spin axis in principal axis spin states.

3.3.1. Body representation: Triaxial ellisoid

A 3-axis ellipsoid shape can be a fairly good approximation for the majority of cases to describe the magnitude variation of an asteroid due to its change in the geometry from the observer point of view (Connelly and Ostro 1984, Michałowski 1993, Torppa et al. 2008). Such ellipsoid can be defined as the region bound by a surface given by the equation:

$$(x/a)^2 + (y/b)^2 + (z/c)^2 = 1 \tag{3.4}$$

where a,b and c are the semi-axes and satisfy the condition $a \geq b \geq c$. An example of an ellipsoid in the principal axis spin state (c axis coincident with the spin axis) is shown in Fig. 3.2.

Most of the asteroids show two maxima and two minima per rotational cycle. Such a lightcurve can be explained considering a ellipsoidal shape rotating about its spin axis (λ, β) in principal axis spin state with a given sidereal period (P). The shape of the ellipsoid is then defined by two parameters, namely, the ratios of the lenghts of the principal axes ($\frac{b}{a}$ and $\frac{c}{a}$). A model relying on such a representation of shape is completed with an initial rotation angle ϕ_0 and the sense of rotation of the body (prograde or retrograde). Using these parameters, it is possible to explain the variation in brightness of an asteroid, not only due to a rotation itself, but also due to the changes of the viewing geometry for the Sun–*Gaia*–asteroid system. Analytically, the brightness of the asteroid at a given time t, is proportional to the surface area seen from a given reference frame (cross-section of the asteroid presented to the observer). The cross-section can be calculated using the following equation:

$$S = \pi \sqrt{\frac{e^t Q e}{detQ}} \tag{3.5}$$

where e is the unit vector pointing from the asteroid to *Gaia*, and $detQ = \frac{1}{a^2 b^2 c^2}$.
We can rewrite the equation in the reference frame of the asteroid using:

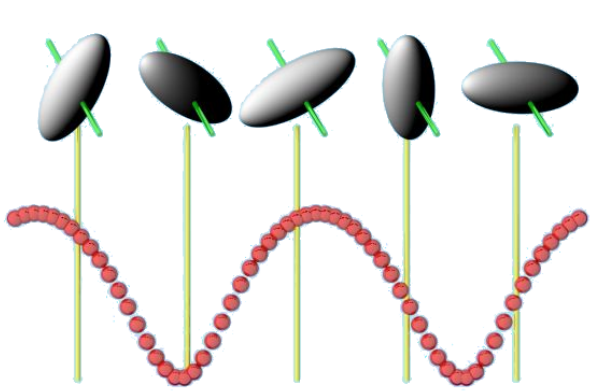

Figure 3.3: A sinusoidal lightcurve can be simply explained based on the rotation of an ellipsoid.

$$\begin{bmatrix} x \\ y \\ z \end{bmatrix} = T \begin{bmatrix} X \\ Y \\ Z \end{bmatrix} \tag{3.6}$$

where the vector on the left is the reference frame of the asteroid, and the vector on the right is the reference frame of the observer, where T is the transformation matrix, which can be written in terms of the asteroid's rotation angle ϕ and the aspect angle γ (the angle between the rotation axis and the asteroid–*Gaia* line of the sight):

$$T = \begin{bmatrix} \cos\phi & \sin\phi & 0 \\ -\sin\phi & \cos\phi & 0 \\ 0 & 0 & 1 \end{bmatrix} \begin{bmatrix} \cos\frac{\pi}{2}-\gamma & 0 & -\sin\frac{\pi}{2}-\gamma \\ 0 & 1 & 0 \\ \sin\frac{\pi}{2}-\gamma & 0 & \cos\frac{\pi}{2}-\gamma \end{bmatrix} \tag{3.7}$$

rewriting the cross-section in these terms we obtain:

$$S = \pi abc \sqrt{\frac{\cos^2\phi\sin^2\gamma}{a^2} + \frac{\sin^2\phi\sin^2\gamma}{b^2} + \frac{\cos^2\gamma}{c^2}} \tag{3.8}$$

As we change the rotation angle ϕ, so does the cross-section observed, thus we obtain a sinusoidal variation on the brightness, as seen in Fig. 3.3.

To complete this model, we must assume some light-scattering law for the asteroid surface. This feature is described in section 3.3.5.

3.3.2. Body representation: Non-convex shape

In order to generate more realistic simulations, with the aim of testing the *Gaia* inversion algorithm (that is described in chapter 4), the posibility of simulating the brightness of random non-convex shapes was included to the Poznań's *Gaia* simulator. The procedure used is as follows:

At first we introduce the main reference frame, defining a Cartesian coordinate system of axes with the origin located in an arbitrary point of a random initial body

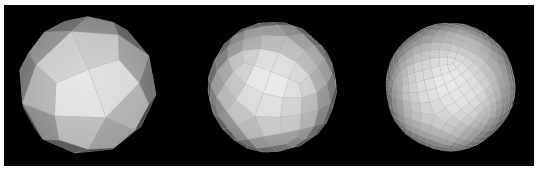

Figure 3.4: Example of the Catmull-Clark subdivision process.

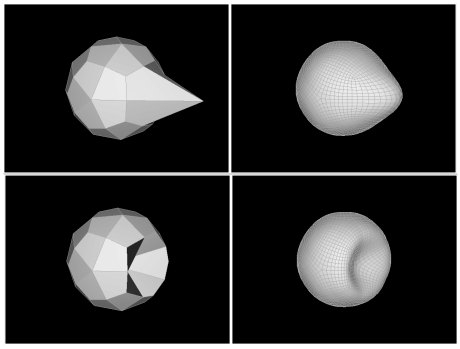

Figure 3.5: Example of local deformations without affecting the global shape of the body. Our genetic algorithm creates shape models like the ones on the left. The Catmull-Clark method is then applied and the resulting shape (on the right) is used to generate the synthetic photometry.

shape. This shape is described by a mesh consisting of 62 vertices. Then, using the Catmull-Clark method (Catmull & Clark, 1978), we obtain a mesh with a higher resolution which allow us to describe smoother shapes (Fig. 3.4). The method can be recursively applied to generate surfaces that approximate points lying-on a mesh of arbitrary topology. In each iteration, the method considers a standard bicubic B-spline patch on a rectangular control-point mesh. The shape of such a patch is regulated by 16 control-points. In subdividing this patch into 4 subpatches, 25 subcontrol points are generated.

One good reason for using this method (and not, for example, spherical harmonics) is that it gives freedom to create local deformations in the shape without having an impact on the rest of the body (an example can be seen in Fig. 3.5).

3.3.3. Center of mass, moments of inertia and the rotation matrix

In order to calculate the moments of inertia of the body, we use the formulae described by Dobrovolskis (1996). We assume that the body in question is homogeneous, with uniform density ρ and total mass $M = \rho V$. Then each simplex is also homogeneous, with mass $\Delta M = \rho \Delta V$. To find the center of mass $\boldsymbol{R}$ of the body as a whole, recall that its moment of mass $M\boldsymbol{R}$ is just the sum of the mass moments $\Delta M \; \Delta \; \boldsymbol{R}$ of all the simplices. Therefore, the centre of mass location is given by the vector $\boldsymbol{R}$

$$\boldsymbol{R} = \sum \frac{\Delta M \Delta \boldsymbol{R}}{M} = \sum \frac{\rho \Delta V \Delta \boldsymbol{R}}{\rho V} = \sum \frac{\Delta V \Delta \boldsymbol{R}}{V}, \tag{3.9}$$

and the origin of the system of axes can be translated to be coincident with the position of the centre of mass. The rotational inertia of a rigid body may be characterized by its inertia tensor

$$I_{j,k} = \begin{bmatrix} I_{x,x} & I_{x,y} & I_{x,z} \\ I_{x,y} & I_{y,y} & I_{y,z} \\ I_{x,z} & I_{y,z} & I_{z,z} \end{bmatrix}. \tag{3.10}$$

and in the given situation, $I_{j,k}$ is relative to the center of mass.

Then the main rotational moment of inertia of the body is calculated, and the main reference axes are redirected so the Z-axis coincides with the principal axis of rotation of the body. We will henceforth call this system the body frame and its axes X_B, Y_B and Z_B.

The attitude matrix is usually expressed in terms of the 3-1-3 set of the Euler angles: rotation angle ψ, nutation angle θ, and precession angle φ (Goldstein, 1980). Although the Euler angles are quite useful in describing rotation, they also possess serious drawbacks: they become undetermined for $\theta = 0$ or $\theta = \pi$, and the elements of the attitude matrix depend on trigonometric functions of the angles. The latter property implies that their use in numerical integration is rather costly. In these circumstances, we prefer to use the Euler parameters (Goldstein, 1980). Although the vector of the Euler parameters $\boldsymbol{q} = (q_0, q_1, q_2, q_3)^{\mathrm{T}}$ consists of four elements (one more variable, compared to the Euler angles), the elements $M_{i,j}$ of the attitude matrix are easily expressible in terms of $\boldsymbol{q}$

$$\begin{aligned}
M_{1,1} &= q_0^2 + q_1^2 - q_2^2 - q_3^2, \\
M_{1,2} &= 2\,(q_1\,q_2 + q_0\,q_3), \\
M_{1,3} &= -2\,(q_0\,q_2 - q_1\,q_3), \\
M_{2,1} &= 2\,(q_1\,q_2 - q_0\,q_3), \\
M_{2,2} &= q_0^2 - q_1^2 + q_2^2 - q_3^2, \\
M_{2,3} &= 2\,(q_2\,q_3 + q_0\,q_1), \\
M_{3,1} &= 2\,(q_1\,q_3 + q_0\,q_2), \\
M_{3,2} &= 2\,(q_2\,q_3 - q_0\,q_1), \\
M_{3,3} &= q_0^2 - q_1^2 - q_2^2 + q_3^2,
\end{aligned} \tag{3.11}$$

involving only products or squares.

The relation between the Euler angles and $\boldsymbol{q}$, often required in order to input the initial conditions, is

$$\begin{aligned}
q_0 &= \cos\tfrac{\theta}{2}\,\cos\tfrac{\varphi+\psi}{2}, \\
q_1 &= \sin\tfrac{\theta}{2}\,\cos\tfrac{\varphi-\psi}{2}, \\
q_2 &= \sin\tfrac{\theta}{2}\,\sin\tfrac{\varphi-\psi}{2}, \\
q_3 &= \cos\tfrac{\theta}{2}\,\sin\tfrac{\varphi+\psi}{2}.
\end{aligned} \tag{3.12}$$

When the body rotates, the Euler parameters change according to the differential

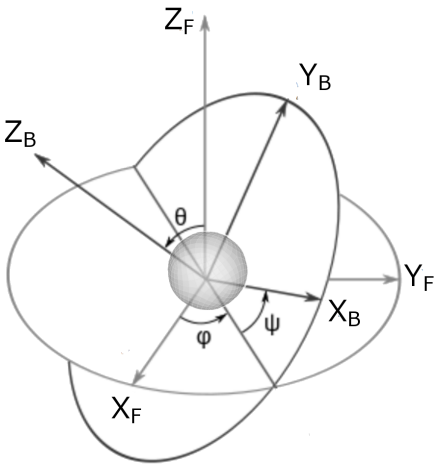

Figure 3.6: This scheme illustrates the Euler angles (ψ,θ,φ), relating the fixed frame (F) to the body frame (B).

equations

$$\dot{\boldsymbol{q}} = \frac{1}{2} \begin{pmatrix} -q_1 & -q_2 & -q_3 \\ q_0 & -q_3 & q_2 \\ q_3 & q_0 & -q_1 \\ -q_2 & q_1 & q_0 \end{pmatrix} \boldsymbol{\Omega}, \tag{3.13}$$

where $\boldsymbol{\Omega} = (\Omega_1, \Omega_2, \Omega_3)^{\mathrm{T}}$ is the angular rate vector in the body frame. Except for the components of $\boldsymbol{q}$, subscripts 1, 2, 3 refer to the axes X_B, Y_B, and Z_B respectively.

3.3.4. Generating synthetic lightcurves

In order to generate a synthetic picture of the body, we introduce a new Cartesian coordinate system of axes (X_F,Y_F,Z_F) that we call the fixed frame. This system of axes is related with the body frame using the attitude matrix described in the previous section (an illustration can be seen in Fig. 3.6).

The fixed frame is a heliocentric system, where we can define $\boldsymbol{S}_A$ and $\boldsymbol{S}_E$ as the vectors in a given moment of time towards the asteroid and *Gaia* respectively. Those vectors can be either calculated using Keplerian orbits and the analytical expressions described in Soma, Hirayama & Kinoshita (1988) or can be obtained by an ephemeris computation service such as Horizons[†].

Additionally, we make use of the body frame, to describe the body spin axis using angles ψ and θ, while we use φ to characterize the body rotation. We also define the vectors $\boldsymbol{A}_E$ and $\boldsymbol{A}_S$ as the vectors towards *Gaia* and the Sun from the body frame (i.e. the *Gaia* and Sun asterocentric positions), and its transformation to the fixed frame becomes straighforward using the $M_{i,j}$ attitude matrix:

$$\begin{aligned} \boldsymbol{A}_E &= M_{i,j} \boldsymbol{S}_E, \\ \boldsymbol{A}_S &= M_{i,j} \boldsymbol{S}_A. \end{aligned} \tag{3.14}$$

[†]http://ssd.jpl.nasa.gov/horizons.cgi

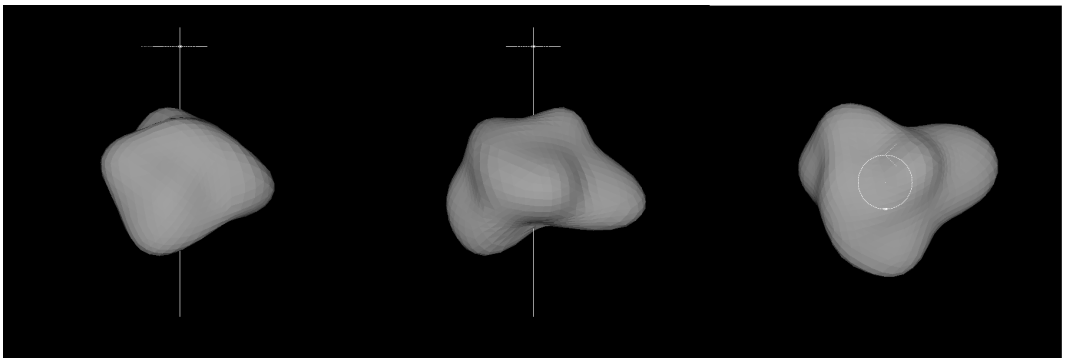

Figure 3.7: Different projections of a 3D shape for a random asteroid generated using spherical harmonics.

As a means to calculate the illumination of the body, we define a square Virtual CCD Frame with the dimensions $2\,rs \times 2\,rs$ (rs being the norm of the vector from the center of the body to the circumscribed circle over the projected shape of the body.). Each frame is divided into $N \times N$ pixels and its plane is perpendicular to the direction of $\boldsymbol{A}_S$ and placed in an infinite distance behind the body. Then we make use of a Z-Buffer standard graphic method described by Catmull (1974), projecting the body triangular mesh onto the Virtual Frame. For each pixel in the frame we allocate a buffer with an initial value defined at an infinite distance. Before storing the number of a projected triangle of the body mesh, the program checks the distance to the Virtual Frame. If the distance is smaller than the stored value, the new value is written. Once all the triangles are projected, we are able to determine which ones (and to what extent) are hidden by other triangles, or which are not illuminated.

Finally, to calculate the brightness as seen from the observer point of view, we make the plane perpendicular to $\boldsymbol{A}_E$ (*Gaia*-pointing vector). The above described Z-Buffer procedure is repeated, with the brightness being now stored in the Virtual Frame. When the procedure is done, the brightness of the body is computed by taking the sum of all stored values.

3.3.5. Light scattering properties

As all the *Gaia* observations of main belt objects are done in phase angles values between 10 and 30 degrees, the relation between the asteroid phase angle and its magnitude should be almost linear. For this reason, a geometric scattering law can be a reasonable first-order approximation of the phase-magnitude relation.

However, the Poznań *Gaia* simulator can easily incorporate more sophisticated scattering laws, as they are called as an external module during the brightness computation. Thus, when computing the brightness, we take into account the projective shadowing (in case of non-convex shapes or binary systems) and we can use linear combinations of different scattering laws, just defining the ratio between them (the most common combination used is 0.1 for the Lambert law and 0.9 for the Lommel-Seeliger law following Kaasalainen & Torppa, 2001).

An example of a simulation obtained with the Poznań *Gaia* simulator can be seen in Fig. 3.8, where each point represents a *Gaia* photometric measurement plotted against

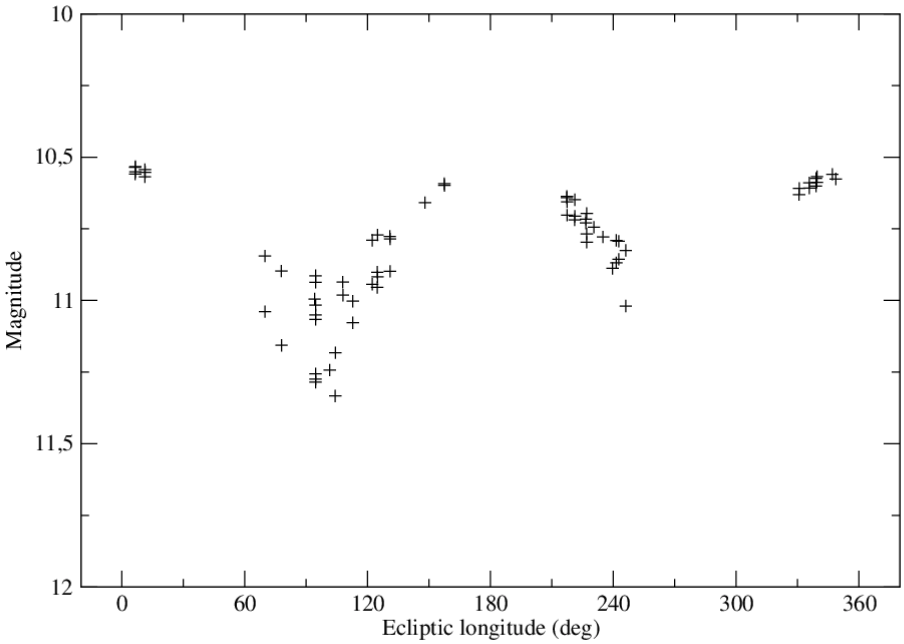

Figure 3.8: An example of the *Gaia* photometry generated with the simulator developed at the Poznań Observatory. The simulation shows the magnitude of the asteroid grouped at 4 different geometries. This is a standard feature of the *Gaia* observations for Main Belt objects, as each object will be observed at least during 4 apparitions for the 5 years *Gaia* operations.

the ecliptic longitude of the asteroid at the moment of its observation. The magnitude was generated using a triaxial ellipsoid model for a given pole orientation, rotation period and axes ratio, while the epochs were obtained with the *Gaia* transit predictor. The full simulation covers the expected five years of *Gaia* operations.

3.4. Simulations of the *Gaia* observations for binary asteroids

One particularly interesting case are the asteroids with satellites. Such systems are specially appreciated by the Solar System researchers as they give a unique opportunity to derive the mass of the components directly from the third Kepler's law. For this reason, they are invaluable targets for studies on internal structure and composition, and therefore it is crucial to develop techniques enabling to detect them among *Gaia* photometry.

We currently know more than a hundred of binary asteroids in the main-belt, and about three hundred in total adding binary NEAs and TNOs. The majority of them have been discovered by recording their mutual events in a classical dense lightcurve. Resolved observation such as the ones obtained from radar or adaptive optics have allowed to confirm or, in a few cases, discover such objects. The number of asteroids with known satellites it is expected to be increased significantly due to the huge amount of data expected from surveys like *Gaia*. To that end, it is necessary to develop automated strategies to find binary candidates in such large datasets. In that purpose, simulations of synchronous binary systems as observed by the *Gaia* photometer were generated with the Poznań *Gaia* simulator. In this section the methodology for conducting the simulations is presented, while the inversion results are analyzed in chapter 5.

3.4.1. Defining the two bodies

The two-body system consists of two independent components, each described by 62 vectors uniformly distributed in space and with a common origin (geometric centre of the body). These vectors define a mesh of 62 vertices called a generator shape. The directions of these vectors are fixed, while their lengths can be modified in order to deform the body. Once the generator shape is ready, the Catmull–Clark subdivision method is applied, following the same procedure described in section 3.3.2. The centre of mass is then calculated for each object, considering the components to be homogeneous with uniform density ρ and total mass $M = \rho V$. The rotational inertia of each component is characterized by its inertia tensor $I_{j,k}$, so the inertia tensor relative to the centre of mass of the system is used in order to find the system principal moments and axes. Finally, the main reference axes are redirected so the Z-axis coincides with the principal axis of rotation. We will henceforth call this system the body frame and its axes are X_B, Y_B and Z_B. An example of the described process can be seen for two different asteroid shapes in Fig. 3.9 and Fig. 3.10.

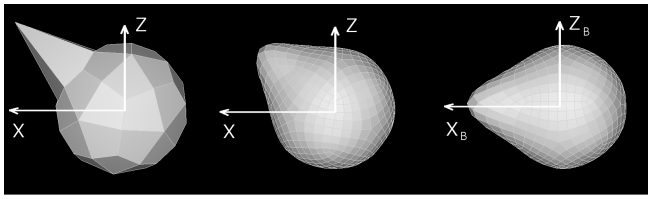

Figure 3.9: An example of the procedure followed by the algorithm to define each component. The first shape on the left is the generator shape, i.e. a starting mesh with 62 vertices. The one in the middle is the result of applying the Catmull–Clark subdivision method to the first shape. The last step is shown on the right, where the body is oriented so that the Z-axis coincides with the principal axis of rotation of the body and the origin of the body frame is translated to the position of the centre of mass.

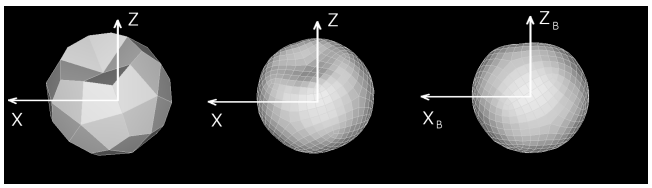

Figure 3.10: The same procedure described in Fig. 1 but for a body with a concavity.

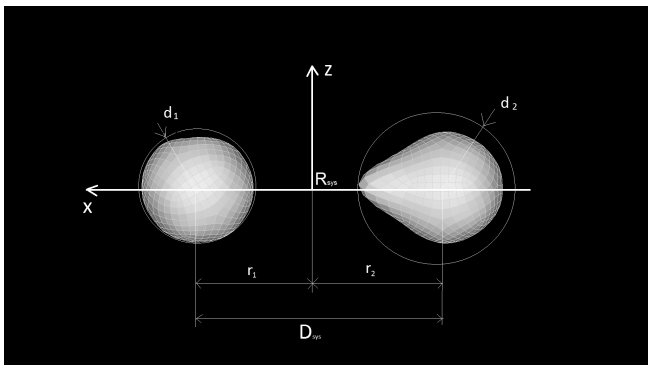

Figure 3.11: Representation of the resulting system configuration after following the described procedures. D_{sys} and d_1/d_2 are the parameters used to relate the two bodies during the minimization process, while $\boldsymbol{r}_1$ and $\boldsymbol{r}_2$ are the positions of the body centres of mass with respect to the system's centre of mass.

3.4.2. System reconstruction

We define a Cartesian coordinate system of axes, with the X-axis passing through the centre of mass of the two objects and coincident with the body frame X_B axis of each component. We can then place one object on the positive part of the X-axis and the other on the negative, where the origin of the system is the position of the centre of mass of the whole system ($\boldsymbol{R}_{\rm sys}$). Further, we define $D_{\rm sys}$ as the distance between the centres of mass of each asteroid ($\boldsymbol{r}_1, \boldsymbol{r}_2$) along the X-axis. For each component we also define d_1 and d_2 as the norms of the vectors from the centre of mass of the body to the circumscribed circle over the projected shape of the body, and d_1/d_2 describes the size ratio between the two components. A scheme of the defined binary system can be seen in Fig. 3.11.

These last values, $D_{\rm sys}$ and d_1/d_2, are used to define the relation between the two components. The system is supposed to be in relaxed state. In particular, we only consider the case of synchronous systems with circular orbits. Therefore, the parameters to describe the system include the following.

1. 62 vertex distances from the centre of the first body (generator shape 1).
2. 62 vertex distances from the centre of the second body (generator shape 2).
3. Distance between the centres of mass ($D_{\rm sys}$).
4. Size ratio between the two components (d_1/d_2).
5. Pole orientation (λ, β).

At this point, the centre of mass, moment of inertia and the rotation matrix are calculated following the formulae described in section 3.3.3. Once the system is build, the brightness can be generated with a visualization algorithm (such as Z-buffer) as described in section 3.3.5.

An example of the photometry generated with this method is shown in Fig. 3.12. The model used in this example corresponds to 90 Antiope, which is a synchronous binary with two components of almost the same size (i.e. size ratio between components close to 1). Moreover, both components are not especially elongated, and the system lightcurves present low amplitude when no mutual events can be observed. On the other hand, apparitions with mutual events, present a high-amplitude lightcurve with two sharp minima. In the *Gaia* simulation, these events are appearing as a drop in the photometric measurements. The impact of these drops on the inversion results is presented in chapter 5.

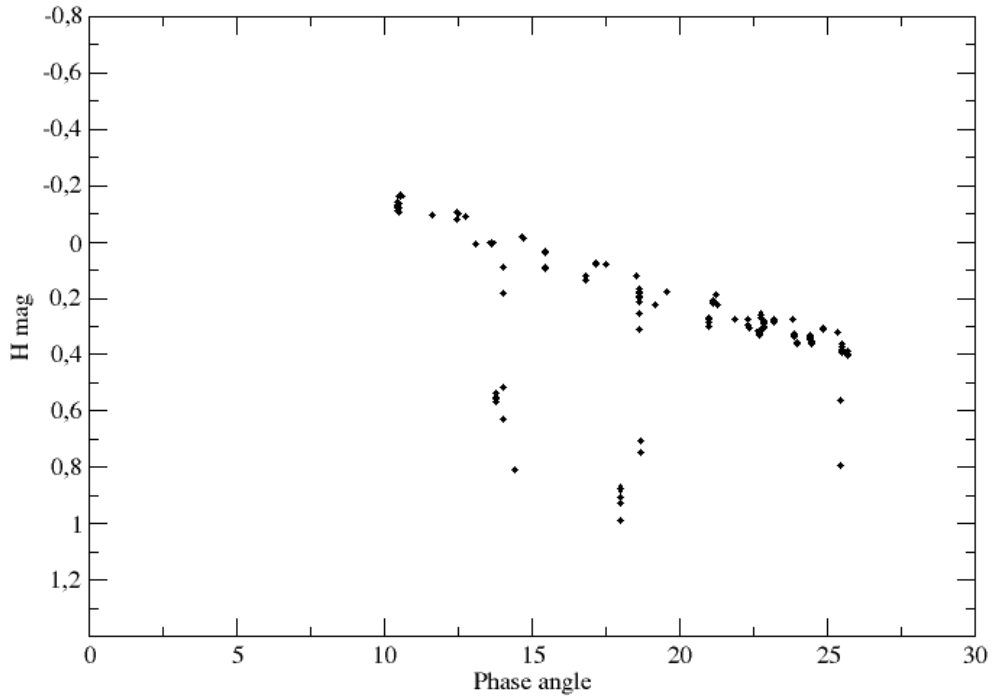

Figure 3.12: Simulation of the photometric measurements of a binary system generated with the Poznań's *Gaia* simulator. The figure shows the observed magnitude as a function of the asteroid's phase angle in degrees. In this case, the mutual events are clearly standing out the magnitude-phase linear relation.

Chapter 4

Inversion of *Gaia* photometry of single asteroids

4.1. Using Poznań simulator to test the *Gaia* inversion algorithm

Although several tests have been done so far for a few selected objects, with the purpose of validating the performance of the inversion code, the algorithm needed to pass through a systematic test covering all the range of possibilites that it will have to face. In particular, the inversion code was build under one main constraint: CPU efficiency to deal with the unprecedentedly great amount of asteroid photometry to be analysed. This forced the *Gaia* Solar System Group to find a compromise between the number of parameters used for solving the inversion problem, and the goodness of this solution. As a result, the solution implemented in the oficial *Gaia* data pipeline is a triaxial ellipsoid representation of the asteroid shape, that is able to give us an idea of the real body's shape with just 2 parameters (i.e. the size ratios between its axes). Moreover, *Gaia* is not going to observe Main Belt asteroids exactly during their opposition (as Main Belt asteroids will be the great majority of the asteroids observed by *Gaia*), but for a certain range of phase angles covering from 10 up to 30 degrees. The magnitude-phase angle relation becomes linear for such values, thus the *Gaia* inversion algorithm is not implementing any specific scattering law to describe the asteroid's reflection under different geometries, but just a linear coefficient that is proportional to the phase angle. The difference between using a scattering law or not is shown in Fig. 4.1, where the first situation corresponds to a simulation of a trixial ellipsoid shape without any scattering law, and the second corresponds to the same body generated with a diffusion law.

Such an approximation should be sufficient for the majority of cases, but it may also be the source of potential bias introduced by inversion failures under certain circumstances. This is a situation that deserves to be studied, as more than 90% of the results generated from the *Gaia* observations of asteroids, will be obtained for objects without any previously derived model. This huge amount of new information will include asteroid rotation periods, pole directions and shapes, and will boost up the asteroid statistics, which can allow us to more accurately reconstruct the formation process of certain asteroid families or even may give clues on the formation of the Solar System

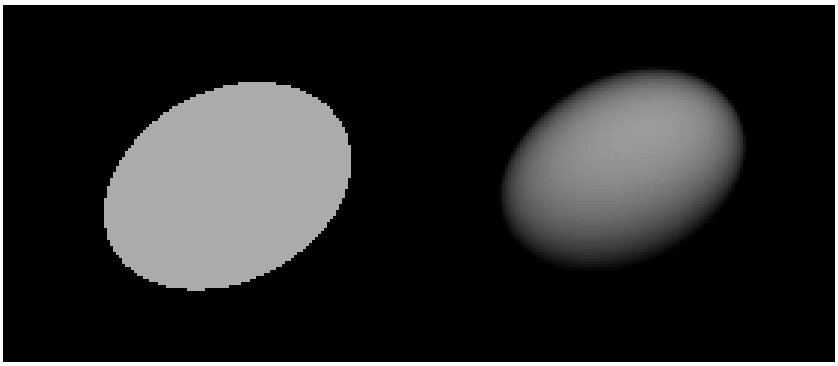

Figure 4.1: The same ellipsoid shapes one generated with a "geometric" scattering law (on the left, the white surface corresponds to the points that were illuminated and visible from the observer point of view), and the other using a diffusion law (on the right, the algorithm is not only checking which points are illuminated and visible, but is also introducing a diffusion function that depends on the dot product between the vector to the observer and the surface normal vector).

itself. But if this new scientific knowledge is systematically corrupted with wrong inversion results, the subsequent analysis may conduct to erroneous conclusions. Therefore the first main objective is to look for systematic problems in the results obtained with the inversion algorithm using realistic *Gaia* simulations. More specifically, we are interested in checking in which situations the assumptions discussed above for the asteroid shapes and its scattering properties, cannot be applied.

4.2. Control test with triaxial ellipsoids and "geometric" scattering law

The first test was performed to detect any systematic divergences between our simulated asteroid magnitudes and the magnitud generated by the *Gaia* inversion algorithm. Since the magnitude–phase relationship is essentially linear for the typical range of phase angles covered by *Gaia* (Zappalà et al. 1990), the inversion algorithm includes a linear parameter to describe this effect. Thus we have not implemented any light-scattering model in this case, but we have considered the geometrical phases (Lindegren 1977). For this test, we simulated *Gaia*-like observations for 10,359 triaxial ellipsoid shapes. This amount of objects is not a random choice, but is the result of generating a set of asteroids having their spin axis directions uniformly distributed. The procedure followed to generate such uniform distribution starts with defining an initial mesh, consisting of eight unit vectors with respect to a common origin, each of those being the vertex of a cube. Then we recursively subdivide the surface with the Catmull–Clark subdivision method (Catmull & Clark, 1978), which smooths the initial mesh surface by dividing the surface's polygons into smaller ones. After seven iterations we obtain a mesh with 10,359 vertices, each of those being the spin axis orientation of a given simulated asteroid.

In order to generate the observational epochs for each object, we have used the *Gaia* mission simulator developed by F. Mignard and P. Tanga at the Observatoire de la Côte

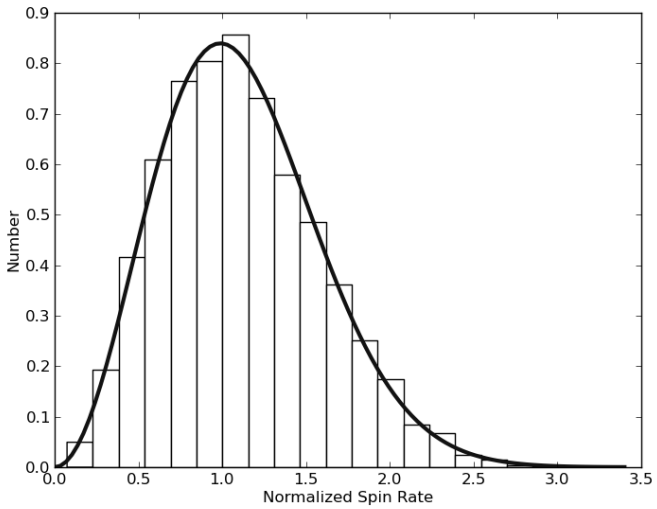

Figure 4.2: Histogram of $f/\langle f \rangle$ for the asteroid population generated for the purposes of this work. The geometric mean spin rate is $\langle f \rangle = 1.8\ d^{-1}$.

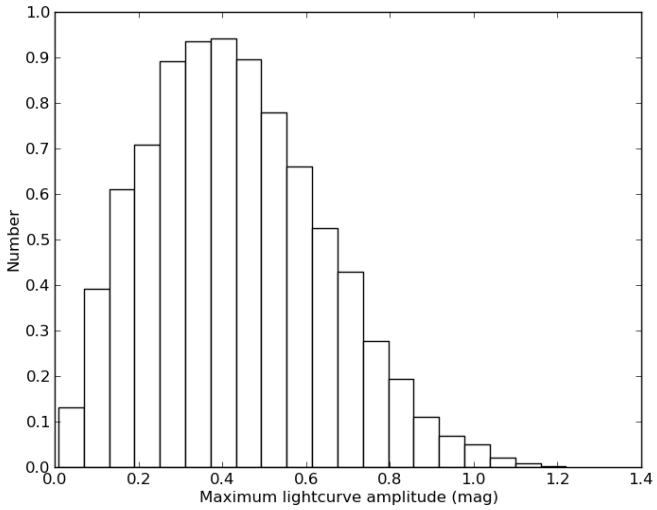

Figure 4.3: Histogram of maximum lightcurve amplitude distribution for the asteroid population generated in our simulations.

Figure 4.4: Image of the Poznań's cluster located in the Observatory of Astronomical Institute basement.

d'Azur (OCA), with a sample of asteroids having typical main-belt orbits. The period distribution within the population is shown in Fig. 4.2, and it was generated following a Maxwellian distribution like the one described in Pravec, Harris & Michałowski (2002). The disk-integrated photometry simulations have been generated using a Z-buffer standard graphic method described by Catmull (1974). Z-buffering works by testing pixel depth. The z-value of any new point to be written into the buffer is compared with the z-value of the point already there. If the new point is behind, it is discarded, whereas if it is in front, it replaces the old value. We note that simpler and more efficient methods exist to generate the brightness of a triaxial ellipsoid, but the main objective of this test was to ensure that the algorithm used to generate the photometric simulations for further tests with more elaborate shape representations was performing well and we were not adding any bias in our analysis. The resulting distribution of magnitudes (i.e. the maximum lightcurve amplitude for each asteroid) is shown in Fig. 4.3.

4.2.1. Test results overview: rotational period, spin axis orientation and overall shape

The inversion run was executed using the Poznań observatory cluster (Fig. 4.4) which consist of 27 workstations equipped with a six-core AMD processors (3 GHz), and the outcome was obtained after one full day of computations. In terms of pole determination, the results were positive, as the inversion algorithm found the correct pole (within 5 degrees of the true value) and shape (within 5 per cent of the true axis ratio) for more than 99 per cent of inversion runs. A few results presented an error in the pole determination, that increased as a function of the pole latitude. This situation can be interpreted as being caused by the double-pole ambiguity of derived spin states of asteroids orbiting close to the plane of the ecliptic. Thus this result is not an intrinsic problem of the method used, but a well-known limitation of the inversion techniques

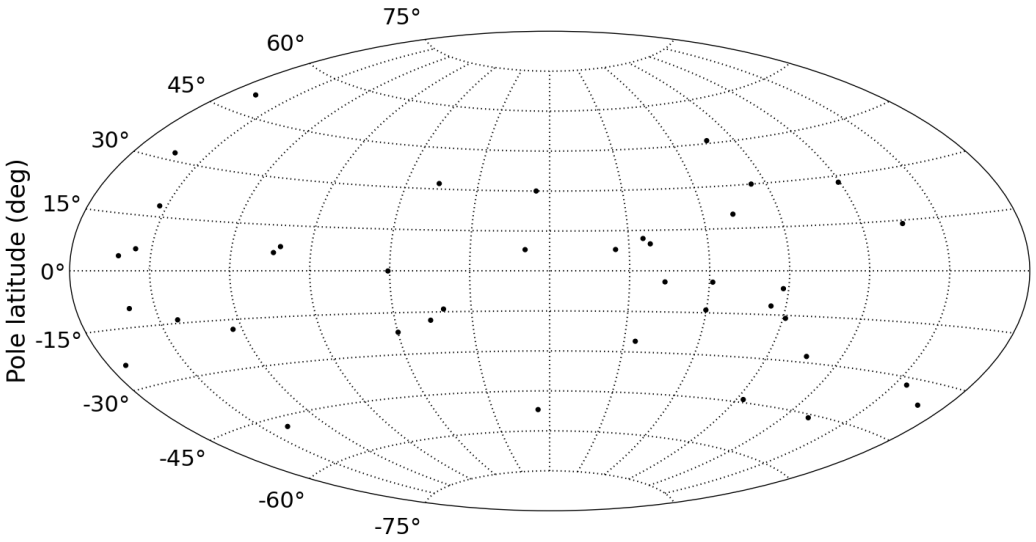

Figure 4.5: Result of the period determination. The black points represent the original pole orientation for the runs which period determination had an error greater than 0.01 per cent. The number of wrong period determination was less than 0.4 per cent of the 10,359 asteroids used in this test.

(Michałowski 1993).

The correct rotational period was also found for the majority of inversion attempts. In particular, for 10,319 of the 10,359 runs the correct value was found with an accuracy better than 0.01 per cent. The original orientation of the spin axis (ecliptic longitude λ and ecliptic latitude β) for the few attempts with a wrong period determination is shown in Fig. 4.5. The majority of the wrong solutions is confined to pole latitudes with $|\beta| <$ 30 degrees, and there was no wrong solution for pole latitudes higher than 60 degrees. As will be shown later, it is a standard behaviour of the method to better perform for asteroids having high pole latitudes. A similar behaviour has been found in the past for other inversion techniques (e.g. in Hanus et al. 2011). As for our case, this effect can be explained by understanding one of the major advantages (paradoxically) of *Gaia*' observations: its capability of seeing asteroids in a wide range of ecliptic longitudes in a *short* period of time (the operational mission phase is planned to last for five years). For instance, if we consider a main-belt asteroid having a pole with $\beta \sim 0$ degrees, the aspect angle (i.e. orientation of the object's spin axis with respect to the direction of sight of the observer) will be very low for two out of five apparitions observed by *Gaia* (see Fig. 4.6). For such apparitions the asteroid's lightcurve is presenting almost no amplitude, resulting in the loss of information about the spin period signal in the sparse-in-time measurements obtained under such circumstances. If the observational sequence for such kind of objects is unluckily distributed, and the majority of measurements are collected under such geometries, the period search would become very sensitive to any asymmetries in the lightcurve, arising for example from an irregular shape. This could cause the genetic algorithm to find alternative solutions, resulting in a warning flag (refusing to generate a solution) or, in the worst case, it could lead to a wrong

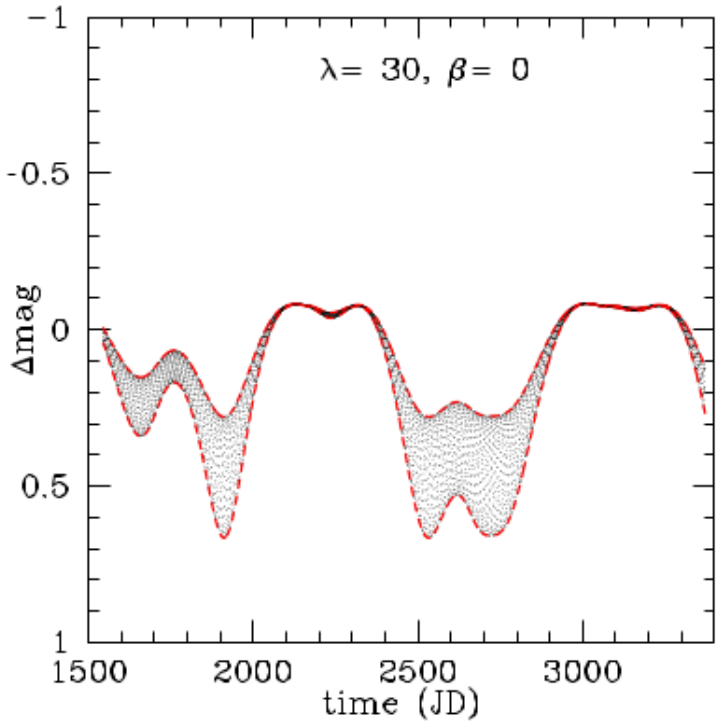

Figure 4.6: Absolute magnitude difference as a function of time, for a simulated object with pole orientation having $\lambda = 30$ degrees in ecliptic longitude and $\beta = 0$ degrees in ecliptic latitude, and for a given sidereal period and axial ratios (Cellino et al. 2006).

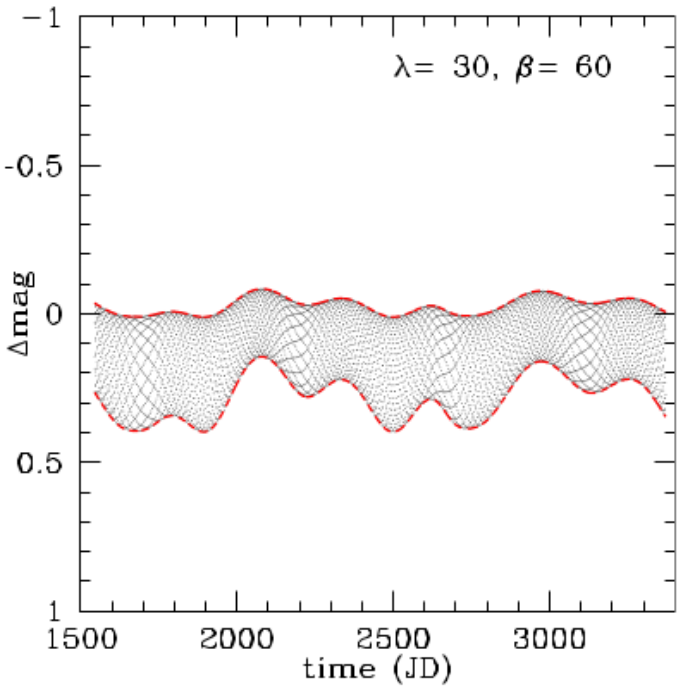

Figure 4.7: Absolute magnitude difference as a function of time, for a simulated object with pole orientation having $\lambda = 30$ degrees in ecliptic longitude and $\beta = 60$ degrees in ecliptic latitude, and for a given sidereal period and axial ratios (Cellino et al. 2006).

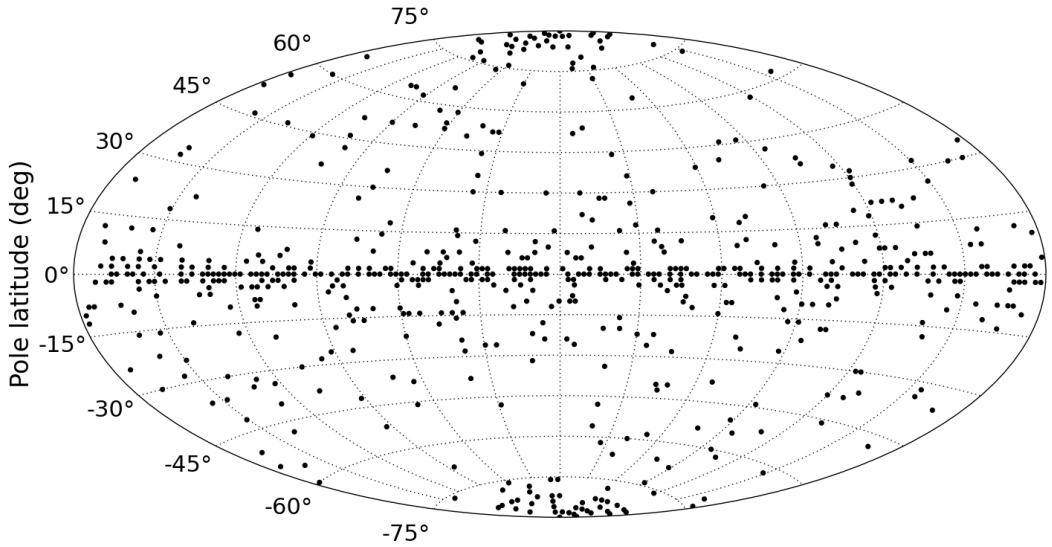

Figure 4.8: Distribution of *warnings* received from the inversion algorithm (see the text).

inversion solution. On the other hand, asteroids with high pole latitudes are always going to be observed under aspect angles far from zero (see Fig. 4.7), thus in such cases, each measurement is bearing valuable information about the spin period. This is because, in such geometries, the instigator of the main periodical signal will be the asteroid axis with the greatest angular momentum (thus the longest). Consequently, the lightcurve amplitude will be near its maximum value and the signals due to any shape irregularity would play a secondary role. Nevertheless, it should be highlighted that the effect of low pole latitude plays in opposite ways for pole determination than for spin period determination. In particular, asteroids having low pole latitudes are ideal for any inversion technique for deriving the pole, due to the high variation in lightcurve amplitude with different ecliptic longitudes.

Concerning other results, we also studied the ellipsoid axis ratio b/a which describes the elongation of the body. This parameter was found with an accuracy better than 5 per cent for more than the 98 per cent of inversion attempts. In this case, no correlation with the pole latitude can be observed. On the other hand, in the case of the c/a axis ratio determination, there is a clear relation between its error and the pole latitude. In particular, the c/a axis ratio was found with an accuracy better than 5 per cent for 95 per cent of the attempts, and almost the totality of the problematic cases – meaning solutions with an accuracy worse than 5 per cent – was found for asteroids with extreme values of $sin\beta$ ($\beta \sim 90$ degrees). This result is not surprising and can be easily explained in terms of observational geometry, as for objects having high pole latitudes and orbits close to the ecliptic, the observations bring no or little information on the c axis.

4.2.2. Results control system

Since *dense* lightcurves are only available for a small number of the asteroids observed by *Gaia*, we would not be able to infer if the inversion results are providing real information of the asteroid's physical parameters or, in contrast, they are the result of an inversion artefact. In order to tackle this problem, the inversion algorithm developed for the *Gaia* data analysis pipeline, is including a *warning* criterion to select the acceptable results. In particular, a *warning* flag will be generated for those cases where the best fit is close to the second-best one, but their inversion solution is substantially different. It is still under discussion if these solutions shall be included in the final catalogue marked with a flag or, instead, they shall remain unpublished. The distribution of such cases can be seen in Fig. 4.8. We received a total of 660 warnings, 59 per cent of them being from asteroids having a pole latitude between $-15 < \beta < 15$ degrees. This shall be taken into account when analysing the *Gaia* inversion statistics, as we expect it to show a lack of asteroids with low pole latitudes. Otherwise, one could tend to mislead this effect with some physical effects, such as non-gravitational forces.

4.2.3. Simulations contaminated with Gaussian noise

The good results obtained in the control test described above allow us to be confident with the methodology used, i.e. we are able to generate photometric simulations which are correctly inverted by the software algorithm that will be used for the analysis of *Gaia* asteroid photometry. However, we cannot expect the inversion of the real observations obtained by *Gaia* to have such a high reliability, as our simulations were generated under ideal assumptions (triaxial ellipsoid, geometric scattering law, no tumbling or binary asteroids, etc). Obviously this is not the situation we are going to face when analysing the *Gaia* photometry. *Gaia* photometric accuracy for each single transit will be of the order of 0.01 mag for objects as faint as $V = 18.5$ m. Thus in the majority of cases the method systematic errors (coming, for instance, from the ellipsoid shape approximation or the scattering law used) will be of greater concern than the errors arising from the photometric accuracy. Thus, we contaminated our photometric simulations with Gaussian noise with different values of σ, and we repeated the inversion process for each case. The results distribution is shown in Fig. 4.9, and two different biases can be observed: 1) population bias, 2) inversion reliability bias. The first one is connected with the warnings obtained from the results control system described above. The number of rejected solutions is not homogeneously distributed, as the majority of them are concentrated around the ecliptic plane (low pole latitudes). The second bias is affecting the reliability of the obtained results. For $\sigma \geq 0.03$ the results reliability is becoming proportional to the asteroid's pole latitude, being worse for the low pole latitudes. Worth noting that the inversion solutions studied are the ones accepted by the algorithm's warning system, thus the first and the second bias are superimposed. The reliability bias is increasing with the photometric noise, as can be seen in Fig. 4.10.

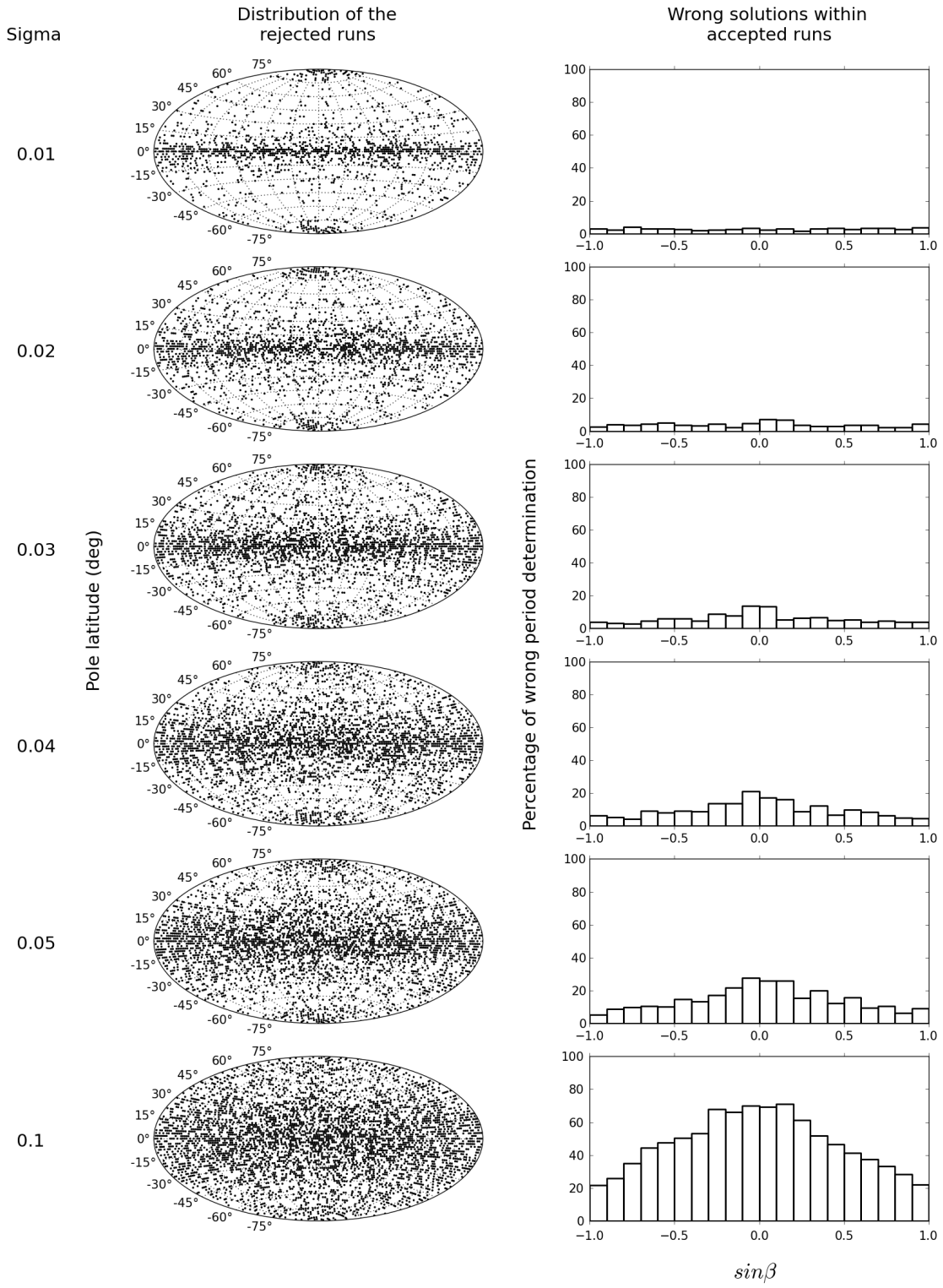

Figure 4.9: Distribution of the inversion results for each σ value for the noise. The projections on the left show the inversion runs for which the solution was not accepted by the algorithm. The histograms on the right show (in per cent) the distribution of the wrong solutions within the accepted runs as a function of the asteroids' initial pole latitude.

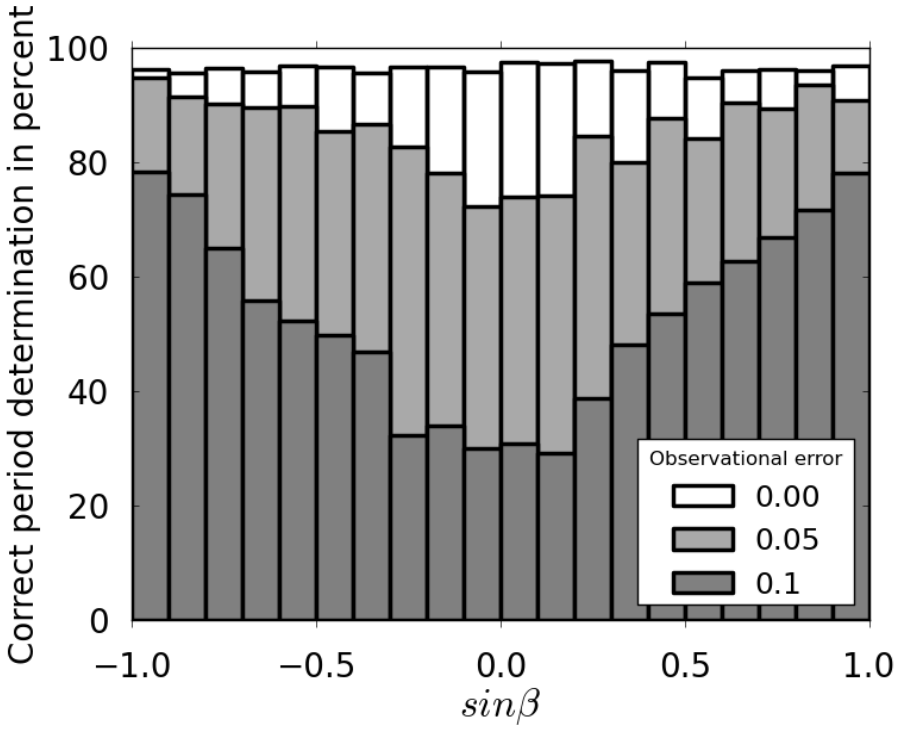

Figure 4.10: Correct period determination in percent versus asteroids' initial pole latitude for different values of the Gaussian noise added to the *Gaia* photometric simulations.

4.3. Realistic test using random non-convex shapes

Once we felt fully confident with our simulation–inversion procedure and after studying the methodological bias, we proceeded with a more demanding test. In order to recreate as close as possible the kind of data which will feed the *Gaia* inversion algorithm we generated a set of 10,359 random non-convex shapes using Gaussian spheres (Muinonen 1998). The spin axis and the rotational period for each object were chosen following the same manner as in the previous tests described above. Next we generated the brightness using the Z-buffer standard graphic method. This method is including the phase angle effects, but unlike the first tests with ellipsoids, this is also including the shadowing effects produced by the irregular surface structures. Consequently, the lightcurves generated by these non-convex shapes presented complex features such as multiple minima and maxima, which cannot be recreated with a simple ellipsoid model. Moreover, once the brightness was simulated, we contaminated the set with a Gaussian noise with $\sigma = 0.03$. As stated before, this is three times the photometric error expected for each single detection made by *Gaia*. But this might allow us to be on the safe side and would cover unexpected methodological errors, for instance, those connected with the scattering properties. Thus, the main question to be answered is whether the *Gaia* inversion algorithm will be able to deal with such complex scenario.

4.3.1. Results overview

The results of the aforementioned test occurred to be very optimistic: 65 per cent of the 10,359 modelled asteroids were accepted by the inversion software and the correct solution was found for 83 per cent of them, or to be more precise, 6,754 inversion results were obtained, from which 5,632 were correct and 1,122 incorrect. If we interpret this results in terms of the expected performance of the *Gaia* mission for Solar System objects, this would allow us to derive correct values for the poles, sidereal periods and axial ratios for several thousand asteroids. Nonetheless, we could find some correlations between the majority of wrong inversions and certain parameters, like the number of observations, the asteroid shape and the object spin axis. Understanding such dependencies would allow us to refuse some of the wrong results or even to correct them.

4.3.2. Influence of the number of measurements on the inversion results

It is of common sense to consider that the more data points the inversion attempt has the better the result will be. And this is, in fact, what our results are confirming. The histogram in Fig. 4.11 is showing the percentage of correct solutions found as a function of number of *Gaia* measurements and the asteroid pole latitude. The majority of regions having 70 measurements or more was found to be above the average of correct solutions. However, for lower regions, we found that the results are acceptable for asteroids having high pole latitudes, but worse than average for asteroids having low pole latitudes. The range of latitudes around zero for which the inversion is presenting a lower reliability is getting wider with decreasing number of measurements. Still, the good news is that, on average, main-belt asteroids will be detected on the *Gaia* focal

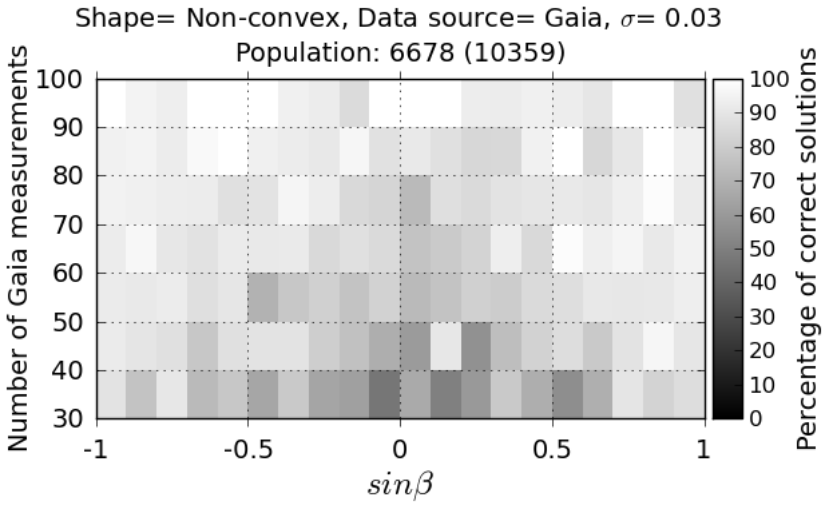

Figure 4.11: Histogram showing the results obtained for the inversion of the simulated set of irregular body shapes. The percentage of correct solutions is plotted as a function of the number of *Gaia* detections for each bin of asteroid's pole latitude. The population number is indicating the amount of obtained solutions and the total of inversion runs executed (in brackets).

plane for a number of times between 60 and 70 during the five-year operational lifetime of the mission (Mignard et al. 2007). Therefore the number of *problematic* asteroids for which *Gaia* photometric inversion might produce wrong solutions will represent a small part (although still several hundreds) of the hundreds of thousands of asteroids observed.

4.3.3. Influence of the asteroid shape on the inversion results

The *Gaia* inversion algorithm is assuming asteroids to have the shapes of triaxial ellipsoids. This approach was chosen mainly due to two reasons: 1) to minimize the CPU time required, 2) a need to produce an automated, standard procedure for working on large amount of data in unattended runs. Although this approximation could seem inaccurate at a first glance, the results are showing that, despite its simplicity, this approach is sufficient to fit the data in the majority of cases. But of course, the shape solution provided by the algorithm is only a first-order approximation of the asteroid's shape and might provide only a general idea of the body elongation.

In order to assess the goodness of the inversion solution we calculated the principal moment of inertia for each random shape, and we determined the triaxial ellipsoid with an equivalent moment of inertia. This operation enables us to obtain an indicator of the elongation of any irregular shape, as the asteroids have been simulated in a relaxed state (i.e. with the rotation axis coincident with its principal axis of rotation). Finally, we divided our set of random shapes into three groups, according to the value of the equivalent b/a axis ratio calculated. The results are presented in Fig. 4.12. As we could expect, the worst results are obtained for the quasi-spherical bodies, in particular for those having a low pole latitude. Such population is presenting the highest ratio of

wrong solutions (around 30 per cent on the average) but also each one out of two solutions is rejected with a warning flag. These results are in agreement with the first tests presented above and can be explained using the same scheme. It is worth pointing out that, by definition, an ideally spherical object cannot be inverted, since the magnitude becomes dependent on the phase angle only. When b/a ratio approaches 1, the lightcurve amplitude becomes very small, and the inversion algorithm will find a large number of equivalent solutions (in terms of residuals) characterized by a large variety of possible poles.

4.4. Distribution of the semi-axes ratios

In spite of its apparent simplicity, a triaxial ellipsoid model provides valuable information about the object's global shape. In addition, uncommon values of the semi-axes solution, such as extremely small ratios, might be a first alarm signal that the given object deserves a closer look. For these reasons, it is worth studying the distribution of the semi-axes of the inversion results presented above.

The histograms for the b/a ratio (Fig. 4.13) and c/a ratio (Fig. 4.16) shows the distribution of the semi-axes of the accepted inversion results (these without a warning flag). The worst results were found for asteroids with spheroidal shapes like the one shown in Fig. 4.14. Half of the population has their semi-major axis between $0.6 < b/a < 0.8$, and 92% has the semi-major axis between $0.4 < b/a < 0.9$. There is only 0.7% of solutions with $b/a < 0.4$. In fact, all of them occurred to be wrong inversion solutions, with an erroneous pole orientation. As explained above, this small fraction of wrong solutions cannot be avoided due to the nature of the genetic inversion algorithm. However, it worth noting that almost all these wrong solutions corresponds to asteroids with less than 50 photometric measurements.

A similar situation was found when analysing the results for the semi-minor axis distribution. As expected, the mean is shifted to a smaller value ($\mu = 0.57$), and 48% of results has the semi-minor axis between $0.5 < c/a < 0.7$, and 91% has the semi-minor axis between $0.3 < c/a < 0.8$. There is 1% of solutions with $c/a < 0.3$ from which 43% also have their semi-major axis smaller than $b/a < 0.4$ (see Fig. 4.15). These cigar-shape solutions are not physical, and are a clear indicator that the inversion has failed.

In order to see more clearly the relation between the semi-axes results, we can plot a 2D histogram for b/a versus c/a. The result is shown in Fig. 4.17, where the solid lines are delimiting the areas around the mean accounting for the 68.27% of the results (1σ), the 95.45% of the results (2σ) and the 99.7% of the results (3σ) respectively. If we consider the 2σ area, we can conclude that the great majority of the solutions are enclosed by $0.5 < b/a < 0.9$ and $0.4 < c/a < 0.8$. All the solutions beyond this area should be double-checked as they could correspond to an inversion failure or an interesting object (such as a binary asteroid, as shown in the next chapter).

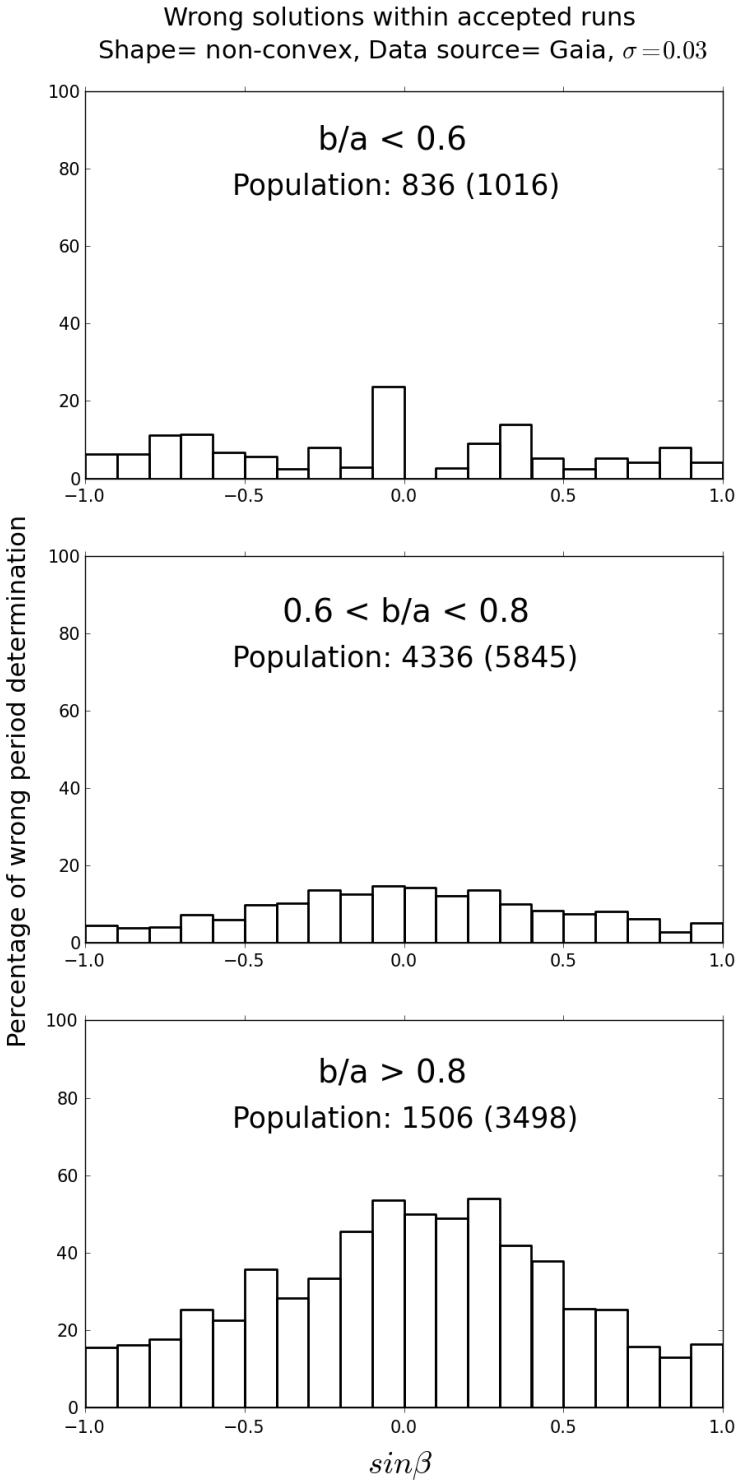

Figure 4.12: Histograms showing the inversion results obtained for three different groups of asteroids as a function of their equivalent b/a axis ratio (see text). The population numbers are indicating the amount of obtained solutions and the total of inversion runs executed (in brackets).

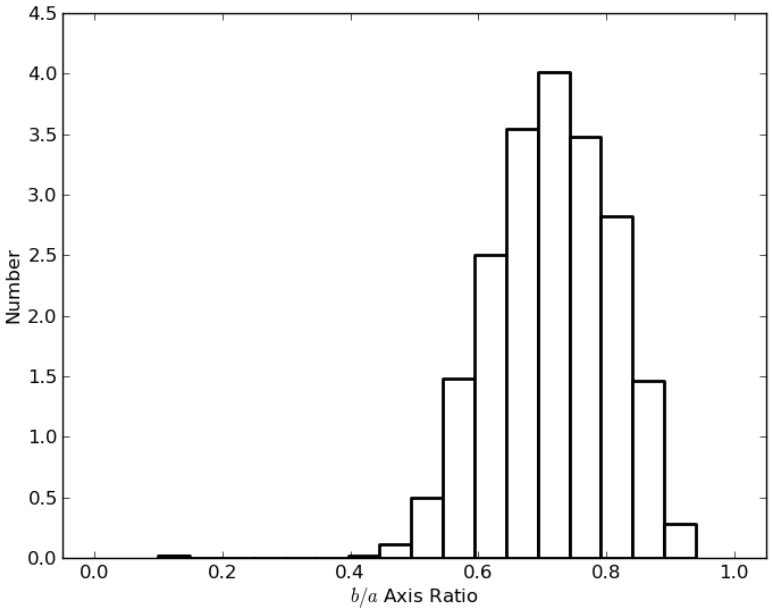

Figure 4.13: Histogram showing the distribution of the semi-major axis results for the accepted runs (these without a warning flag).

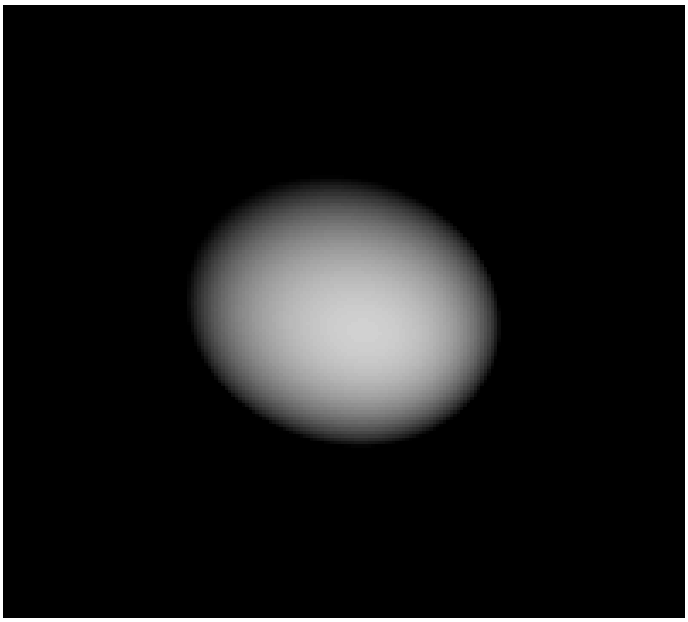

Figure 4.14: Example of a spheroidal-like shape with b/a=0.9 and c/a=0.8.

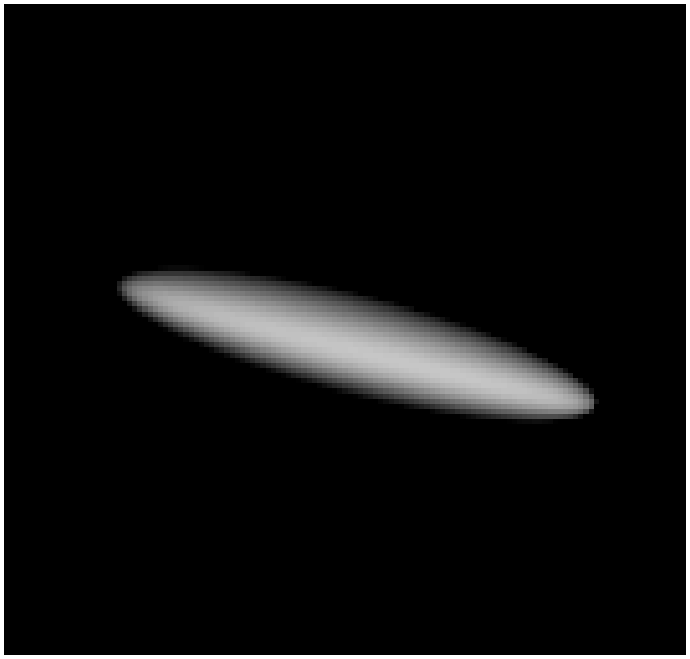

Figure 4.15: Example of a cigar-like shape with b/a=0.3 and c/a=0.2.

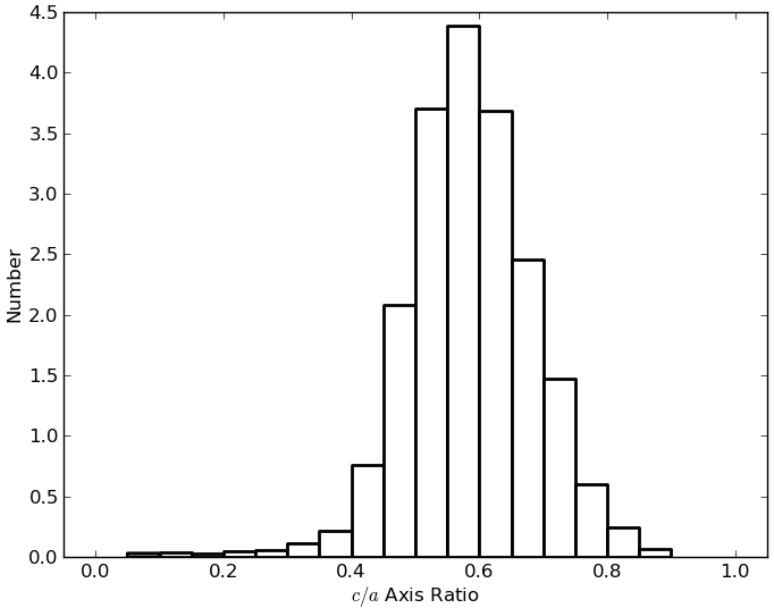

Figure 4.16: Histogram showing the distribution of the semi-minor axis results for the accepted runs (these without a warning flag).

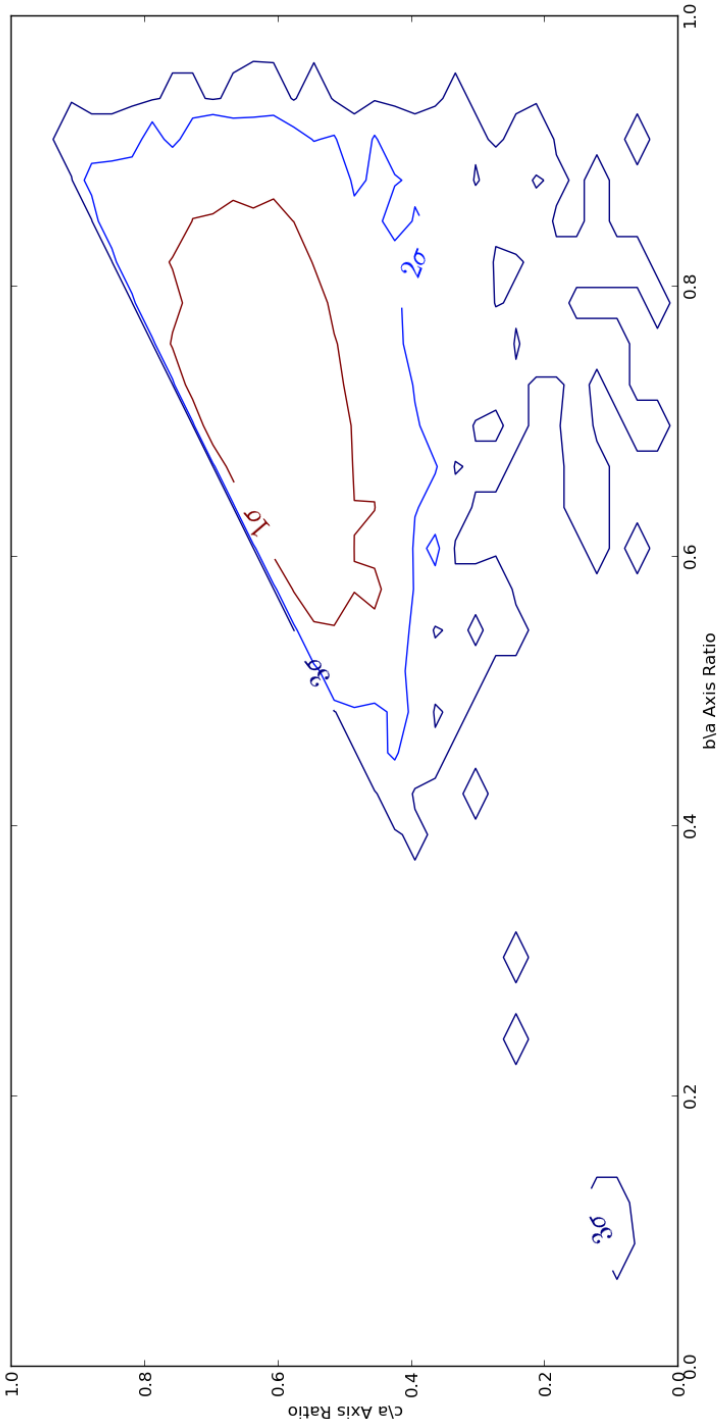

Figure 4.17: A 2D histogram showing the distribution of the semi-axes for the accepted runs (without a warning flag). See the text for the meaning of the σ boundaries.

4.5. Inversion test with real sparse-data

It is not planned to include the *Gaia* photometric measurements of asteroids until the fourth data release expected for 2019 (Prusti 2012). Thus in order to test the *Gaia* inversion algorithm beyond simulations, it is necessary to find other existing data sources. In this sense, sparse photometry of asteroids from a few sky surveys compiled in the Asteroids–Dynamic Site* (AstDyS) provides a good opportunity to practise with a dataset which is similar (to a certain degree) to the data expected from *Gaia*.

However, there are some issues that need to be clarified at this point before proceeding. While *Gaia* photometric accuracy for each single measurement is calculated to be between ∼0.01–0.03 mag, the accuracy of the the AstDyS dataset is 0.1 mag at best, depending on the observatory and the epoch, and in most cases magnitudes are given to one decimal place only. Moreover, each object's dataset has to be scrupulously purged, as it often containts clear outliers (e.g. Fig. 4.18). Another difference relies on the number of measurements. While the number of *Gaia* transits is not correlated with the object's brightness (∼70 transits per object on average), in the AstDyS dataset the quantity of points per object decreases the fainter the asteroid is. In addition, measurements are gathered with different filters and during a long time span (we used data from 1985 until 2015), which potentially implies instrumentation replacements and measurement calibrations beyond our reach.

In spite of all, and taking into account the data limitations previously stated, we used an upgraded version of the *Gaia* inversion algorithm to invert the AstDys sparse data of some selected targets. The program used was the last version of the *Gaia* inversion algorithm, which includes a Lommel-Seeliger light-scattering law (Cellino et al. 2015). For the simulations tests done so far, the light-scattering effects were not relevant for the goals of the study. However, this is not the case when applied to real photometric data, as the light-scattering properties play a role in the results, and therefore they need to be considered in the inversion process.

4.5.1. Data mining of the Asteroids-Dynamic Site

The AstDyS is a service mainly focused on providing multiopposition astrometric information of asteroids, including orbital elements, proper elements and ephemerides. However, some of the observations also contain a photometric measurement as a by-product of the survey operations. In practice this means that, for our purposes, some data mining of the site is required to prepare a dataset ready to be inverted. The steps followed by a script prepared for this aim are described below.

At first, we decided to gather the measurements only from observatories numbered 689, 703 and 950, as they have the lowest observational errors (see Hanus et al. 2011). Then, for a given asteroid, the code extracts the observation epochs which contain photometric measurements in a given filter band.

Next, the code extracts the asteroid's Heliocentric ($\boldsymbol{r_E}$) and Geocentric ($\boldsymbol{r_S}$) carte-

*http://hamilton.dm.unipi.it/astdys

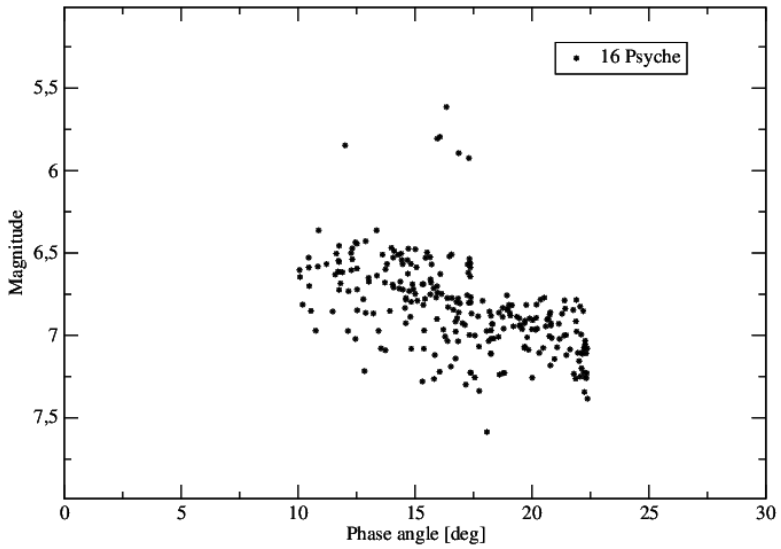

Figure 4.18: Sparse photometry of 16 Psyche against phase angle. A group of points are outlying the magnitude-phase relation. The data was gathered at the 689 U.S. Naval Observatory from 1985 until 2015.

sian coordinates with an automatic query to the Horizons service[†]. However, the *Gaia* inversion algorithms requires the Heliocentric and Geocentric longitude and latitude of the asteroid, which can be calculated following equations 4.1 and 4.2, respectively:

$$\lambda_S = \arctan\left(\frac{y_S}{x_S}\right), \quad \beta_S = \arcsin\left(\frac{z_S}{r_S}\right) \tag{4.1}$$

$$\lambda_E = \arctan\left(\frac{y_E}{x_E}\right), \quad \beta_E = \arcsin\left(\frac{z_E}{r_E}\right) \tag{4.2}$$

Where

$$r_E = \sqrt{\boldsymbol{x}_E^2 + \boldsymbol{y}_E^2 + \boldsymbol{z}_E^2} \tag{4.3}$$

$$r_S = \sqrt{\boldsymbol{x}_S^2 + \boldsymbol{y}_S^2 + \boldsymbol{z}_S^2} \tag{4.4}$$

The last input requirement for the inversion code is the phase angle calculated for each epoch, which is given by equation 4.5

[†]http://ssd.jpl.nasa.gov

$$\alpha = \arccos\left(\frac{\boldsymbol{r}_E \cdot \boldsymbol{r}_S}{r_E r_S}\right) \tag{4.5}$$

Where $\boldsymbol{r}_E \cdot \boldsymbol{r}_S$ is the vector's dot product

$$\boldsymbol{r}_E \cdot \boldsymbol{r}_S = x_S x_E + y_S y_E + z_S z_E \tag{4.6}$$

The photometry published at the AstDyS corresponds to the apparent magnitude of the object at a given epoch. The *Gaia* algorithm was developed to deal with *Gaia* magnitudes, which are not dependent on the asteroid's distance. Thus the code also reduces the asteroid's apparent magnitude to absolute magnitude using equation 4.7

$$H = m - 5log(r_E r_S) \tag{4.7}$$

Where m is the apparent magnitude and H the absolute magnitude.

Finally, the light-time correction needs to be applied to the AstDyS epoch, for which we can use equation 4.8

$$JD_{LT} = JD - 0.005778 r_E \tag{4.8}$$

From the resulting dataset, the code selects all the observations gathered at a phase angle $\alpha > 10$ deg. As previously explained, due to its particular scanning law, *Gaia* will avoid observations close to the asteroid's opposition (see Fig. 2.3). For this reason, the so called opposition effect (the asteroid's brightness boost due to coherent backscattering) is not considered in the inversion algorithm. As a result, only observations collected in the linear part of the magnitude-phase relation should be considered. Otherwise, this would have a direct effect on the inversion process, in particular on the semi-axes determination.

4.5.2. Inversion results

The procedure described above was used to extract observations for the 60 first single asteroids with known inversion solution, and in particular, the DAMIT[‡] list of asteroids was followed. The results obtained are summarized in Table 4.1.

[‡]http://astro.troja.mff.cuni.cz/projects/asteroids3D/

Table 4.1: Results of the inversion of the AstDyS sparse photometry for a set of single asteroids. The results in bold are in agreement with the values in the bibliography given on the right, while the results in italics are in disagreement. The 180 degree ambiguity in the pole ecliptic longitud is taken into account when comparing the results.

Asteroid	λ [°]	β [°]	b/a	c/a	**Period** $[h]$	**Obs**	N_{obs}	**Reference**	λ_R [°]	β_R [°]	Period_R $[h]$
3 Juno	*126*	*50*	0.80	0.69	*9.571881*	689	221	Kaasalainen et al. (2002a)	35	-12	7.81323
5 Astraea	**110**	**52**	0.71	0.54	**16.800705**	689	207	Ďurech et al. (2009)	126	40	16.80061
6 Hebe	*291*	**42**	0.70	0.67	*9.588475*	689	236	Hanuš et al. (2013b)	340	42	7.274471
7 Iris	**194**	**12**	0.74	0.53	**7.138837**	689	254	Kaasalainen et al. (2002a)	196	2	7.138843
8 Flora	*92*	*83*	0.85	0.19	*15.957595*	689	241	Torppa et al. (2003)	155	6	12.86667
9 Metis	**354**	**25**	0.75	0.50	**5.079175**	689	263	Torppa et al. (2003)	180	22	5.079176
10 Hygiea	**133**	**-56**	0.73	0.73	**27.658828**	689	205	Ďurech et al. (2011)	122	-44	27.65905
11 Parthenope	**120**	*71*	0.89	0.45	*15.948561*	689	268	Hanuš et al. (2013a)	129	14	13.72205
13 Egeria	**36**	**27**	0.79	0.73	*6.141342*	689	341	Hanuš et al. (2011)	44	21	7.046671
14 Irene	*308*	*66*	0.77	0.26	*11.963247*	689	223	Hanuš et al. (2011)	95	-11	15.02986
15 Eunomia	*248*	*86*	0.66	0.37	*5.397346*	689	300	Kaasalainen et al. (2002a)	3	-67	6.082753
16 Psyche	**202**	*81*	0.82	0.15	*8.392789*	689	235	Kaasalainen et al. (2002a)	32	-7	4.195948
17 Thetis	**239**	**6**	0.68	0.56	**12.266034**	689	355	Ďurech et al. (2009)	236	19	12.26603
19 Fortuna	*357*	*84*	0.79	0.23	*8.812542*	689	314	Torppa et al. (2003)	98	57	7.443224
20 Massalia	*133*	*54*	0.76	0.76	*25.068970*	689	268	Kaasalainen et al. (2002a)	179	39	8.09902
21 Lutetia	**40**	*56*	0.79	0.53	*15.938479*	689	230	Torppa et al. (2003)	54	-7	8.168269
23 Thalia	**158**	*78*	0.84	0.49	*23.907300*	689	210	Torppa et al. (2003)	159	-45	12.31241
25 Phocaea	*5*	*54*	0.78	0.57	*4.874214*	689	292	Hanuš et al. (2013a)	347	10	9.935397
27 Euterpe	**61**	*80*	0.85	0.19	*16.026684*	689	213	Stephens et al. (2012)	258	-42	10.40828
28 Bellona	**282**	**-17**	0.73	0.60	*23.397361*	689	198	Ďurech et al. (2011)	102	-8	15.70785
29 Amphitrite	**146**	*0*	0.78	0.72	*1.367642*	689	215	Kaasalainen et al. (2002a)	138	-21	5.390119
30 Urania	**284**	*49*	0.77	0.45	*10.645690*	689	193	Ďurech et al. (2009)	284	20	13.68717
32 Pomona	*244*	*78*	0.58	0.45	*11.965098*	689	199	Kaasalainen et al. (2002a)	267	58	9.44767
34 Circe	**262**	**65**	0.84	0.75	*9.441435*	689	155	Ďurech et al. (2009)	275	51	12.17458
37 Fides	*138*	*48*	0.81	0.81	*5.317128*	689	233	Hanuš et al. (2011)	270	19	7.332527

Continued on next page

Table 4.1 – continued from previous page

Asteroid	λ [°]	β [°]	b/a	c/a	**Period** [h]	**Obs**	N_{obs}	**Reference**	λ_R [°]	β_R [°]	Period$_R$ [h]
38 Leda	**166**	**-25**	0.74	0.56	*7.965336*	689	157	Franco et al. (2013)	161	-15	12.83612
39 Laetitia	**323**	**21**	0.62	0.41	**5.138246**	689	285	Kaasalainen et al. (2002a)	323	32	5.138238
40 Harmonia	**17**	**44**	0.76	0.59	*14.191439*	689	261	Hanuš et al. (2011)	22	31	8.908483
41 Daphne*	*34*	*53*	0.71	0.52	*3.990310*	689	285	Kaasalainen et al. (2002b)	198	-32	5.98798
42 Isis	**102**	**52**	0.75	0.63	**13.583584**	689	277	Hanuš et al. (2011)	106	40	13.58364
43 Ariadne	**253**	**-26**	0.44	0.35	**5.761990**	689	222	Kaasalainen et al. (2002a)	253	-15	5.761990
44 Nysa	**107**	**50**	0.63	0.54	**6.421417**	689	238	Kaasalainen et al. (2002b)	99	58	6.421417
45 Eugenia*	**304**	*2*	0.70	0.49	*6.469654*	689	360	Hanuš et al. (2013b)	124	-33	5.699152
52 Europa	*275*	*83*	0.80	0.21	*7.976632*	689	270	Michałowski et al. (2004a)	254	37	5.629962
54 Alexandra	**326**	**19**	0.73	0.71	*9.938751*	689	227	Warner et al. (2008b)	156	13	7.022641
55 Pandora	*33*	*42*	0.67	0.45	*15.946901*	689	119	Torppa et al. (2003)	223	18	4.804043
62 Erato	**92**	**28**	0.74	0.67	**9.218164**	689	138	Hanuš et al. (2011)	87	22	9.21819
63 Ausonia	**300**	*36*	0.41	0.32	**9.297583**	689	207	Torppa et al. (2003)	120	-15	9.29759
64 Angelina	**310**	*75*	0.83	0.20	*18.910090*	689	280	Ďurech et al. (2011)	317	17	8.75032
68 Leto	*341*	*85*	0.83	0.21	*6.837900*	689	180	Ďurech et al. (2011)	103	43	14.84547
69 Hesperia	*171*	*86*	0.81	0.24	*23.928494*	689	229	Hanuš et al. (2011)	250	17	5.655340
72 Feronia	**274**	**-50**	0.75	0.61	**8.090670**	689	188	Hanuš et al. (2013a)	102	-55	8.09068
73 Klytia	*330*	**79**	0.74	0.33	*10.014906*	689	117	Marciniak et al. (2008)	266	68	8.28307
76 Freia	**145**	**30**	0.76	0.55	*26.660772*	689	122	Marciniak et al. (2012)	140	14	9.97306
79 Eurynome	**63**	**39**	0.83	0.66	*15.993495*	689	226	Hanuš et al. (2013a)	228	30	5.977722
80 Sappho	**18**	**-24**	0.67	0.56	**14.030846**	689	343	Ďurech et al. (2009)	194	-26	14.03087
82 Alkmen	**177**	*53*	0.70	0.16	**13.000712**	689	146	Ďurech et al. (2009)	164	-28	13.00079
85 Io	*135*	*21*	0.83	0.74	**6.874811**	689	295	Ďurech et al. (2011)	95	-65	6.874783
87 Sylvia*	**66**	**61**	0.64	0.56	**5.183648**	689	243	Kaasalainen et al. (2002a)	71	66	5.18364
88 Thisbe	**279**	**54**	0.80	0.80	*23.946055*	689	308	Torppa et al. (2003)	72	60	6.04131
89 Julia	*208*	*70*	0.84	0.24	*15.938998*	689	379	Ďurech et al. (2011)	8	-13	11.38834
93 Minerva*	*2*	*57*	0.80	0.37	*7.971605*	689	139	Marchis et al. (2013)	21	21	5.981767
94 Aurora	**51**	*77*	0.77	0.32	*2.279887*	689	264	Marciniak et al. (2011)	58	16	7.226191
95 Arethusa	**155**	*66*	0.63	0.15	**8.702312**	689	150	Ďurech et al. (2011)	149	33	8.70221
97 Klotho	*155*	*58*	0.81	0.44	*18.118041*	689	306	Hanuš et al. (2011)	359	30	35.2510
107 Camilla*	**71**	**61**	0.63	0.35	*9.808441*	689	268	Torppa et al. (2003)	73	54	4.843928

Continued on next page

Table 4.1 – continued from previous page

Asteroid	λ [°]	β [°]	b/a	c/a	**Period** $[h]$	**Obs**	N_{obs}	**Reference**	λ_R [°]	β_R [°]	Period_R $[h]$
110 Lydia	**343**	*87*	0.86	0.15	**10.925814**	689	163	Ďurech et al. (2007)	331	-61	10.92580
115 Thyra	*320*	*89*	0.83	0.49	*23.911656*	689	242	Michałowski et al. (2004a)	35	33	7.23996
119 Althaea	**179**	**-65**	0.69	0.47	**11.465151**	689	147	Hanuš et al. (2011)	181	-61	11.46514

* Asteroid with at least one known small satellite ($d_s/d_p < 0.1$) which photometric signal can be neglected considering the accuracy of the disk-integrated measurements used.

The results are rather poor, as expected for a dataset with such low quality. Nevertheless, while it would be risky to make any conclusions about the physical properties obtained for a given asteroid, this experiment allows us to check to what extent do the results obtained with the Poznań's simulator fit the real data. In Fig. 4.19 the semi-axes results for the AstDyS asteroids are projected to the 2D histogram obtained by means of simulations. The AstDyS results are divided into solutions with correct pole solution (assuming the DAMIT values as correct, and accepting those solutions which differ less than 10 degrees in solid angle) and solution with wrong pole solution. The fit between both experiments is remarkable, as the majority of the correct solutions are fitted in the 2σ area, while the wrong pole solutions are spread along the 3σ area with large b/a ratios but with small c/a ratios. This is confirming that the genetic inversion algorithm tends to deform the body into cigar-shaped solutions when it fails to find the correct pole solution (and in particular, when the pole latitude is wrong).

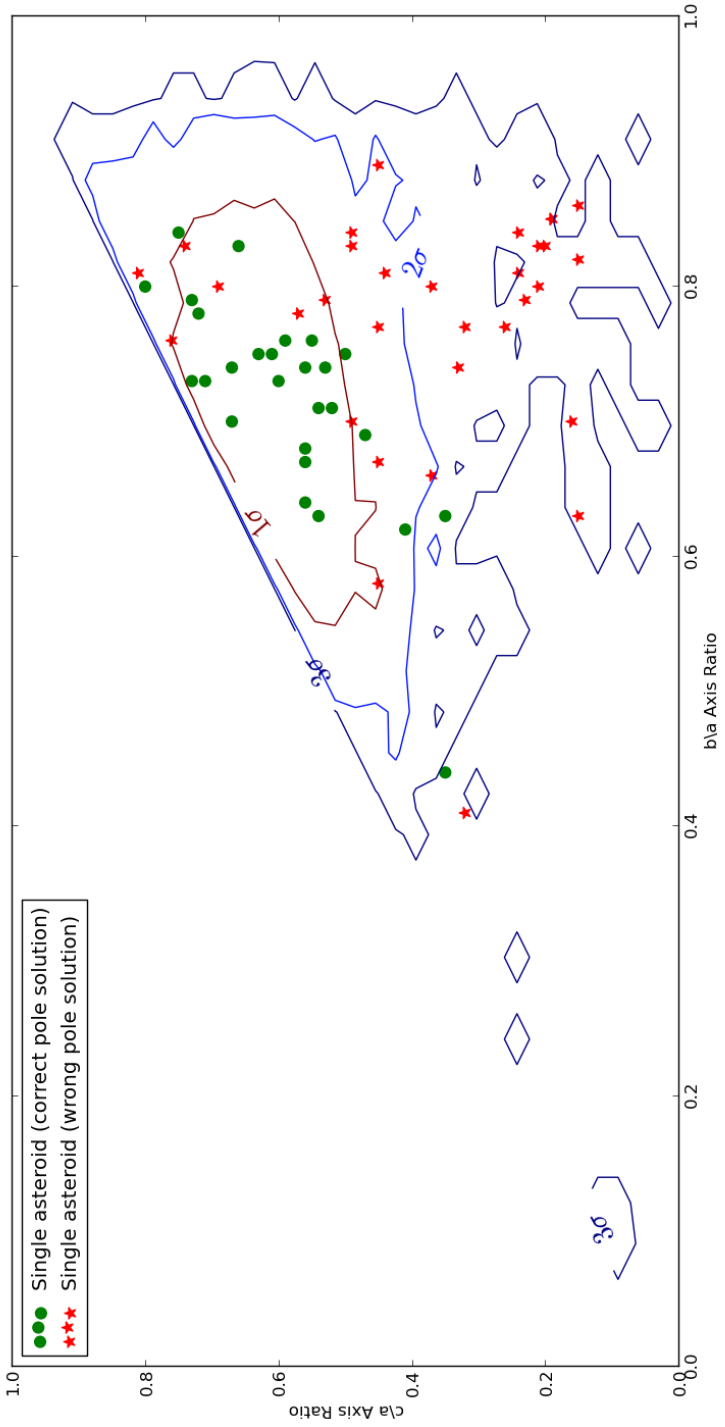

Figure 4.19: Same histogram as Fig. 4.17 with the projection of the semi-axes results obtained using real AstDyS sparse data. The results are divided into correct pole solutions and wrong pole solutions, assuming the DAMIT solutions as correct. See text for the meaning of the σ boundaries.

Chapter 5

Inversion of *Gaia* photometry of binary asteroids

As previously stated, *Gaia* is going to generate an unprecedently huge quantity of asteroid data, of the order of dozens of milions of measurements. As a consequence, all the processes conected with the data treatment and its analysis must be totally automatic. If we want to discover interesting objects among all this data, at first we need to know what kind of objects we are looking for, and even more importantly, what impact might this asteroid's peculiarity have on the *Gaia* photometry. One particularly interesting case constitute the asteroids with satellites. Such systems are especially appreciated by astronomers as they give an unique opportunity to derive mass of the components directly from the third Kepler law. We currently know about one hundred binary asteroids in the main belt (compiled by R. Johnston on his site*), and more than two hundred in total adding NEAs and TNOs. The majority of them have been discovered by recording their mutual events in a classical full-lightcurve observation. In other words, without any previous knowledge of the asteroid, discovering such meaningful objects is practically a matter of luck. For that reason, a main objective of this work is to study the impact of such systems to the *Gaia* photometric measurements of asteroids and to point out strategies to detect them.

The Poznan photometric team is leading the research of binary systems modelling, and during the last years it has produced several publications, particularly focused on synchronous binary systems (e.g. Michałowski et al. 2002, Michałowski et al. 2004 and Kryszczyńska et al. 2009). Recently we have developed a new algorithm capable to generate model solutions for binary asteroids using a nonconvex shape representation of the components (Bartczak, Michałowski, Santana-Ros et al., 2014). As the model is able to reproduce body concavities, the relative volume obtained for the components is more accurate than for the previous models, which were based in Roche elipsoids (Descamps et al. 2009), having a direct impact on the density calculation. Taking profit of all this experience on binary systems modeling, we have developed a different version of the *Gaia* simulator able to generate photometry for binary asteroids. Each component is described following the same procedure used for a single body, but the algorithm is also taking into consideration the size ratio between the two bodies and, consequently, the distance stability considering that the two bodies have the same

*www.johnstonsarchive.net/astro/asteroidmoons.html

composition, therefore the same density.

As shown in chapter 3, the are some cases for which we already know that it will be possible to detect the system mutual events. However, it would be not feasible to check each observation one by one, thus it is necessary to develop mathematical technics to automatically detect such potential binary objects among the 300.000 observed asteroids.

The following sections describe the *Gaia* photometric simulations of binary asteroids generated with the Poznań simulator, as well as the results obtained with the *Gaia* inversion algorithm. The inversion results are then analysed with the aim of detecting the differences between single and binary populations. Similarly to the previous chapter, the inversion results for simulations are cross-checked against the results obtained from the inversion of AstDyS real data for selected binary asteroids.

5.1. A modified version of the Poznań simulator for binary asteroids

The simulations were performed using a modified version of the Poznań simulator described in previous chapter. In particular, the same number of asteroids was generated (10.359) and their spin axis directions were uniformly distributed following the same procedure as described above. The orbits and, consequently, the transit epochs were considered to be the same as for the single cases. However, the rotation period distribution used in the single asteroid case would not be realistic for the binary population. Thus the rotation period population was created using a pseudorandom generator with values from 11h to 50h mimicking the observed boundaries (Polishook & Brosch, 2006). The shape representation of binary asteroids consist of two triaxial ellipsoids, with the axes ratio values generated as for the single population, which are mutually orbiting in a synchronous system. The size relation between both components was also generated with a pseudorandom procedure with values $0.7 < r_2/r_1 < 1$, which corresponds to the observed boundaries of synchronous systems known. An example of a binary system simulation, including the shadowing effects is shown in Fig. 5.1.

5.2. Inversion results of the binary asteroids simulations

5.2.1. General overview of the results

In general terms, the results obtained have been similar to the ones described for the single asteroid simulations with a photometric error of $\sigma = 0.04$. A total of 6,535 solutions were accepted by the inversion algorithm (63% of the simulated asteroids). The distribution of these rejected cases because of the warning flags is again biased, grouping towards low pole latitudes as shown in Fig. 5.2. This means that the solutions produced by the *Gaia* inversion algorithm will miss binary systems having low pole latitudes, or in other words, binary systems discovered by analyzing the *Gaia* inversion results, will tend to have high pole latitudes.

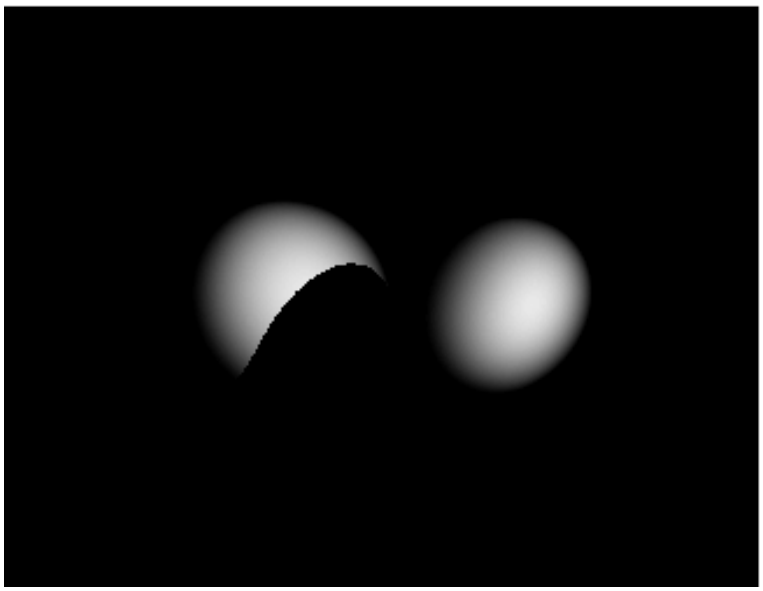

Figure 5.1: Example of a binary system representation using 3-axis ellipsoids. The component on the right is projecting its shadow to the component on the left due to the viewing geometry for the Sun–Observer–asteroid system.

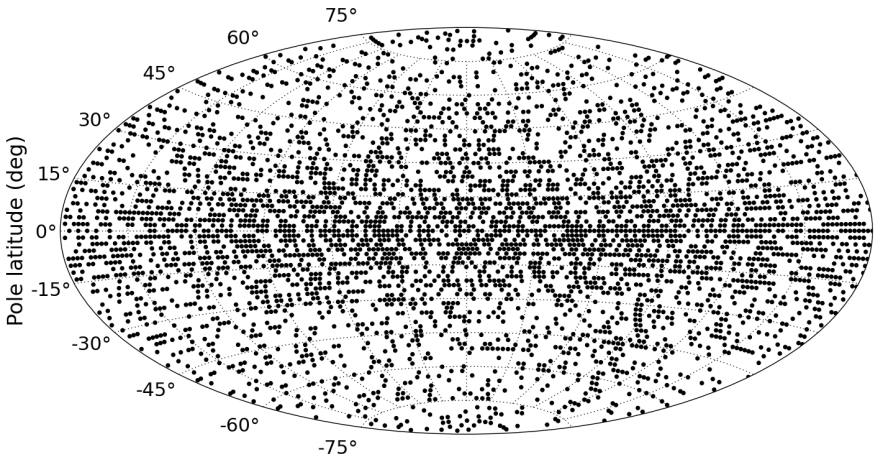

Figure 5.2: Distribution of *warnings* received from the inversion of the binary asteroid population.

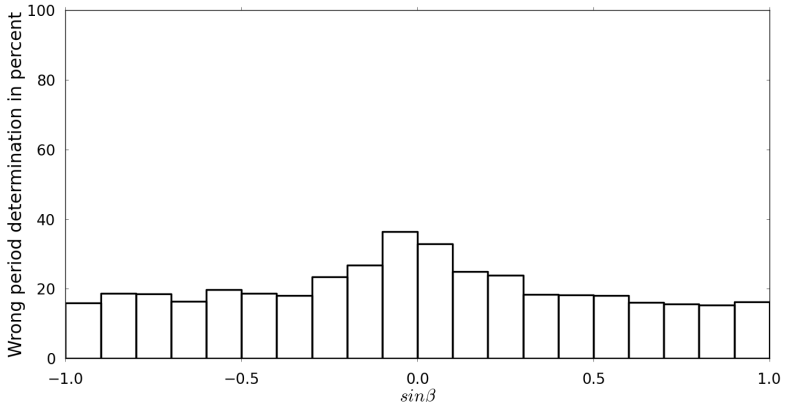

Figure 5.3: Wrong period determination in percent versus the binary asteroids system orbital pole latitude.

The reliability of the rotational period determination is also biased against low pole latitudes, as shown in Fig. 5.3. However, the wrong period determinations appears to be higher than for the single asteroids results for high pole latitudes, with almost 20% of the inversion results with a wrong solution.

The distribution of the percentage of correct solutions as a function of the number of *Gaia* transits and the pole latitude is also following the same scheme as in the single case, as can be seen in Fig. 5.4. However, the number of generated solutions is smaller, as the number of warning flags is higher compared to the singular case. The number of transits is specially crucial for the detection of binary systems, as the bigger the number of transits, the higher the probability of catching a mutual event. In the case of synchronous binary systems with comparable component sizes, each mutual event causes a significant magnitude drop, which might be crucial for the correct period determination. On the contrary, a small number of transits might result in few or no mutual events observed, which can entangle the correct period determination.

In order to understand the results obtained, it is worth to study the distribution of the mutual events in the simulated photometry. The magnitude drop produced by a mutual event is mainly related to the size ratio of the two components of the system. For instance, in the ideal case of two perfect spheres observed at zero phase angle, the maximum magnitude drop can be simply calculated as a function of the radius of the components (Descamps et al. 2007):

$$\Delta mag = 2.5 \log \left(1 + \frac{R_2}{R_1}\right) \tag{5.1}$$

where R_1 and R_2 are the radii of the components.

In a more general approach, a magnitude drop observed in a mutual event at zero phase angle will be proportional to the body's cross-sectional area eclipsed by the second component. For observations obtained at higher phase angles, the mutual shadowing effects have to be also taken into account. Each body casts cylindrical shadows according to its cross-sectional area, producing a magnitude drop if this cylinder intersects the other component.

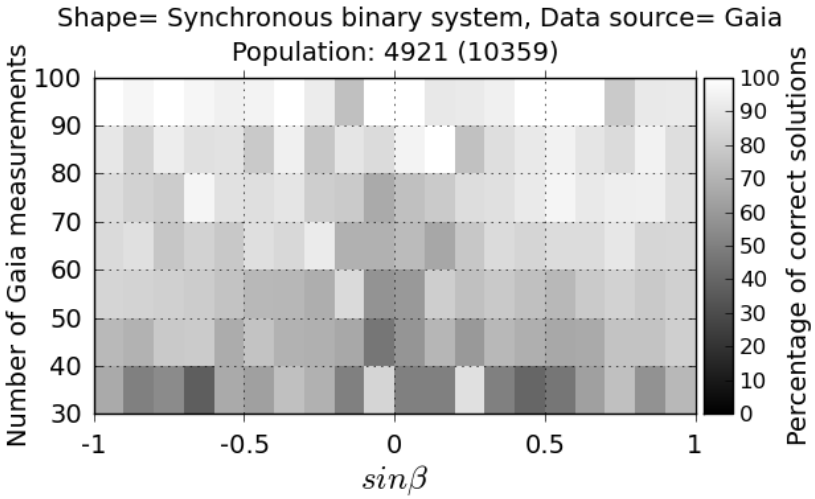

Figure 5.4: Histogram showing the results obtained for the inversion of the binary asteroids population. The percentage of correct solutions is plotted as a function of the number of *Gaia* detections for each bin of asteroid's pole latitude. The population number is indicating the number of obtained solutions and the total of inversion runs executed (in brackets).

In order to estimate the impact of the mutual events on the *Gaia* photometry simulations, the drop in magnitude (Δmag_i) was analytically calculated for each single measurement, including the eclipses and the shadowing effects. Next the arithmetic mean of the mutual events (Δm) was calculated by adding all the magnitude drops and dividing by the number of transits (N) when they were observed:

$$\Delta m = \frac{1}{N} \sum_{i=1}^{N} \Delta mag_i \tag{5.2}$$

The results of these calculations allowed to understand better the behaviour of the inversion algorithm. For the majority of binary systems simulated, the impact of the mutual events in the *Gaia* photometric simulations was almost negligible. In particular, 4,783 asteroids (73% of the results accepted by the inversion algorithm) had a mean $\Delta m < 0.02$ mag. For the modelling purposes, this means that the effects of the mutual events were comparable to the noise level. On the other hand, in case of weakly elongated bodies, the lack of mutual events implies a lightcurve with low amplitude. As previously stated, this is the worst scenario for an inversion problem with sparse data, as several solutions might generate equivalent fits. In other words, the increment of inversion warnings and wrong period determinations for asteroids with low pole latitudes compared to the single case is due to the lack of measurements of mutual events. Regarding the rest of the results, 1,065 asteroids (16% of the results accepted) had a mean between $0.02 < \Delta m < 0.04$ mag, only 308 (5% of the results accepted) had $0.04 < \Delta m < 0.06$ mag, and 379 (6% of the results accepted) had a strong impact on the photometry having $\Delta m > 0.06$ mag.

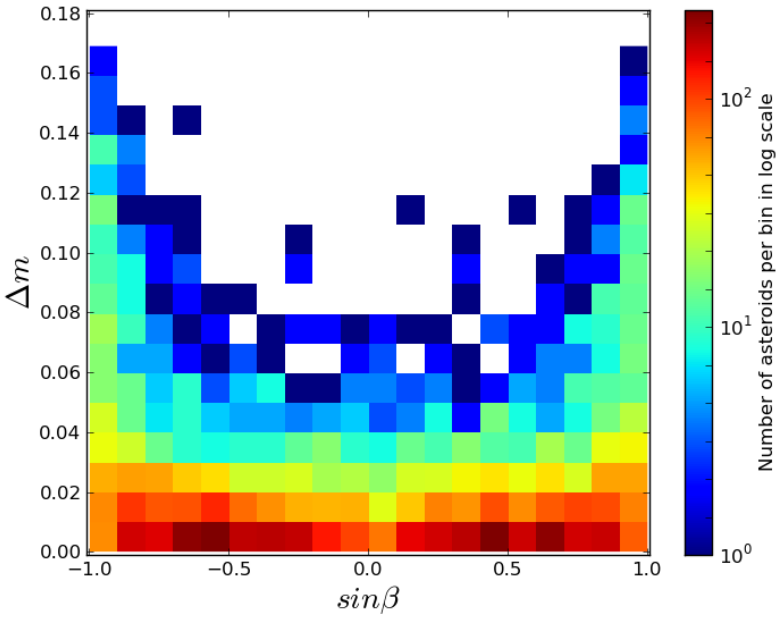

Figure 5.5: Distribution of the average drops in magnitude per single observation and per object (see text) as a function of the asteroid's pole latitude. The population shown is not including those asteroids for which a warning was obtained in the inversion run. The logarithmic colormap shows the number of asteroids per bin.

When studying the results dependency on the system's pole, it is clear that the majority of detections of mutual events corresponds to asteroids with high pole latitudes. This result is not surprising, as systems having high pole latitudes present mutual events in almost every apparition, as the aspect angle is always close to 90 degrees. In Fig. 5.5 obtained distribution of Δm as a function of the asteroids' pole latitude is shown. The color of each bin indicates the number of asteroids found with a given value of Δm and $sin\beta$. A logarithmic scale was chosen in order to visualize the few results with mutual events, which have a clear dependency on the pole latitude.

5.2.2. Distribution of the semi-axes ratios

The most interesting result was found to be connected with the distribution of the semi-axes ratios. A histogram showing a comparison between the semi-major axes obtained for the single and binary populations is shown in Fig. 5.6. Despite both results being similar, the mean is slightly shifted to a higher value for the binary results. This effect is related to the lack of observed mutual events discussed previously. However, a longer tail can be observed for small values of the b/a axis ratio. A small fraction of the results include ratios smaller than $b/a < 0.5$ whereas such values were practically not existing in the single asteroids results. These results correspond to the systems with observed mutual events.

The differences between semi-minor axis results are even more noticeable. The mean of the binary results is clearly shifted to a higher value. A histogram showing a

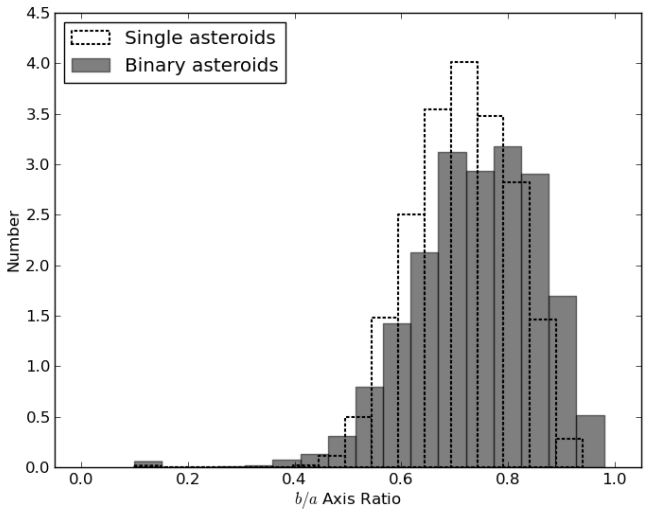

Figure 5.6: Histogram showing the distribution of the semi-major axis found for the accepted results (without a warning flag).

comparison between the semi-minor axes obtained for the single and binary populations is shown in Fig. 5.7. This shift to higher values is also due to the absence of mutual events for the majority of observed systems.

Both shifts described can be explained by calculating the cross-sectional area observed for the single and binary cases. Observations near a pole-on geometry have a higher cross-sectional area for a binary system than for a single body. If mutual events are observed in another geometry, the lightcurve amplitude will be high and the inversion algorithm will tend to create a cigar-like shape solution, with a very elongated triaxial ellipsoid. However, if no mutual events are observed, the semi-minor axis solution will tend to have its maximum value, and so will the value of the semi-major axis. Such tendency of equalizing the semi-axes results can be better seen in Fig. 5.8, where a 2D histogram shows the correlation between both semi-axes results.

Besides the aforementioned effect, a cluster of solutions is formed in the region comprised by $0.5 < b/a < 0.7$ and $0.1 < c/a < 0.3$. These solutions correspond to systems with mutual events observed but a wrong determination of the pole orientation. As exposed in the single asteroids case, the inversion algorithm tends to choose very low values of the semi-minor axis in order to compensate for the wrong determination of the pole. However, in the single case such solutions presented a higher value of the semi-major axis, as the lightcurve amplitude was lower. Therefore, despite knowing that the solutions in this area might be wrong, they could indicate that the asteroid might potentially be a binary system. The differences between the single and binary distributions can be more clearly seen in Fig. 5.9 where the histogram for the single asteroid results has been substracted from the histogram obtained for the binary systems. The resulting diagram shows the area where it is more probable to find a binary system in the inversion results.

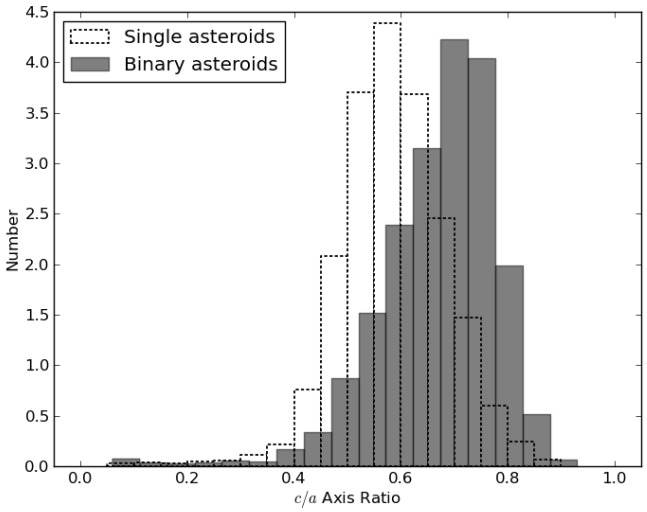

Figure 5.7: Histogram showing the distribution of the semi-minor axis found for the accepted results (without a warning flag).

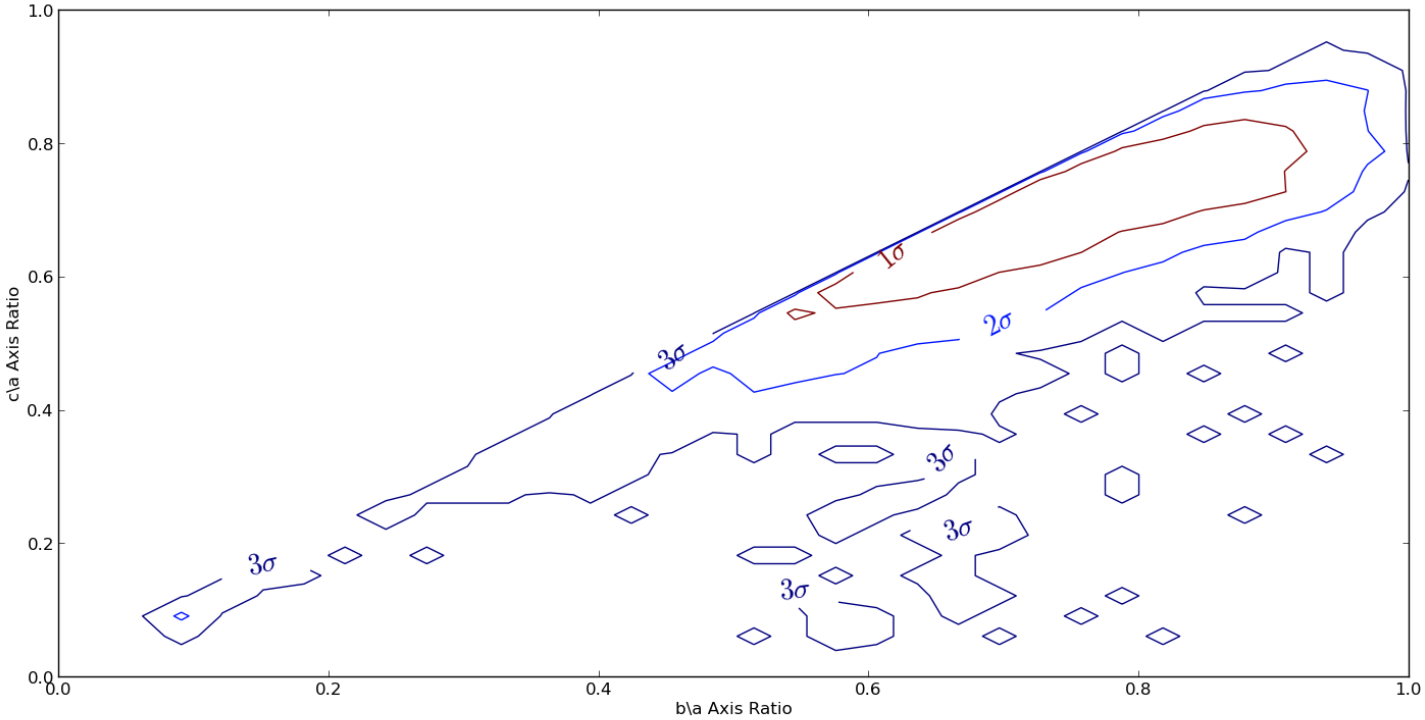

Figure 5.8: A 2D histogram showing the distribution of the semi-axes for the accepted runs from the inversion of simulated measurements of binary asteroids (without a warning flag).

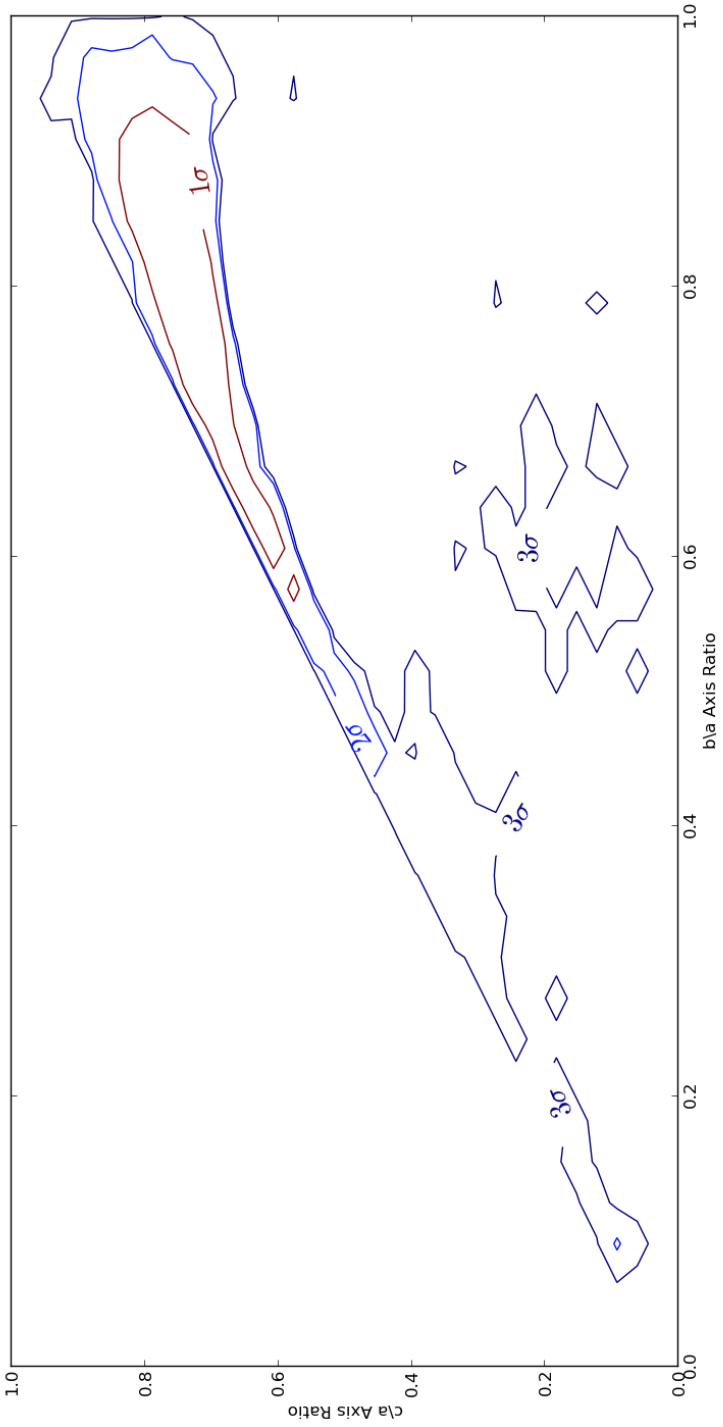

Figure 5.9: Diagram obtained after subtracting the single population histogram from the binary population histogram. The plot shows the areas of the semi-axes' results with a higher probability of finding a binary asteroid among the inversion results.

In order to confirm the results interpretation given above, we plotted the distribution of the average drops Δm as scatter points in the 2D histograms. The impact of the mutual events on the simulations is quantified as previously explained by calculating Δm, which is divided into four intervals in the diagram shown in Fig. 5.10. As expected, asteroids without mutual events (blue points) observed are concentrated at higher values of the semi-major axis, while asteroids with a high impact of the mutual events in the photometry are mainly aligned along the $b/a = c/a$ area.

Finally, Fig. 5.11 is showing the same distribution of the average drops projected to the diagram resulting from substracting the histogram of the single population to the one obtained for the binary population. This diagram might be useful to identify the scenarios for which it will be possible to differentiate, at least with a probabilistic approach, the binary population from the single one. Binary systems without mutual events observed should accumulate in the area comprised by $b/a > 0.8$ and $c/a > 0.7$, while binary asteroids should be found in the $b/a = c/a$, with $b/a < 0.7$ and in the wrong-pole-determination are with $c/a < 0.3$ and $0.5 < b/a < 0.7$. The rest of the semi-axes results, despite containing observations with mutual events, might not be distinguished from the single asteroids population, at least not by applying this criteria.

Nevertheless, it is worth noting that in this work the binary systems were simulated following an isotropic distribution of orbit poles. The absence of mutual events in the majority of simulated observations is a direct effect of the pole distribution chosen. Some authors suggest that the orbit poles of binaries is anisotropically distributed, preferring higher pole values (Pravec et al. 2012). If the results obtained with the *Gaia* inversion presents an excess of solutions with $b/a > 0.8$ similar to our inversion results for binaries, this would indicate that binary systems with low poles are underestimated in the actual distribution, as they are harder to be discovered (mutual events are only observable in specific geometries). And on the contrary, if the distribution of semi-axes are fitting the prediction pattern shown for single asteroids, this would support the theory of the pole anisotropy of binary systems.

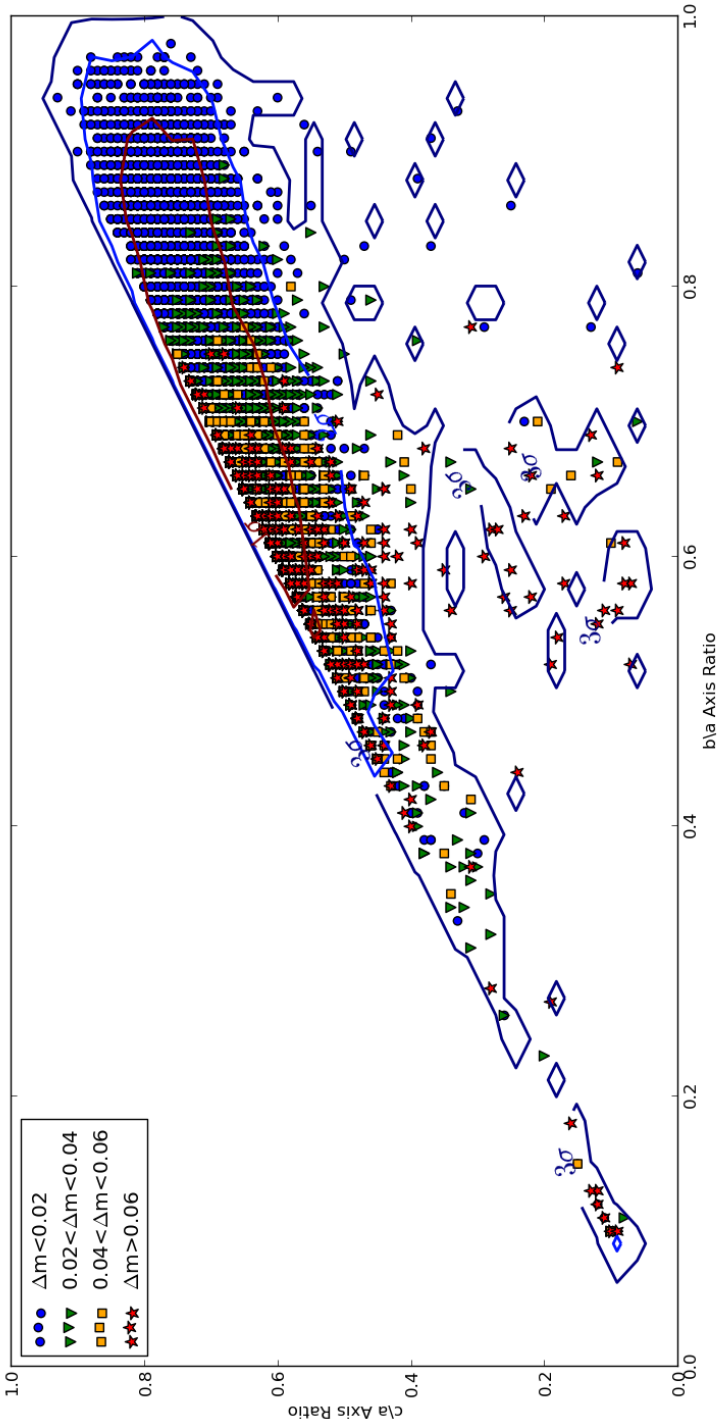

Figure 5.10: Scattered points show the average drops in magnitude per single observation and per object (see text) as a function of the semi-axes' results. The solid line shows the density distribution of the results as shown in Fig .5.8.

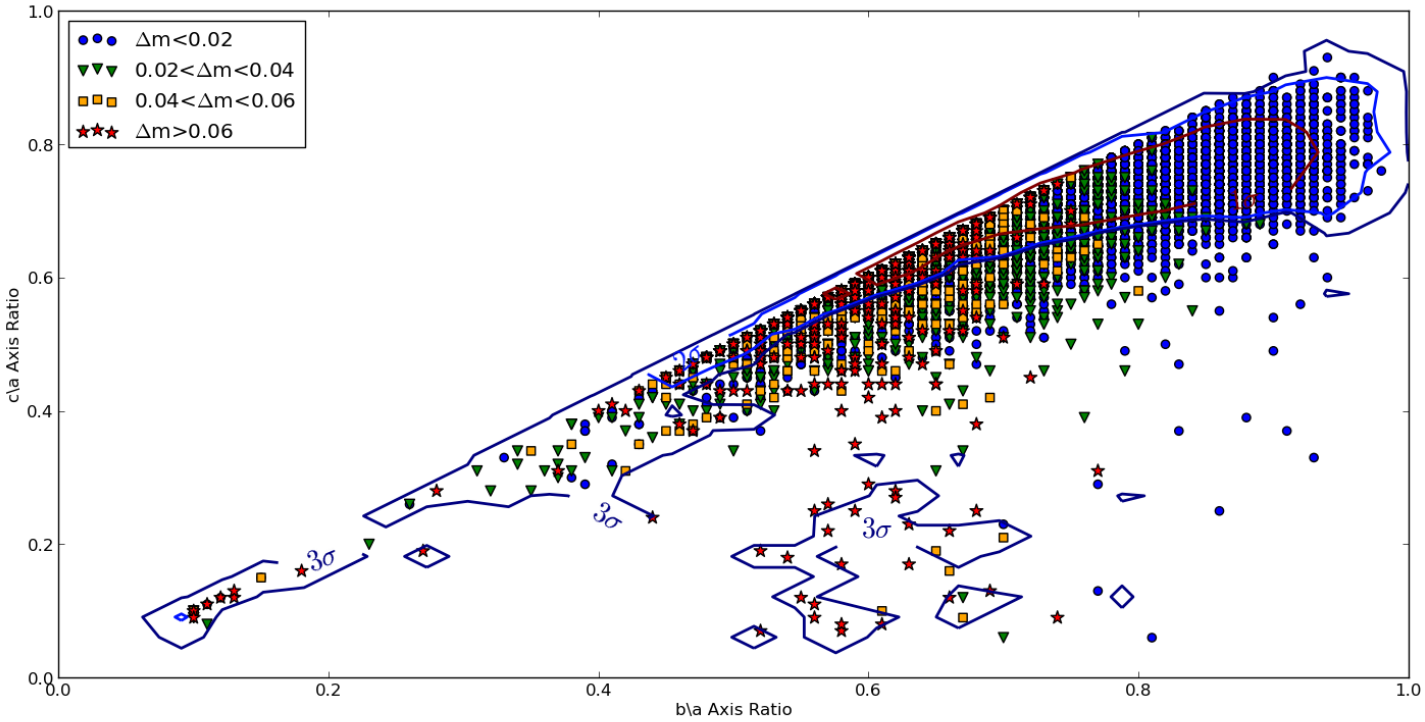

Figure 5.11: Scattered points show the average drops in magnitude per single observation and per object (see text) as a function of the semi-axes' results. These results are projected in the diagram obtained after substracting the single population histogram from the binary population histogram.

5.3. Inversion test with real sparse-data

The same inversion experiment with sparse-data for single asteroids described in section 4.5 was repeated for known binary systems. The objects selected were confirmed binary asteroids, both synchronous and asynchronous. However, not all known binaries have been inverted, as the quality of the available sparse data and the quantity of apparitions with measurements is restricting the number of systems for which the inversion could be applied. In fact, quality of the data was acceptable only for the brighter binary systems known.

A total of six synchronous binary asteroids were inverted. Despite the low quality of the data used, the correct period (i.e. in agreement with the period published by other authors on the basis of full lightcurves) was derived for five of them. For three of them, the pole solution was in agreement with other published works, for two of them no pole solution could be found in the references, and one had a wrong pole solution. The results and the references used for comparison reasons are summarized in Table 5.1. It is worth mentioning that the inversion with a wrong period determination corresponds to the asteroid with, by far, a smaller number of measurements (*809 Lundia*, with 53 data points).

The results for the asynchronous binary systems were clearly worse. A total of nine asynchronous systems were inverted, with only two correct period determinations. Both correct solutions correspond to asteroids with a high pole latitude solution ($\beta > 80$ deg). However, no comparison can be done for their pole solutions, as no model exists in the bibliography. Three models could be found in the bibliography for the remaining asteroids; one of the results was in agreement with the references while the two others were in disagreement. The majority of the pole solutions are, thus, new results. The models' parameter as well as the bibliography consultated are summarized in Table 5.2.

From these results, it can be stated that the *Gaia* inversion algorithm works fine for synchronous systems, as they only present one periodic signal, and thus the inversion problem can be faced with a single object approach. However, asynchronous systems presents two periodic signals, due to the rotation of the primary and the asynchronous mutual events. If the latter are numerous enough and the magnitude drop is significant enough, such problem can not be solved with a single body model.

Table 5.1: Table with the results obtained for synchronous binary asteroids. The results in bold are in agreement with the values in the bibliography given on the right, while the results in italics are in disagreement. The results written in plain font at present lack the counterpart in the literature. The 180 degree ambiguity in the pole ecliptic longitud is taken into account when comparing the results.

Asteroid	λ [°]	β [°]	b/a	c/a	**Period** $[h]$	**Observatory**	N_{obs}	**Reference**	λ_R [°]	β_R [°]	Period_R $[h]$
90 Antiope	**200**	**22**	0.74	0.67	**16.505064**	689	161	Bartczak et al. (2014)	199	38	16.505046
809 Lundia	**135**	**28**	0.50	0.39	*7.868180*	689	53	Kryszczyńska et al. (2014)	122	22	15.41574
1089 Tama*	**358**	**40**	0.61	0.32	16.456907	689	103	Hanuš et al. (2013a)	193	32	16.4461
1139 Atami	90	34	0.60	0.28	**27.471666**	703	179	Manzini et al. (2006)	–	–	27.45
1313 Berna	188	29	0.51	0.41	**25.471945**	689	149	Behrend et al. (2006)	–	–	25.464
3169 Ostro*	*306*	*39*	0.25	0.25	**6.509161**	703	137	Michałowski et al. (2014)	238	-61	6.509
* Contact binary											

Table 5.2: Table with the results obtained for asynchronous binary asteroids. The results in bold are in agreement with the values in the bibliography, while the results in italics are in disagreement (the data of the primary component is considered for comparison purposes). The results written in plain font at present lack the counterpart in the literature. The 180 degree ambiguity in the pole ecliptic longitud is taken into account when comparing the results.

Asteroid	λ [°]	β [°]	b/a	c/a	**Period** [h]	**Observatory**	N_{obs}	**Reference**	λ_R [°]	β_R [°]	Period_R [h]
22 Kalliope	*0*	*15*	0.72	0.55	*3.817228*	689	216	Kaasalainen et al. (2002a)	196	3	4.148200
107 Camilla	**71**	**61**	0.63	0.35	*9.808441*	689	268	De Angelis (1995)	73	54	4.843928
317 Roxane	148	86	0.47	0.15	**8.169585**	689	133	Harris et al. (1992)	–	–	8.169
762 Pulcova	214	38	0.60	0.60	*23.854082*	689	137	Davis (2001)	–	–	5.839
939 Isberga	*317*	*56*	0.36	0.36	*23.957256*	689	79	Carry et al. (2015)	225	86	26.6304
1052 Belgica	91	34	0.54	0.54	*16.817451*	689	83	Franco et al. (2013)	–	–	2.7097
1333 Cevenola	184	80	0.42	0.42	**4.879335**	689	69	Warner (2002)	–	–	4.88
1338 Duponta	40	41	0.72	0.72	*3.962982*	703	80	Gajdos et al. (2007)	–	–	3.8543
2121 Sevastopol	306	43	0.60	0.60	*16.810518*	703	120	Higgins et al. (2010)	–	–	2.90640

The semi-axes ratios results are also interesting to be studied in this case. In general, they are in agreement with the predictions presented above on the basis of the simulations. The semi-axes obtained from the inversion of real data for both synchronous and asynchronous cases are projected to the density distribution diagram (Fig. 5.12). The inversion solutions of real data are shown as scattered points which are mostly located inside the areas gathered on the basis of the simulations results. The real data results present a tendency to be located close to the $b/a = c/a$ line, with the exception of three cases which are located in the area with $c/a < 0.3$, which was identified as an inversion-artifact's solution area for wrong pole determinations. It worth noting that none of the results has a nearly spherical shape ($b/a > 0.8$ and $c/a > 0.8$) despite the results based on simulations predicted a high density of solutions with such values. As previously shown, these nearly spherical solutions correspond to asteroids which observations does (almost) not include mutual events. However, it would be wrong to consider that an absence of this results implies that such binary systems do not exist, as it is necessary to keep in mind that the selection of asteroids to test the inversion algorithm with real sparse data is heavily biased for two main reasons: 1) only the brighter asteroids (thus bigger binary systems, which may have some primordial preference for spin axis position) were selected, as they present the best photometry available and 2) all binary systems used in this research had been discovered by observing the traces of their mutual events in their lightcurves, thus their sparse measurements collected under different geometries might include them as well.

In order to check if the results obtained on account of simulations can be used to differentiate single and binary populations, we created a new plot including the results from the inversion of sparse data of single and binary asteroids (Fig. 5.13). In this plot, the semi-axes results for real data are shown as scatter points while the solid lines show the density distribution of the results obtained for the simulated sets after deducting the single histogram from the the binary histogram. As a result, the diagram is identifying the areas whith higher probability of finding a binary system among the inversion results. Almost all the results of the binary asteroids are inside the predicted area, while the majority of results of single asteroids are found outside. This diagram can, therefore, be useful when analyzing the *Gaia* inversion results. Asteroids having their semi-axis ratio inside the high density area might be considered as binary candidates, thus they will be good targets for further observation.

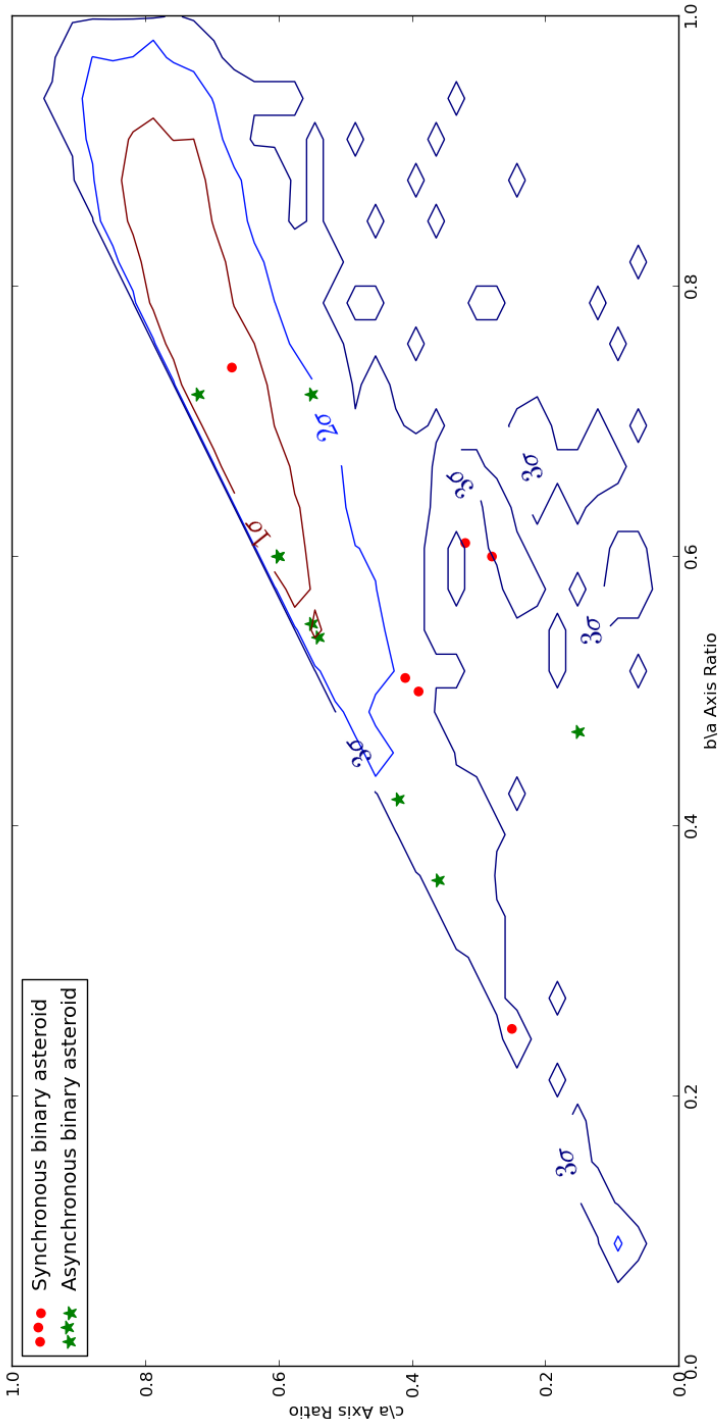

Figure 5.12: Same as histogram in Fig. 5.8 with the projection of the semi-axes' results obtained with real AstDyS sparse data of known binary asteroids. The results are divided into synchronous binary asteroids and asynchronous binary asteroids. See text for the meaning of the σ boundaries.

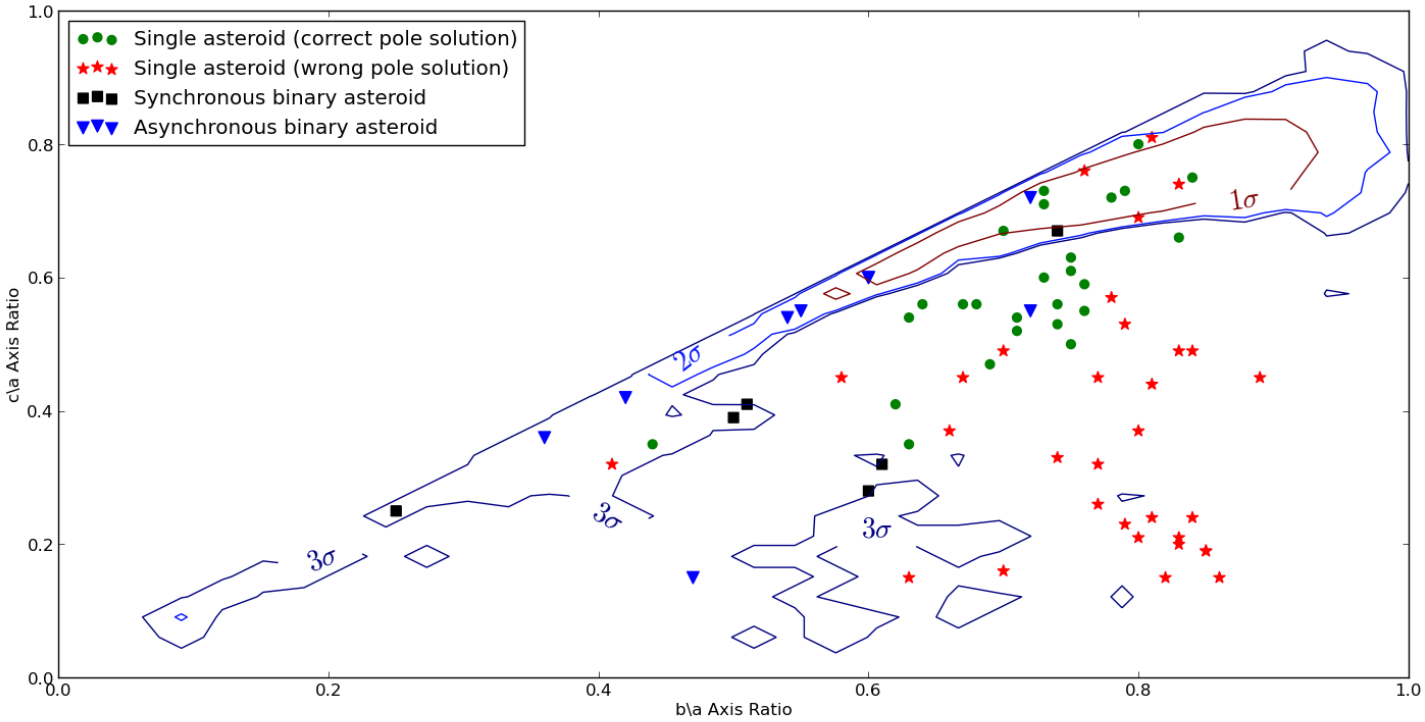

Figure 5.13: Diagram showing the result of subtracting the 2D histogram for the single asteroids simulations from the 2D histogram for the binary asteroid simulations. The boundaries show the areas where it is more probable to find isolated binary candidates. See text for the meaning of σ.

Chapter 6

Combining dense lightcurves with *Gaia* photometry of asteroids

Another strategy for optimizing the *Gaia* results is performing ground-based follow-up observations. Now that all the parameters of the *Gaia* scanning law are fixed, we are able to predict exactly the observation sequence for Solar System objects. It means that we can observe the same target from the ground at the same time as *Gaia* does. For example, we can very easily add a full rotational (dense) lightcurve around (or very close to) an isolated observation made by *Gaia*. The link between the two data sets would then be very strong, as a single *Gaia* measurement provides a very precise absolute magnitude that can be used to calibrate the ground-based lightcurve. The question is: how many such lightcurves per object we need to obtain a substantial improvement of the inversion? Maybe a single one? Or more? Therefore, this part of present work is thought to address such questions and lay the foundations for a collaboration involving coordinated observations from the ground.

6.1. *Gaia* photometry combined with ground-based observations

Combining *Gaia* observations of asteroids with ground-based lightcurves becomes straightforward when both observations are taken simultaneously. In contrast, if the lightcurve obtained from the ground is not close to the epoch of observation by *Gaia*, there may be problems to link the *Gaia* observation to the rotational phase, and to calibrate the magnitudes of the ground-based data, especially in cases when the lightcurve is complex and the period resulting from the lightcurve is uncertain.

In order to support an observational campaign, it would be a good idea to publish the *Gaia* observation sequence for Solar System objects, allowing the observers to obtain a lightcurve of a certain asteroid at the same time as *Gaia* is collecting a very precise photometric measurement. Later on, it will be possible to calibrate the ground-based observation (even if it is relative photometry) with *Gaia* absolute magnitude, and proceed with the inversion process normally. Formally, the only difference between data sources will appear during the preparation of the input file containing the photometric error associated with each observational instrument and the position vectors of the observer.

In order to study the impact of adding ground-based observations to *Gaia* data inversion we have simulated a full lightcurve with 60 point measurements for the asteroids with non-convex shapes. The particular geometry of the scan movement of *Gaia* telescopes, which never point on the Sun nor its opposition, results in observations taken at relatively high phase angles. For instance, considering the *Gaia* observations of a main-belt asteroid, the measurement with the lowest phase angle will be usually above 10 degrees. As the asteroid's magnitude becomes fainter for increasing phase angles, we selected the date of the *Gaia*'s measurement with the lowest phase angle as an epoch to generate the lightcurve. This choice was made taking into account that ground-based supporting observations of asteroids will probably be done by small or mid-sized telescopes, and moreover, we are not interested in the projecting shadows appearing at higher phase angles. Finally, we contaminated all the simulated lightcurves with Gaussian noise ($\sigma = 0.03$). It should be pointed out that the results presented here are limited to the specific choice made when adding dense lightcurves and they could be different for observations obtained around opposition, with more than one curve, etc.

6.1.1. Impact on the results as a function of the asteroid shape

After combining the simulated *Gaia* photometry and a full lightcurve, we used the resulting data set to feed the inversion algorithm. The results resemble the ones obtained for the *Gaia* data alone, i.e. a good overall performance, albeit worse reliability for nearly spherical bodies. In Fig. 6.1, we show the percentage of wrong solutions as a function of the asteroid's pole latitude and the equivalent b/a ratio, as well as the improvement gained when combining both data sets. It turned out that, with the exception of nearly spherical objects, the improvement was almost negligible. It is worth noting that the relative improvement on the results is not caused by an increment of the correct inversions, but the reduction of the accepted wrong solutions.

6.1.2. Impact on the results as a function of the number of measurements

If we analyse the results as a function of the amount of points collected by *Gaia*, the improvement can be clearly appreciated for asteroids having less than 50 detections. The results of the inversion run of the *Gaia* data with an additional lightcurve, and the relative improvement reached with respect to the results obtained for *Gaia* data alone are shown in Fig. 6.2. For the majority of asteroids for which supporting ground-based observations will be planned, we would not have any a priori information of the physical parameters. In contrast, the total number of observations for each asteroid can be already calculated as all the parameters of the *Gaia* scanning law are already fixed and the mission has started its science phase. Considering that it is not feasible to obtain one lightcurve for each of the ~300.000 asteroids observed by *Gaia*, it would be necessary to draw up an observational plan, thus we conclude that, for these purposes, the number of expected *Gaia* measurements can be a good selection criterion.

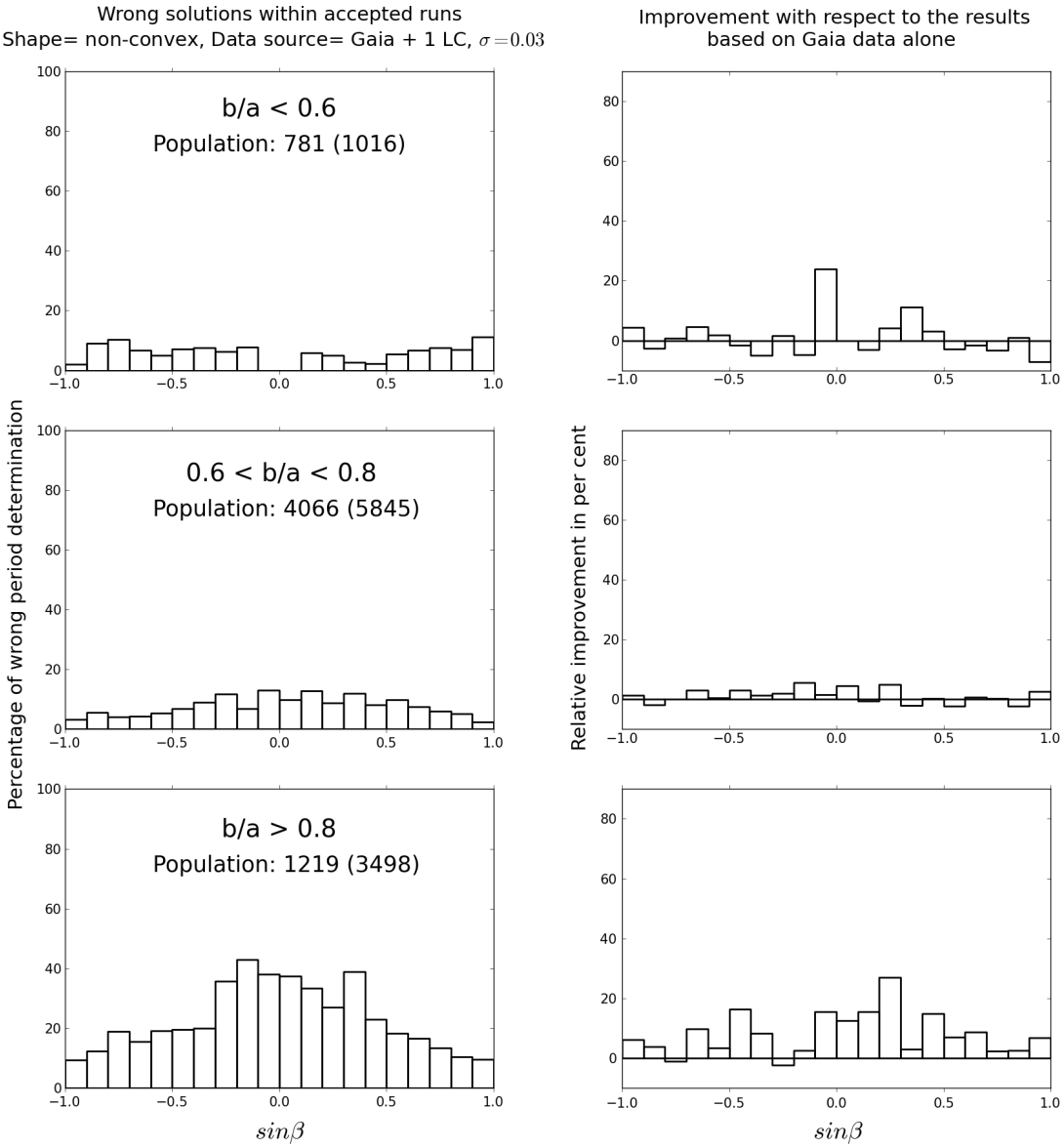

Figure 6.1: Histograms on the left show the inversion results obtained for a data set combining *Gaia* photometry and one full lightcurve. The results are divided into three groups as a function of the asteroids' equivalent b/a axis ratio and are plotted as a function of the asteroids' pole latitude. Histograms on the right show the relative improvement comparing with the inversion results obtained for *Gaia* data alone.

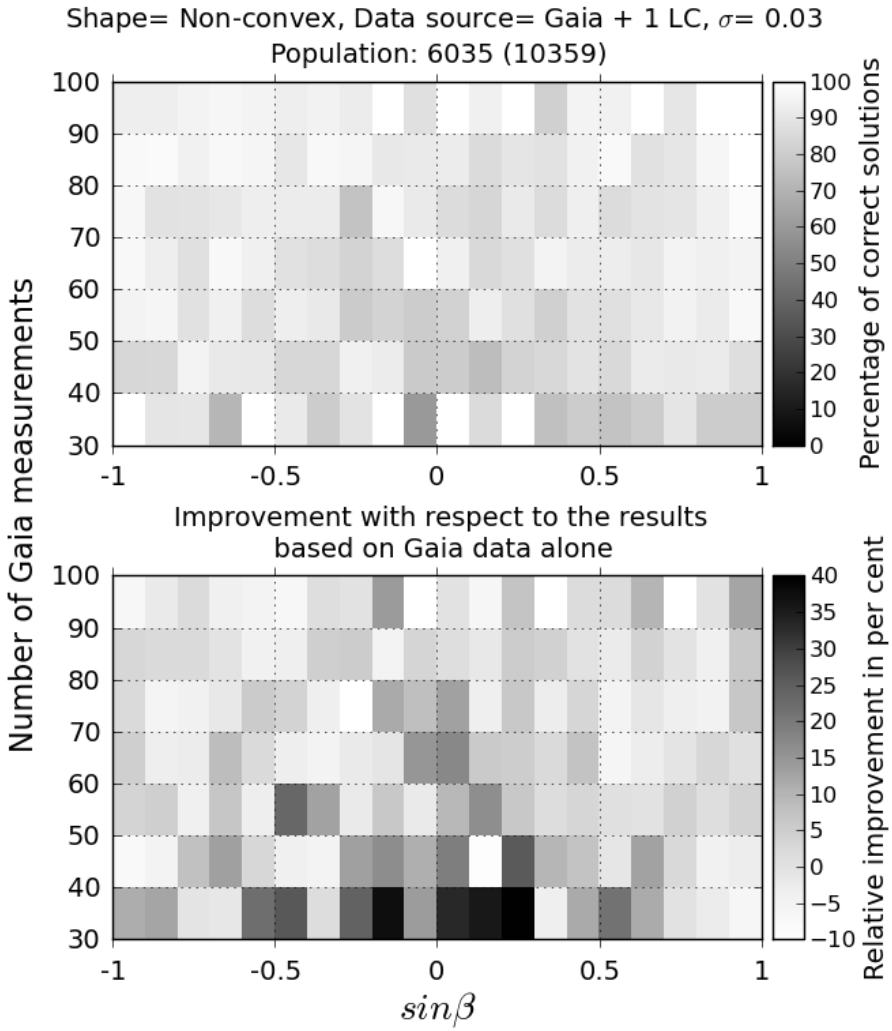

Figure 6.2: The histogram on the top shows the results obtained for the combined data set. The percentage of correct solutions is plotted as a function of the number of *Gaia* detections for each bin of asteroids' pole latitude. The population number is indicating the amount of generated solutions and the total of inversion runs executed (in brackets). The histogram on the bottom shows the relative improvement compared to the inversion results obtained for *Gaia* data alone.

6.1.3. Discussion of the results

The results presented above could seem counter-intuitive. In particular, one could argue how it is possible that the addition of a full lightcurve does not generally improve the reliability of the method. In order to understand the situation, we should clarify some points:

1. *The actual version of the inversion algorithm treats each single measurement equally.* The goodness of the inversion solution is estimated on the basis of the fit between computed and observed single measurements. In the case of asteroids with abundant *Gaia* observations (for instance, more than 80 points), a single lightcurve will have a negligible influence on the inversion result, especially for lightcurves with low amplitude (Marciniak & Michałowski, 2010). This situation can be faced by increasing the weight of the ground-based lightcurve to the detriment of the *Gaia* data.
2. *The additional lightcurves were blindly simulated in terms of asteroid's aspect angle.* Observations obtained at high aspect angles represent the best-case scenario for deriving the rotation period, as asteroid lightcurve is then at its maximum amplitude. However, it would require us to know in advance the spin axis orientation of the given asteroid so to predict the appropriate observational epoch. For the great majority of asteroids observed by *Gaia* this is not feasible, as we do not know their rotational states. For this reason, the only selection criterion used when generating the additional lightcurves was the asteroid's phase angle (see the beginning of the section), thus some of the lightcurves presented low amplitudes. In this particular situation, the inversion fit's residual is very low no matter the rotation period, and so the impact on the inversion results is negligible.
3. *The triaxial ellipsoid assumption of the inversion algorithm might have not well-behaved cases.*
   While it has been proven to work well for the majority of cases, the triaxial ellipsoid assumption might cause the inversion to fail under tough circumstances. For instance, very irregular shapes can generate lightcurves with multiple extrema, which cannot be inverted using a triaxial ellipsoid assumption, no matter how much of complementary data are used.

Chapter 7

Coordinated observations to enhance *Gaia* asteroid science

Nowadays, more and more people possess or have access to astronomical instruments which may be a source of observation material valuable for professional astronomical research. Although amateur astronomers are well equipped they usually observe and practice astrophotography only to experience beauty of the universe. Some of them having ambition to go beyond esthetic sensations do not have any idea how to do it. But there are some initiatives that address this problem and provide amateur observers with knowledge how to employ their enthusiasm and capabilities in service of contemporary science. As a result of these initiatives, statistics show a significant increase of the publications involving amateur observers over the last years (e.g. Mousis et al. 2014). Conducting some of professional activities requires performing both numerous and precise observations along with covering many targets in a relatively short period of time. Such research activities involve objects and phenomena including follow-up of newly discovered Near Earth Objects (NEOs) or measurement of the timings of star occultations by asteroids. Since the access to the scientific-valuable equipment is no longer an issue, ones should intensify the effort towards providing more opportunities for amateurs to have input in the professional astronomical research. The *Gaia* mission provides a great opportunity to take advantage of the professional and amateur collaborations.

7.1. Introducing *Gaia*-GOSA

7.1.1. Motivation

We already know that the main challenge to be solved when inverting sparse data is the correct determination of the rotation period. On the other hand, all the parameters of the *Gaia* scanning law are very stable on long periods of time, thus we are able to predict exactly the observation sequence for Solar System Objects (SSO). That means that we can plan to observe from the ground at the same time as *Gaia* in order to obtain a full rotational lightcurve of the target. This lightcurve not only can be used to improve the results derived from the *Gaia* photometry inversion of asteroids, but also the rotation period acquired from the lightcurve can be useful to check the inversion

reliability.

However, the asteroid observing predictions by *Gaia* are in a very specialized format, created for Data Processing and Analysis Consortium (DPAC) internal use only. This fact is preventing many potential observers to take part in a coordinated campaign. Moreover, publishing the whole list of predictions without promoting an observational campaign would not solve the problem, as coordination between observers is needed in order to cover the full asteroid lightcurve, as their typical rotation periods range between 2 and 40 hours. Thus, in order to optimize the enhancement of the *Gaia* SSO results, the observers should focus on interesting targets pre-selected by researchers, also avoiding those with the rotation period already determined. Another issue related with the observational campaigns is the data reduction standardization. There are several tools available for lightcurve analysis and period determination, meaning that if the data processing is performed by the observer, we cannot have any certainty about the quality of the analysis process, thus it become a black box.

7.1.2. Concept

In order to lay the foundations for a worldwide collaborative network of observers, we have created a web service called *Gaia*-Groundbased Observation Service for Asteroids (*Gaia*-GOSA) presented in Santana-Ros et al. 2014. The service has been funded under the ESA Contract No. 400011266014/NL/CBi: "Gaia-GOSA: An interactive service for asteroid follow-up observations.". The main goal of *Gaia*-GOSA service is to support observers (both amateur and professional) in preparation and planning asteroid photometric observations, so that they can generate scientifically valuable data. Such data will result in a standardised catalogue with physical information of asteroids ready to be used for enhancing the final *Gaia* SSO release. Any registered user of the service is able to easily create an account, acquire the list of observation targets (in accordance with the *Gaia* observations) adapted for the specific user's instrument and observation site. The users are also able to upload the registered observation data to the server as the material for further research. This research will mainly help to determine asteroids' synodic period. The ranking of registered observers based on the scientific value of uploaded data is publicly available, encouraging the observers to keep on with their work and enabling them to experience the excitement of being part of a real space mission. The service is available for the general public, but the registered users are able to enjoy a more personalised service experience. We make use of the information provided during their registration process (e.g. instrument characteristics, observing site) to refine the object selection according to their individual observing possibilities. In order to obtain the *Gaia* transit predictions we have been collaborating with the Observatoire de la Côte d'Azur (OCA) which has the leadership of Solar System processing and simulations in *Gaia*-DPAC (CU4, Development Unit 460). We also considered necessary to have a mobile version, in order to facilitate the observation planning and enable checking updated information of other observers operations anywhere one wants. Hence, we started collaborating with the *Gaia* UB Research group in Barcelona in order to integrate the service to the official *Gaia* mission app developed by them.

The project collaborations are schematically summarized in Fig. 7.1

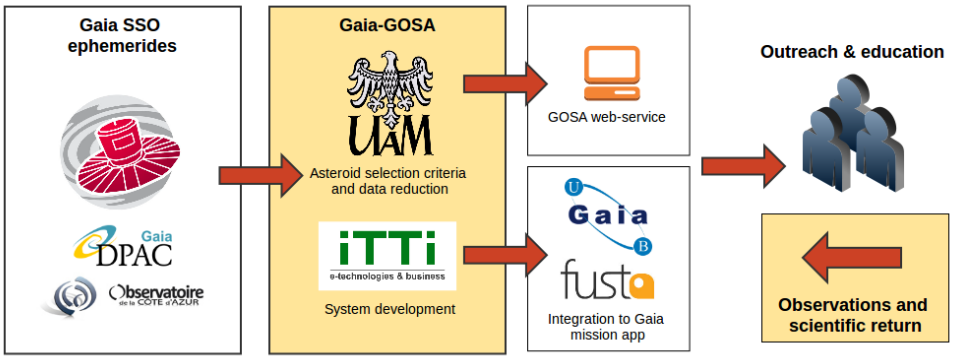

Figure 7.1: *Gaia*-GOSA organizational chart showing the project's dependencies between collaborators and users.

7.1.3. Objectives

The final goal of the project is to create a volunteer observers network that will obtain valuable photometric measurements of asteroids under the guidance of a professional group of astronomers. In order to achieve this goal the following requirements have to be met:

1. Coordination between observers is essential to fulfill the aims of the program
2. It is necessary to publish the predictions of the *Gaia* transit times
3. It is not feasible to collect lightcurves for each of the asteroid observed by *Gaia*, thus a pre-selection of interesting targets is needed

Our team is responsible for the data analysis and is planning to produce a catalogue with the collected results, which will contribute to enhance the scientific impact of *Gaia* on Solar System science. Such complementary data might also be used for validation purposes to assess the quality of the photometric inversion performed by DPAC (in the frame of unit CU9). In contrast to other collaborative projects in which the full photometry process is performed by the observer (from obtaining the data, to its reduction and analysis), in our project we aim only to "educate" the observers so as many of them as possible could generate useful data (see section below). However, the full analysis process will be performed by our team using standard and professional analysis tools. This way, we ensure that the results generated by the *Gaia*-GOSA will have high-quality standards, ready to be used by the *Gaia*-DPAC.

In sum, *Gaia*-GOSA shall enable observers (both amateur and professional) to choose a target from a pre-selected list of scientifically interesting objects and plan its observing run. Moreover, the *Gaia* transit times will be published for each target, allowing the observers to collect lightcurves of an asteroid at the same time *Gaia* is obtaining a very precise absolute magnitude. We will later analyse the data in order to extract the rotational period and lightcurve amplitude. The final goal of the project is to use the physical parameters derived from lightcurves to enhance the scientific impact of *Gaia* on Solar System science.

7.1.4. Observation strategy

The main challenge to face when inverting *Gaia* sparse-in-time data of asteroids is the correct determination of the rotation period. If any lightcurve is available for the object it can become a cornerstone when solving the problem. For instance, ground-based observations may be used to reject solutions containing alias period values.

Photometric observations of selected targets are thus required, including calibration frames (flat field, dark and bias). Photometry should be aimed to have 0.05 magnitude precision at worst. GOSA observing campaign relies on optimised observing strategy and careful planning of possible phase coverage from multiple stations. To complete a lightcurve we aim to collect at least 50 well placed data points. As a general rule, the longer the asteroid is observed the better. When the rotation period is still not known, a general practice is to image the asteroid in series of exposures of 2 to 5 minutes and a few hours in length (depending on the object brightness). The GOSA service will advise the user in each case, helping on the planning of the observing run.

7.2. GOSA project execution

The project started on January 2015 and has received funding from ESA until January 2017. The GOSA service has been designed to be easily portable. This means that, if no funding extension is received, the service might be exported to another institute willing to continue GOSA's operations at the end of the UAM's contract with ESA. At the moment, a first version of the GOSA service is already publicly available, and works are in progress for the final version of the service which should be available before the end of the year 2015. The project's work plan is summarized in the sections below.

7.2.1. Prediction of transits of Solar System objects

GOSA aims to release part of a highly specialized product generated within the *Gaia*-DPAC Solar system group to the general public. In order to make this product useful to the general community it should accomplish the following points:

1. *It shall be understandable without any previous knowledge of the Gaia mission*
2. *It cannot contain specialized information or too much data*
3. *It shall provide clear instructions on how to use the product*

The prediction of transits of Solar System objects will be calculated approximately once per year, due to the impossibility of predicting some of the input parameters for a longer period. For each release, we aim to select the most interesting targets under a scientific criteria and publish their predictions at GOSA webpage. In return, we expect gathering observations from the users, which will be analysed at the UAM Observatory. The results obtained will be published, while feedback about the observation quality will be sent to the users. The full expected flowchart of the data processing design is shown in Fig. 7.2.

As a starting point for the selection of targets for the GOSA it was required to obtain the transits of Solar System objects in the *Gaia* FOVs for the current year. These predictions were generated by F. Mignard from the OCA using the transit predictor

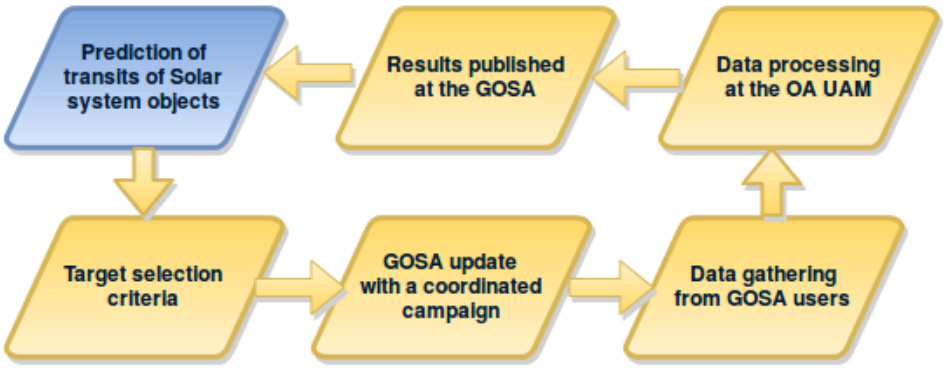

Figure 7.2: Flowchart of the GOSA data processing design.

```
Sun Aspect Angle                        :     45.00
Precession rate in rev/yr               :      5.80
Spin rate in arcsec/s TCB               :   59.960499070315
Initial precession phase                :      52.660
Initial spin phase                      :     339.000
Ref date (JD) of the initial phases     : 2456536.500
Beginning (JD) of the simulation        : 2456923.500
Duration (days) of the simulation       :     460
Number of planets processed             :  650000
Limit magnitude                         :     20.50
```

Figure 7.3: Input parameters used for generating the predictions.

developed within the DPAC-CU4/SSO (*Gaia*-C4-TN-OCA-FM-056-1). The standard output from the predictor comes as a single text file (250 MB) with one record per planetary transit. The file is sorted in increasing transit times. The input parameters used for generating the predictions are shown in Fig. 7.3, and includes the computation of the orbits of 650.000 minor planets. The resulting number of transits is over two millions for only one year of integration.

Each transit position contains technical information of the event. However, not all the information is relevant for the GOSA operations. For our purposes we extracted the values in Table 7.1:

Table 7.1: Input parameters of the asteroid visibility computations.

Transit TCB	Transit time (JD-2455197.5)
Planet	Asteroid id
FOV	Field of view (*Gaia* mirror 1 or 2)
Mag	*Gaia* magnitude
Date UTC	Transit time in UTC
RA	Right ascension
Dec	Declination

These are the input values of the mathematical software developed in the Poznań's Observatory, which computes the visibility of any asteroid transiting the *Gaia* FOVs for a given site on the Earth.

7.2.2. Target selection criteria

The results presented in Santana-Ros et al. (2015) are defining the first target selection criteria for the *Gaia*'s follow-up observations: additional ground-based observations are sought for asteroids with low pole latitudes, suspected nearly spheroidal shapes, and those with less than 50 *Gaia* transits. However, we are not able to predict all the transits of Solar System objects until the end of the mission, as the predictions require regular corrections due to unpredictable parameters, such as micrometeorite impacts on the spacecraft surface. Thus, for such group of objects, it will be necessary to perform data mining at the end of the *Gaia* mission in order to enhance their inversion results. In addition to these results, it is obvious that asteroids which might be scientifically interesting for the Solar System science community should also be observed. Such objects would include:

- Known or suspected binary asteroids
- Suspected fast rotators (period shorter than 1 hour) for which *Gaia* could have problems for the period determination
- Interesting categories, including strange spectral types, asteroid families, slow rotators, etc.

Based on these considerations, we have prepared a preliminary list of interesting targets (henceforth "Hot targets"), which are included in the first release of the GOSA service. However, this list should be considered to be dynamic, in the sense that more targets can (or shall) be included. Some examples might be: newly discovered NEOs, targets of opportunity for other observational techniques (radar echo, adaptive optics,

stellar occultations) or objects for which a new important discovery has been made. For this reason, we plan to allow GOSA users to submit requests to add objects to the target list if they can prove them to be scientifically meaningful. At this first stage, such requests will be placed in a special post in the site's forum. In consequent versions, we consider including a request form, or even organizing polls to allow the users choose their favourite targets.

7.2.3. Data processing

We will encourage users to store observations using the most commonly used digital formats in astronomy, such as FITS (Flexible Image Transport System) or SDF (Single-dimensional Format). In order to reduce the data, we have developed a procedure based on the Starlink open source code. The Starlink Project was a long running UK Project supporting astronomical data processing. It was closed in 2005 but the software continued to be developed at the Joint Astronomy Centre until March 2015, and is now maintained by the East Asian Observatory. We will also make use of in-house developed software (in C and C++) for format converting and SExtractor (Source-Extractor) for automatization purpouses. Other data formats like IRAF, PNM or TIFF will be also accepted only if the user is including the HEADER data in Table. 7.2.

Table 7.2: Header requirements for GOSA observations.

OBJECT	Asteroid id and/or name
OBSERVER	Observer's name
OBSERVING SITE	Telescope position: longitude (in degrees east of Greenwich) and latitude
TELESCOPE	Telescope diameter
DETECTOR	CCD model
COLUMNS	Filter used (C for clear)

Each frame should also include the Julian Date of the exposure start or a date with a Zero-time reference. Observations gathered in these formats will be reduced using a software based on a license-free IRAF version. IRAF is written and supported by the National Optical Astronomy Observatories (NOAO) in Tucson, Arizona.

7.2.4. Data analysis and lightcurve composition

For image analysis we have developed a C++ routine. The code allows to manually define the photometric aperture for the target and three comparison stars. When the apertures are defined, the code proceeds to measure the mean counts for the first image. The following frames are automatically analysed, as the software has the capability of detecting moving sources, thus it corrects the aperture position of an asteroid. An example of this procedure can be seen in Fig. 7.4.

The spin period of asteroids typically spans from 2 hours to a few days. This means that for asteroids with slow rotation, the full lightcurve cannot be obtained in a single observing run. Therefore, it is necessary to compose several fragments of the lightcurve, obtained during different nights and/or different observers. The UAM Observatory (OA UAM) has a 30 year tradition in the Solar System science field.

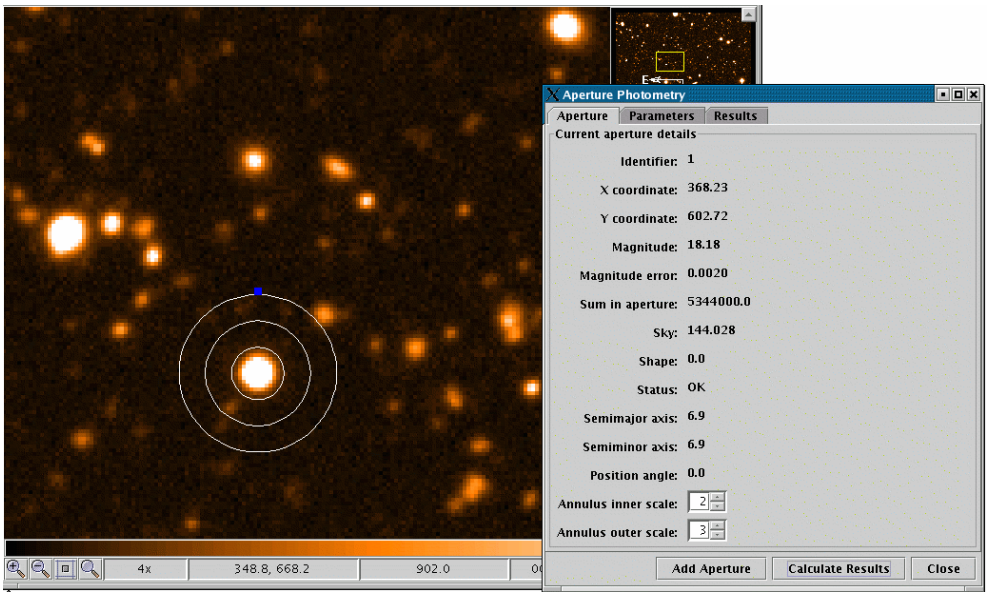

Figure 7.4: Example of an aperture photometry.

During that time Fortran, C and C++ algorithm solutions have been developed for lightcurve composition and period determination. These codes allow for composition of observations obtained at different sites. They also account for filter corrections, when different filters were used, and they take into account the magnitude-phase variation effects.

7.2.5. Storage of the results

Obtained results will be stored at the OA UAM local server. A database has been created using the LAMP open source Web development platform. We have adopted a standard format for storing the results: the Asteroid Lightcurve Data Exchange Format (ALCDEF, Stephens et al. 2010), which is a widely accepted standard format among the community (e.g. observations stored in the Minor Planet Center). The database is including the fields detailed in Table. 7.3.

7.3. GOSA website

The Gaia-GOSA service is already available at `www.gaiagosa.eu`. The website aims to be a specialized social network for asteroid observers seeking to collaborate within the *Gaia* mission. The website software design as well as its contents are described in the following sections.

7.3.1. Software static and dynamic architectures

The front-end component consists of the following sections: Home page, Guide and FAQ. The software dynamic architecture shows a typical interaction between elements of the system which is summarized in Fig. 7.5.

Table 7.3: Parameters stored after analysing the data (after Stephens et al. 2010).

OBJECTNUMBER	Asteroid id
OBJECTNAME	Asteroid name
CONTACTNAME	Observer
CONTACTINFO	Observer's e-mail and address
OBSLONGITUDE	Longitude of the observer's site
OBSLATITUDE	Latitude of the observer's site
SESSIONDATE	UT date of the observation
SESSIONTIME	UT time of the observation
FILTER	Filter used (C for clear)
MAGBAND	Indicates the color band of the magnitudes for the target
DIFFERMAGS	Indicates if the magnitude values for the target are differential or "standard" magnitudes
OBJECTRA	The approximate Right Ascension of the object at the given SESSIONDATE and SESSIONTIME
OBJECTDEC	The approximate Declination of the object at the given SESSIONDATE and SESSIONTIME
PHASE	The solar phase angle (Earth-Sun angle as seen from the asteroid) at the given SESSIONDATE and SESSIONTIME
CICORRECTION	Indicates whether or not a color index correction has been applied to the magnitudes in the DATA section
COMMENT	Provides additional information that is not covered by one of the recognized keywords
JDDATA	Julian date of the observation
MAGDATA	Magnitude of the target at the given Julian date

The interaction relies on a local communication between various elements. The sequence triggered by the user can be described in the following steps.

1. Home page interaction:
   - The user enters the home page and is able to share on social media (e.g. on Facebook, Twitter) the Gaia-GOSA service by clicking a proper button.
2. Observation planner interaction:
   - The user enters the observation planner page.
   - The system displays a form in which the user can specify its observational preferences.
   - The user confirms the specified preferences.
   - The system calculates the list of suggested objects.
   - The user selects their objects of interest.
   - The system calculates the ephemerides for selected objects and displays them in a form of a table.
   - The user is able to download the whole table on request (as a pdf or xls file).
3. Observation processing:

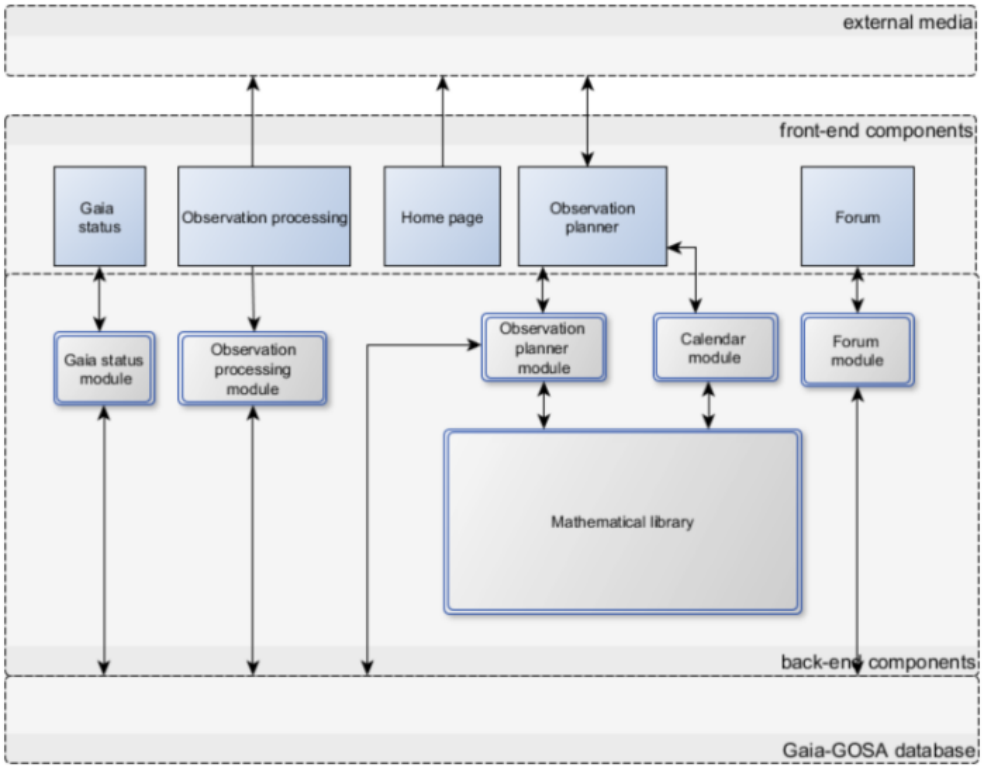

Figure 7.5: Dynamic architecture of Gaia-GOSA web service.

- The user enters the observation processing page.
- The system displays a table with observations that are currenly being processed or are queued.
- The user is able to upload the observations using the form.
- The system verifies the header data (image header) of the user's observations and asks to provide any missing information (if necessary).
- The system accepts the data, if all necessary information is provided.

4. Forum:
   - The user enters the Forum webpage.
   - The system displays all the active threads in which the user can create a new topic or contribute to any existing topic.

7.3.2. Software behaviour

The system responds to the user's requests in the way described below.

- **Request 1: *Gaia* status table interaction**
  When the user enters the *Gaia* status web page, the system back-end (*Gaia* status module) downloads a list containing current transits of minor bodies in the *Gaia*'s focal plane (from the *Gaia* status database) and displays them in a table. The user is able to modify the dimensions of the *Gaia* status table on demand. Any transit

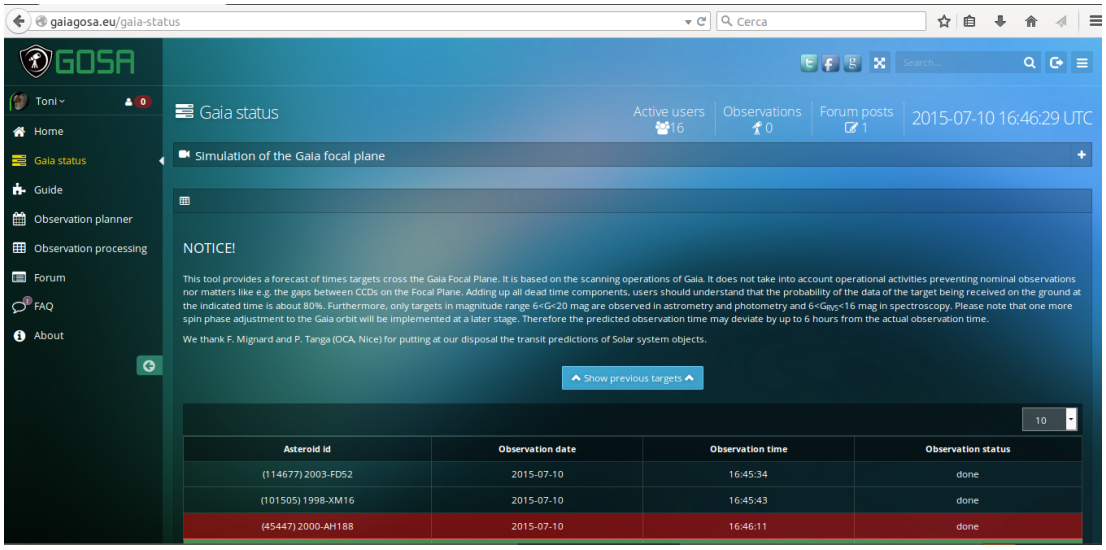

Figure 7.6: View of the *Gaia* status page.

event happening in real time is displayed with a green highlight. An example of the *Gaia* status page is shown in Fig. 7.6.

– **Request 2: Observation planner interaction**
When the user enters the observation planner page, the system back-end (Observation planner module) asks the user for a permission to utilize its geographical position (based on Geo IP). By referring to the Geo IP, the system zooms the map to the user's location. If the user rejects the use of auto-localisation, it is still possible to manually enter its position using a drop-down list. On account of the user's position, the system filters the targets list looking for visible targets which are planned to be observed by *Gaia* within the next 24 hours. Moreover, the user can filter the targets as a function of its observing capabilities, which are specified taking into account the magnitude range for the user's instrument and timestamp (Calendar module) of the planned observation entered by the user. After providing these filters, the system suggests a complete list of objects which are ready to be observed by the user. The system, basing on the filtered list, automatically adds a list of objects with high observation priority previously defined (the "Hot targets") to the user's targets. After the acceptance of the prepared target list by the user, the system displays the final targets list in a form of a table, containing the targets coordinates on the celestial sphere (in equatorial coordinate system and horizontal coordinate system), the *Gaia*'s transit time, the target's visibility time range for the given location and the expected magnitude. The system allows to download this table as a pdf or xls file. The user is also able to generate a star chart generated for the observation's start date. The chart is centered on the target, and includes the surrounding stars within a field of view defined by the user. An example of the observation planner page is shown in Fig. 7.7.

– **Request 3: Observation processing interaction**
The observation processing page allows the user to upload its new observational data to the system. During the validation process the system checks the completeness of

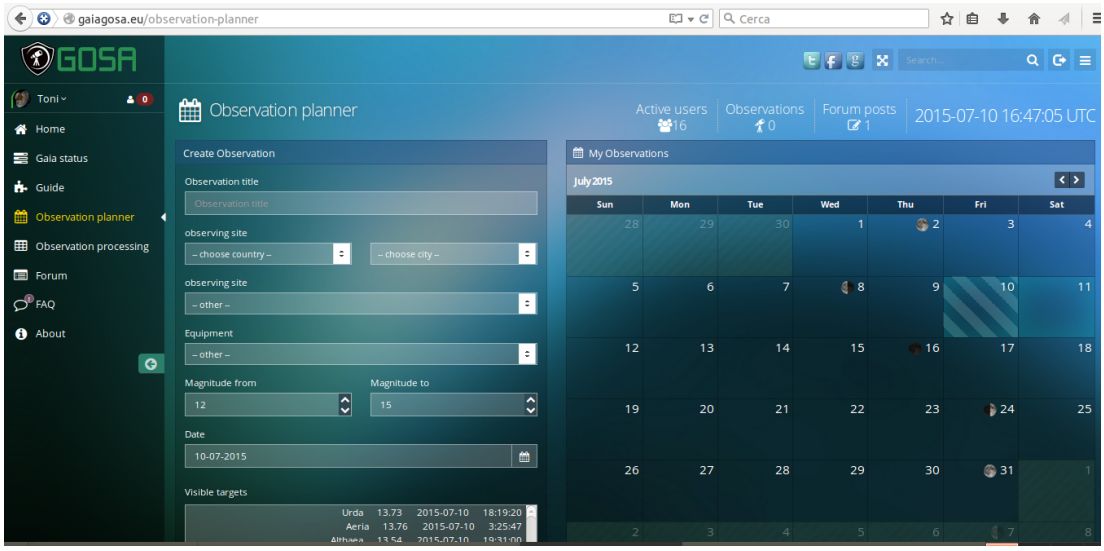

Figure 7.7: View of the Gaia-GOSA observation planner.

information of every image header. If any information from the header is missing, the system asks the user to manually provide it. Only when this information is complete, the system accepts the observational data. When the user enters the observation processing page, the system (observation processing module) displays all uploaded data and their current status (in process, accepted, rejected) in the form of a table. When the data analysis process is completed, the results obtained (period derived, lightcurve amplitude, comments on the quality of the observations) are returned to the user and published in the site. In addition, the system allows the user to publish the results obtained on external media (Facebook, Twitter and/or Google+).

– **Request 4: Home, Guide and FAQ interaction**
Based on the user's request, the system displays the corresponding static text content. The Home page containts news about the *Gaia* mission and about the GOSA service, as well as a list of priority targets (Hot targets) visible during the following night (Fig. 7.8). On the other hand, the Guide page displays step by step information and hints on how to correctly gather photometric observations (Fig. 7.9). Finally, the FAQ page is answering the frequently asked questions received (Fig. 7.10).

7.3.3. Interfaces context

Fig. 7.11 presents the Gaia-GOSA service components which are used by the external interfaces. The Home page component and the Observation processing component are using the external interface for communicating and publishing information from Gaia-GOSA web service in social media such as Twitter, Facebook, Google+. The Observation planner is using the external interface for communication with the Google Maps service. In the case of social media, the communication is unidirectional, while in the case of the Maps module, the communication is bidirectional. The system is using the Google Maps API to display the geographical coordinates specified by the user.

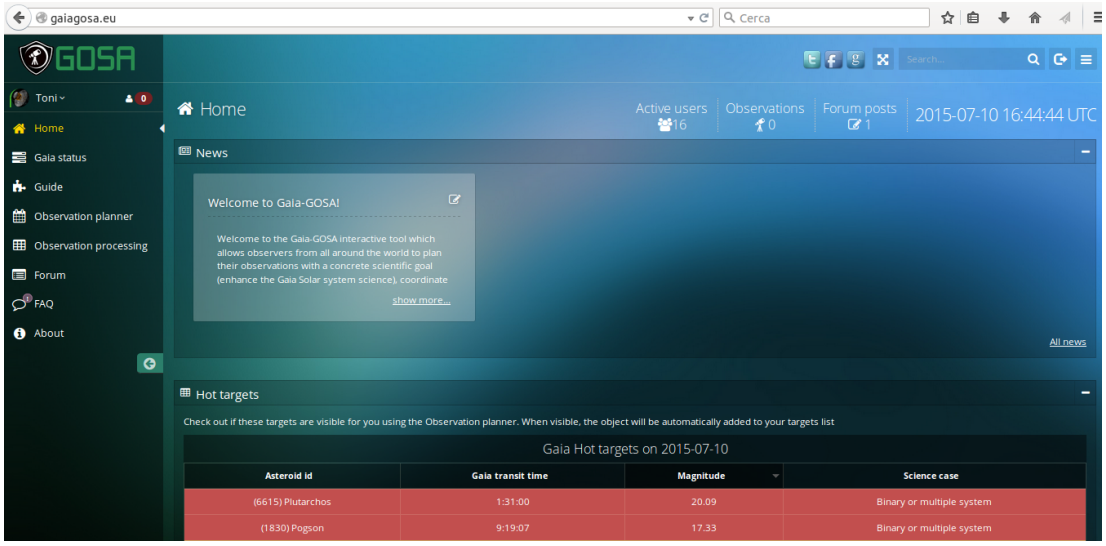

Figure 7.8: View of the Gaia-GOSA home page.

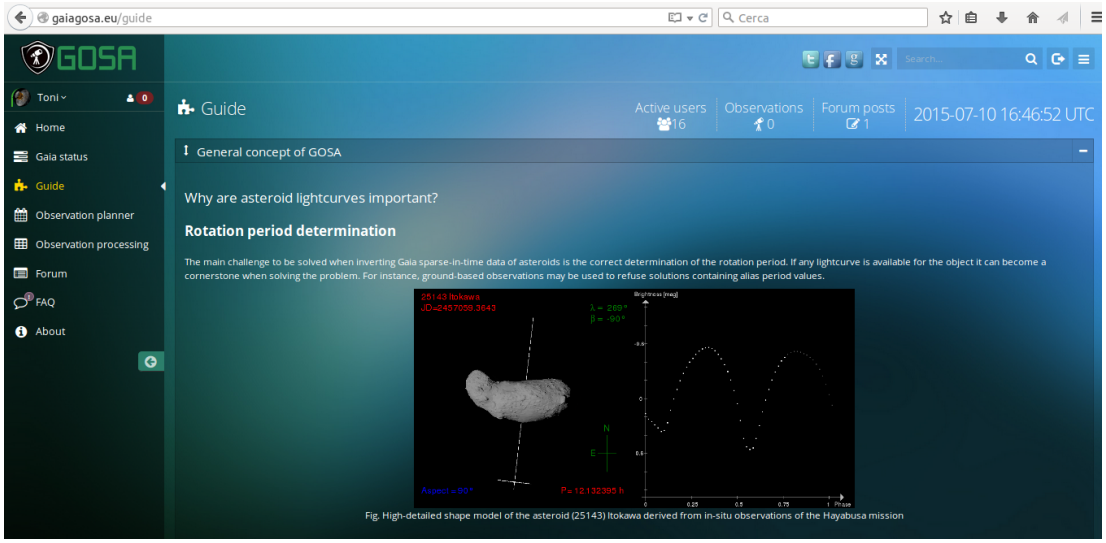

Figure 7.9: View of the Gaia-GOSA users' guide.

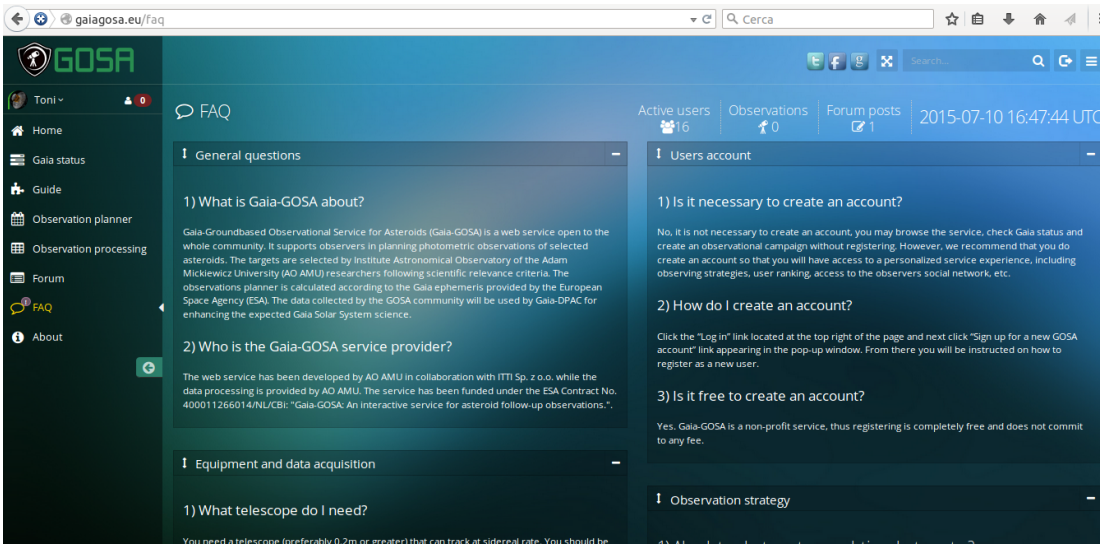

Figure 7.10: View of the Gaia-GOSA's frequently asked questions page.

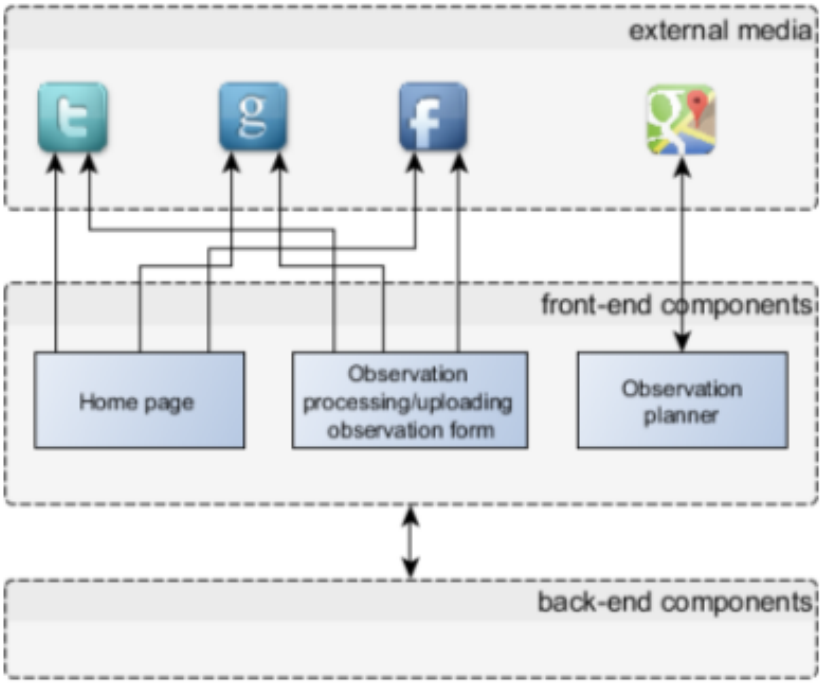

Figure 7.11: Gaia-GOSA external interfaces.

Chapter 8

Conclusions

We stand on the threshold of a new era in the Solar System science. The *Gaia* mission is surveying the sky and will produce a photometric catalogue with several tens of measurements for more than 300,000 asteroids with an unprecedented quality. To analyze such huge quantity of data it will be necessary to apply unattended procedures which have to be tested in simulations before being applied to real *Gaia* data. The tool developed for the analysis of the sparse photometric measurements of asteroids collected by *Gaia* is a genetic inversion algorithm which derives a simple triaxial ellipsoid model of the body in order to obtain its rotational period and pole orientation.

The work presented in this dissertation allows for a better understanding of the *Gaia* inversion algorithm and the results expected from the photometric data of asteroids generated during the *Gaia* mission operations. In this study, the inversion algorithm has been fed with realistic simulations of single asteroids and the results are encouraging. The number of correct inversions remain above 80 per cent even for photometric data burdened with error of 0.03 mag. Moreover, the most problematic scenarios for the inversion method have been detected: 1) asteroids having a quasi-spherical shape, 2) asteroids with low pole latitudes, and 3) asteroids with less than 50 data points. As a consequence, the inversion results produced by this method are severely biased, which has to be considered before drawing physical interpretations from future inversion results. Otherwise, the detected biases could be erroneously misled with physical effects, like an overinterpretation of the YORP effect, resulting from loss of many cases having poles far from being perpendicular to the orbital plane.

A large part of the work has also been devoted to the study of the photometric observations of binary asteroids by *Gaia*. In particular, it has been shown that a simple triaxial model can be positively used to derive the pole and period of a synchronous binary system relying on these observations. The impact of the mutual events on the inversion results has been studied and a detection strategy based on the results for semi-axes distribution has been proposed in order to detect such precious objects within the full catalogue of asteroids. It has been found that the semi-axes distribution resulting from the *Gaia* results can be a good indicator to confirm or deny the anisotropy observed in the distribution of orbit poles of binary asteroids.

The inversion algorithm has also been fed with real photometric sparse data gathered by ground-based surveys. Although the accuracy of these datasets is almost ten times worse than the *Gaia* photometry, the results allowed to confirm the results ob-

tained by means of simulations. In addition, the results include the inversion solutions of known synchronous binary systems, including their rotational periods and pole orientations. Real sparse data was also used to confirm that the inversion method fails for asynchronous binary systems. Such asteroids might be difficult to detect among the regular solutions, which might be an additional error source for the inversion results. However, an estimation of the impact of such objects on the final *Gaia* catalogue of asteroids shall be studied by aims of simulations. The development of strategies for the detection of two periodic asynchronized signals (due to the primary and the secondary lightcurve components) might be a possible way to tackle the issue.

We have also shown that it is possible to reduce the number of wrong solutions by adding a single lightcurve to *Gaia* measurements. Thus pre-selected targets can be used to coordinate an observational campaign with the aim of enhancing the *Gaia* Solar System science output. This is the main goal of the *Gaia-GOSA* service, which has been created on the basis of this work. This dissertation includes the requirements that were needed to create the *Gaia-GOSA* service which allows to coordinate a worldwide observational campaign. It is shown that in order to achieve the scientific goals, coordination between observers is required, as well as a pre-selection of interesting targets within the thousands of asteroids observed by *Gaia*.

It is also of utmost importance to develop strategies for collaboration with ground-based optical surveys that in the near future will produce sparse photometric measurements similar to the ones produced by *Gaia* in terms of quantity and quality. The most outstanding project for the next decade is LSST, which, up to some extent, could be understood as a ground extension of the *Gaia* mission. In this sense, the *Gaia*'s inversion algorithm can be easily adapted to process and combine data from other surveys. Such collaboration shall greatly improve our statistical picture of physical parameters of Solar System objects and will allow us to derive shapes and spin states of asteroids far beyond the main belt.

Bibliography

Binzel R.P. & Mulholland J.D. 1983. „A photoelectric lightcurve survey of small main belt asteroids." *Icarus* **56**, 519

Bartczak P., Michałowski T., Santana-Ros T. & Dudziński G. 2014. „A new non-convex model of the binary asteroid 90 Antiope obtained with the SAGE modelling technique" *Mon. Not. R. Astron. Soc.* **443**, 1802

Bartczak P., Santana-Ros T. & Michałowski T. 2014. „Non-convex shape models of asteroids based on photometric observations" *Asteroids, Comets, Meteors 2014* **29B**

Barucci M. A. et al. 1987. „Classification of asteroids using G-mode analysis" *Icarus* **72**, 304

Behrend R. et al. 2006. „Four new binary minor planets: (854) Frostia, (1089) Tama, (1313) Berna, (4492) Debussy" *Astron. Astrophys.* **446**, 1177

Bottke W. F. et al. 2001. „Dynamical Spreading of Asteroid Families by the Yarkovsky Effect" *Science* **294**, 1693

Bottke W. F. et al. 2006. „The Yarkovsky and Yorp Effects: Implications for Asteroid Dynamics" *Annual Review of Earth and Planetary Sciences* **34**, 157

Braga-Ribas F. et al 2014. „A ring system detected around the Centaur (10199) Chariklo" *Nature* **508**, 72

Bus S. & Binzel R. 2002a. „Phase II of the Small Main-Belt Asteroid Spectroscopic Survey. The Observations" *Icarus* **158**, 106

Bus S. & Binzel R. 2002b. „Phase II of the Small Main-Belt Asteroid Spectroscopic Survey. A Feature-Based Taxonomy" *Icarus* **158**, 146

Carbognani A. et al. 2012. „The representation of asteroid shapes: A test for the inversion of Gaia photometry" *Planetary and Space Science* **73**, 80

Carry B. et al. 2012. „Shape modeling technique KOALA validated by ESA Rosetta at (21) Lutetia" *Planetary and Space Science* **66**, 200

Carry B. et al. 2015. „The small binary asteroid (939) Isberga" *Icarus* **248**, 516

Catmull E. 1974. „A subdivision algorithm for computer display of curved surfaces" *Ph.D. Thesis, University of Utah*

Catmull E. & Clark J. 1978. „Recursively generated B-spline surfaces on arbitrary topological meshes" *Comput. Aided Des.* **10**, 350

Cellino A., Bus S., Doressoundiram A. & Lazzaro D. 2002. „Spectroscopic Properties of Asteroid Families" *Asteroids III, ed. W. F. Bottke, A. Cellino, P. Paolicchi & R. P. Binzel, University of Arizona Press* **633**

Cellino A. 2000. „Minor bodies: spectral gradients and relationships with meteorites" *Space Science Reviews* **92**, 397

Cellino A. et al. 2006. „Rotational properties of asteroids from Gaia disk-integrated photometry: A "genetic" algorithm" *Advances in Space Research* **38**, 9

Cellino A. et al. 2009. „Genetic inversion of sparse disk-integrated photometric data of asteroids: application to Hipparcos data" *Astron. Astrophys.* **506**, 935

Cellino A. 2014. „The expected Gaia revolution in asteroid science: Photometry and spectroscopy" *Asteroids, Comets, Meteors 2014* **85C**

Cellino A. et al. 2015. „Inversion of sparse photometric data of asteroids using triaxial ellipsoid shape models and a Lommel-Seeliger scattering law" *Planetary Space Science* **Submitted**

Colas F. et al. 2012. „Shape and size of (90) ANTIOPE derived from an exceptional stellar occultation on July 19, 2011" *Asteroids, Comets, Meteors 2012* **6427**

Connelly R. & Ostro S. J. 1984. „Ellipsoids and lightcurves" *Geometriae Dedicate* **17**, 87

Davis R. G. 2001. „High precision lightcurves for 762 Pulcova" *Minor Planet Bulletin* **28**, 10

Davis R. G. et al. 1989. „Asteroid collisional history - Effects on sizes and spins" *Asteroids II, ed. R. P. Binzel, T. Gehrels, & M. S. Matthews, University of Arizona Press* **805**

De Angelis G. 1995. „Asteroid spin, pole and shape determinations" *Planetary and Space Science* **43**, 649

Delbo M. et al. 2012. „Asteroid spectroscopy with Gaia" *Planetary and Space Science* **73**, 86

Descamps P. et al. 2007. „Figure of the double Asteroid 90 Antiope from adap-

tive optics and lightcurve observations" *Icarus* **187**, 482

Descamps P. et al. 2009. „A giant crater on 90 Antiope?" *Icarus* **203**, 102

Dobrovolskis A. R. 1996. „Inertia of Any Polyhedron" *Icarus* **124**, 243

Ďurech J. et al. 2007. „Physical models of asteroids from sparse photometric data" *Proc. IAU Symp. 236, Cambridge University Press* p.**191**

Ďurech J. et al. 2009. „Asteroid models from combined sparse and dense photometric data" *Astron. Astrophys.* **493**, 291

Ďurech J. et al. 2011. „Combining asteroid models derived by lightcurve inversion with asteroidal occultation silhouettes" *Icarus* **214**, 652

Eyer L. & Mignard F. 2005. „Rate of correct detection of periodic signal with the Gaia satellite" *Mon. Not. R. Astron. Soc.* **361**, 1136

Franco L., Pilcher F. & Ďurech J. 2013. „Lightcurve inversion for 38 Leda" *Minor Planet Bulletin* **40**, 229

Gajdos S. et al. 2007. „(1338) Duponta" *Central Bureau Electronic Telegrams* **910**, 1

Goldstein H. 1980. „Classical Mechanics" *Addison-Wesley, Reading, MA*

Hanuš J. et al. 2011. „A study of asteroid pole-latitude distribution based on an extended set of shape models derived by the lightcurve inversion method" *Astron. Astrophys.* **530**, A134

Hanuš J. et al. 2013a. „Asteroids' physical models from combined dense and sparse photometry and scaling of the YORP effect by the observed obliquity distribution" *Astron. Astrophys.* **551**, A67

Hanuš J., Marchis F. & Ďurech J. 2013b. „Sizes of main-belt asteroids by combining shape models and Keck Adaptive Optics observations" *Icarus* **226**, 1045

Harris A. W. et al. 1992. „Asteroid lightcurve observations from 1981" *Icarus* **95**, 115

Higgins D. et al. 2010. „(2121) Sevastopol" *Central Bureau Electronic Telegrams* **2427**, 1

Kaasalainen M. 2004. „Physical models of large number of asteroids from calibrated photometry sparse in time" *Astron. Astrophys.* **422**, L39-L42

Kaasalainen M. & Torppa J. 2001. „Optimization Methods for Asteroid Lightcurve

Inversion. I. Shape Determination" *Icarus* **153**, 24

Kaasalainen M., Torppa J. & Piironen J. 2002a. „Models of twenty asteroids from photometric data" *Icarus* **159**, 369

Kaasalainen M., Torppa J. & Piironen J. 2002b. „Binary structures among large asteroids" *Astron. Astrophys.* **383**, L19

Kryszczyńska A. et al. 2009. „New binary asteroid 809 Lundia. I. Photometry and modelling" *Astron. Astrophys.* **501**, 769

Kryszczyńska A. et al. 2014. „Non-convex model of the binary asteroid (809) Lundia and its density estimation" *Asteroids, Comets, Meteors 2014. Proceedings of the conference.* **297K**

Lindegren L. 1977. „Meridian observations of planets with a photoelectric multislit micrometer" *Astron. Astrophys.* **57**, 55

Manzini F. et al. 2006. „(1139) Atami" *Central Bureau Electronic Telegrams* **430**, 1

Marchis F. et al. 2006. „Shape, size and multiplicity of main-belt asteroids. I. Keck Adaptive Optics survey" *Icarus* **185**, 39

Marchis F. et al. 2013. „Characteristics and large bulk density of the C-type main-belt triple asteroid (93) Minerva" *Icarus* **224**, 178

Marciniak A. & Michałowski T. 2010. „Asteroids' spin axis distribution" *Icarus* **512**, A56

Marciniak A. et al. 2008. „Photometry and models of selected main belt asteroids. V. 73 Klytia, 377 Campania, and 378 Holmia" *Astron. Astrophys.* **478**, 559

Marciniak A. et al. 2011. „Photometry and models of selected main belt asteroids. VIII. Low-pole asteroids" *Astron. Astrophys.* **529**, A107

Marciniak A., Bartczak P., Santana-Ros T. et al. 2012. „Photometry and models of selected main belt asteroids. IX. Introducing interactive service for asteroid models (ISAM)" *Astron. Astrophys.* **545**, A131

Michałowski T. 1993. „Poles, shapes, senses of rotation, and sidereal periods of asteroids" *Icarus* **106**, 563

Michałowski T. et al. 2002. „Eclipsing events in the binary system of the asteroid 90 Antiope" *Astron. Astrophys.* **396**, 293

Michałowski T. et al. 2004a. „Photometry and models of selected main-belt as-

teroids (I): 52 Europa, 115 Thyra, and 382 Dodona" *Astron. Astrophys.* **416**, 353

Michałowski T. et al. 2004b. „Eclipsing binary asteroid 90 Antiope" *Astron. Astrophys.* **423**, 1159

Michałowski T. et al. 2014. „(3169) Ostro: A single body or a contact binary asteroid?" *Asteroids, Comets, Meteors 2014. Proceedings of the conference.* **351M**

Mignard F. 2011. „From Gaia frame to ICRF3?" *Proceedings of the JournÃ©es 2011* **Vienna University of Technology**

Mignard F. 2015. „Transits of Solar system objects in 2015" *Gaia-DPAC documentation* **GAIA-C4-TN-OCA-FM-056-1**

Mignard F. et al. 2007. „The Gaia Mission: Expected Applications to Asteroid Science" *Earth, Moon and Planets* **101**, 97

Mouret S., Hestroffer D. & Mignard F. 2008. „Asteroid mass determination with the Gaia mission. A simulation of the expected precisions" *Planetary and Space Science* **56**, 14, 1819

Mousis O. et al. 2013. „Instrumental methods for professional and amateur collaborations in planetary astronomy" *Experimental Astronomy* **38**, 91

Muinonen K. 1998. „Introducing the Gaussian shape hypothesis for asteroids and comets" *Astron. Astrophys.* **332**, 1087

Muinonen K., Virtanen J., Granvik M. & Laakso T. 2005. „Asteroid Orbits with Gaia: Inversion and Prediction" *Proceedings of the Gaia Symposium "The Three-Dimensional Universe with Gaia* **ESA SP-576**

Polishook D. & Brosch N. 2006. „Many binaries among NEAs." *arXiv* **2006astro.ph..7128P**

Pospieszalska-Surdej A. & Surdej J. 1985. „Determination of the pole orientation of an asteroid. The amplitude-aspect relation revisited." *Astron. Astrophys.* **149**, 186

Pravec P., Harris A. W. & Michałowski T. 2002. „Asteroid Rotations" *Asteroids III* **2002**, 113

Pravec P. et al. 2012. „Binary asteroid population. 2. Anisotropic distribution of orbit poles of small, inner main-belt binaries" *Icarus* **218**, 125

Prusti T. 2012. „Gaia intermediate data release scenario" *Gaia documentation* **GAIA-CG-PL-ESA-TJP-011-01**

Santana-Ros T. et al. 2014. „Gaia-GOSA: an interactive service for asteroid follow-up

observations" *EAS Publications Series*, 67-68, 109

Santana-Ros T. et al. 2015. „Testing the inversion of asteroids' *Gaia* photometry combined with ground-based observations" *Mon. Not. R. Astron. Soc.* **450**, 333

Soma M., Hirayama T. & Kinoshita H. 1988. „Analytical expressions of the Earth's position and velocity for the calculation of apparent positions" *Cel. Mech.* **41**, 389

Stephens R., Warner, B.D. & Harris, A.W. 2010. „A Proposed Standard For Reporting Asteroid Lightcurve Data" *American Astronomical Society, DPS meeting* **42**, 1035

Stephens R. et al. 2012. „A shape model of the main-belt asteroid 27 Euterpe" *Minor Planet Bulletin* **39**, 2

Tanga P. & Delbo M. 2007. „Asteroid occultations today and tomorrow: toward the GAIA era" *Astron. Astrophys.* **474**, 1015

Tholen D. J. 1984. „Asteroid taxonomy from cluster analysis of photometry" *Ph.D. Thesis, University of Arizona, Tucson*

Torppa J. et al 2003. „Shapes and rotational properties of thirty asteroids from photometric data" *Icarus* **164**, 346

Torppa J. et al 2008. „Asteroid shape and spin statistics from convex models" *Icarus* **198**, 91

Viikinkoski M., Kaasalainen M. & Ďurech J. 2015. „ADAM: a general method for using various data types in asteroid reconstruction" *Astron. Astrophys.* **576**, A8

Warell J. & Lagerkvist C. I. 2007. „Asteroid taxonomic classification in the Gaia photometric system" *Astron. Astrophys.* **467**, 749

Warner B. D. 2002. „Asteroid photometry at the Palmer Divide Observatory: Results for 1333 Cevenola and 2460 Mitlincoln" *Minor Planet Bulletin* **31**, 67

Warner B. D. et al. 2008b. „Shape and spin models for four asteroids" *Minor Planet Bulletin* **35**, 167

Zappalà V. et al. 1990. „An analysis of the amplitude-phase relationship among asteroids" *Astron. Astrophys.* **231**, 548

Zellner B., Tholen D. J. & Tedesco E. F. 1985. „The eight-color asteroid survey - Results for 589 minor planets" *Icarus* **61**, 355